NASA Technical Memorandum 104581

Empirical Wind Model for the Middle and Lower Atmosphere— Part 1: Local Time Average

A. E. Hedin
NASA Goddard Space Flight Center
Greenbelt, Maryland

F. J. Schmidlin
NASA Goddard Space Flight Center
Greenbelt, Maryland

E. L. Fleming
Applied Research Corporation
Landover, Maryland

S. K. Avery
University of Colorado
Boulder, Colorado

A. H. Manson
University of Saskatchewan
Saskatchewan, Canada

S. J. Franke
University of Illinois
Urbana, Illinois

National Aeronautics and
Space Administration

Goddard Space Flight Center
Greenbelt, Maryland 20771

1993

Contents

1. Introduction

The recently published Cospar International Reference Atmosphere (CIRA 1986 or CIRA-86) contains monthly tabulations of zonal mean wind from 0 to 120 km [Fleming et al., 1990] derived from a tropospheric climatology by Oort [1983] and use of the gradient wind approximation with the temperature and pressure tables derived from satellite remote sensing data by Barnett and Corney [1985] for the middle atmosphere and the mass spectrometer and incoherent scatter (MSIS-83) empirical model [Hedin, 1983] for the thermosphere. The MSIS-83 model was the predecessor of the MSIS-86 model [Hedin, 1987] model which constitutes the thermosphere portion of the CIRA-86 density and temperature model [Hedin, 1988].

The CIRA-86 tabulations are the successor to CIRA 1972 (CIRA-72) which contained wind tabulations [Groves, 1972a] based largely on rocket and some radar measurements. However, the CIRA-86 tabulations were derived independently of the prior rocket data or tabulated models. Monthly wind models for the upper mesosphere and lower thermosphere based entirely on MF (medium frequency) and meteor radar data have also been prepared [Miyahara et al, 1991].

Thermospheric wind data from satellites and ground based incoherent scatter radar and Fabry-Perot optical interferometers have been combined [Hedin et al., 1991] to generate an analytic empirical horizontal wind model (HWM90) of winds above 100 km using a limited set of vector spherical harmonics to describe spatial and temporal variations in the exosphere and at selected altitude nodes with cubic spline interpolation between nodes. The formulation of this wind model is analogous to the MSIS-86 density and temperature model and allows the user to obtain atmospheric parameters at an arbitrary location and time. The MSIS-86 model was recently extended [Hedin, 1991] into the lower atmosphere to provide a single analytic reference model [MSISE-90] of temperature and density from the ground to the exosphere. While the lower atmosphere portion was essentially derived from the CIRA-86 tabulations, the structure in the upper mesosphere was adjusted to best fit historical rocket data as well as maintain overall hydrostatic equilibrium while smoothly joining the previous upper thermosphere model.

It is the goal of the HWM93 model described herein to extend the formulation of the HWM90 wind model into the mesosphere and to the surface so as to provide a description of the average (climatological) wind system throughout the atmosphere. The model is based not only on the CIRA-86 tabulations, but selected historical rocket data, previous rocket data based tabulations, meteor radar and MF radar data, and lower thermosphere incoherent scatter data previously used for HWM90. The new model thus represents a compromise between data sources in the upper stratosphere, mesosphere, and lower thermosphere, while closely following CIRA-86 in the lower stratosphere and troposphere and HWM90 in the thermosphere. Model results and data comparisons are given with emphasis on the mesosphere and lower thermosphere and include also gradient winds calculated from MSISE-90. The HWM90 model parameters

1

were changed at 100 km to provide a smoother transition into the mesosphere but otherwise remain unchanged in the thermosphere.

2. Data Sources

The data used to generate this model were derived from published tabulations, figures, and original data bases as summarized in Table 1. The number and diversity of data sources is greatest in the mesosphere and lower thermosphere consistent with availability and the emphasis of this paper.

In the mesosphere and lower thermosphere the techniques and sources represented include incoherent scatter radar, MF radar, meteor radar, rocketsondes, rocket grenade soundings, and gradient winds. These data were given the most weight in deriving the model. Although MF radar data appear in later plots at their nominal attributed altitude, they were given considerably less weight in the fit above 100 km because their real and apparent altitudes are different near the total reflection height. In addition, tabulations in CIRA-72 [Groves, 1972a], GROVES-69 [Groves, 1969], and CAO-83 (Central Aerological Observatory) [Koshelkov, 1983] summarizing largely older or different rocket data and tabulations from CIRA-86 [Fleming et al., 1990], providing global coverage largely based on gradient wind calculations, were included with approximately a factor of two less weight. Gradient winds derived from MSISE-90 were weighted a factor of ten less than the rocket and radar data and thus are only included for comparison purposes below 85 km. However, the CIRA-86 winds were weighted less above 85 km by a factor of sixteen in order to give some precedence to the newer MSISE-90 representation of the mesosphere/thermosphere transition region.

In the stratosphere the data include rocketsondes, and rocket grenade soundings, CIRA-72, CAO-83, tabulations from CIRA-86 and MSISE-90 gradient winds (Table 1). For the troposphere, only the CIRA-86 tabulations and MSISE-90 gradient winds are used.

While the data sources are largely independent, there are also significant overlaps which should be kept in mind. The data sets will now be described with this aspect in mind as far as is known.

Unlike earlier CIRA tabulations, the CIRA-86 reference atmosphere winds in the stratosphere and mesosphere are inferred from satellite remote sounding pressure and temperature data and a thermospheric density and temperature model and make no direct use of rocket or radar wind data. The CIRA-86 winds were largely derived from the gradient wind equation. However, equatorial winds were based on the second derivative of pressure where the geostrophic formulation fails, troposphere winds were based on a published data summary, and very high latitude winds were based on a dynamical constraint (see Fleming et al., 1990). For longitudinal variations the CIRA-86 tabulations were supplemented with gradient wind calculations of wave 1 amplitudes and phases for the zonal and meridional wind [Fleming et al., 1988]. These gradient winds were favorably compared with radar derived winds by Manson et al. [1991]. Gradient winds (including equatorial winds

using the second derivative formulation) were also derived from the MSISE-90 density and temperature model and will be similar to the CIRA-86 winds, since MSISE-90 is based heavily on the same CIRA-86 pressure and temperature tabulations. However, there are differences, particularly in the upper mesosphere/lower thermosphere, and these are greatest near the equator. Also, winds derived from the MSISE-90 model will have smoother variations as a function of latitude and month than the CIRA-86 tabulations since MSISE-90 represents a smoothed version of density and temperature variations.

The CIRA-72 zonal winds (no meridional winds were published) are largely determined by rocket wind data and early radio-meteor results available at that time. Much of the data was from reports and private sources not readily available today, but there is some overlap with rocket data used here. Below 60 km there are separate tables for American and European longitudes and these were arbitrarily taken to apply to 90W and 20E.

The CAO-83 southern hemisphere reference tabulations (only zonal wind) are derived largely from Russian rocket data but probably overlap slightly the data used in CIRA-72. A later version [Koshelkov, 1990] incorporates more rocketsonde data but also radar data that is separately included here.

The GROVES-69 tabulations are an older version of CIRA-72 for both zonal and meridional winds and include some of the early rocket data. Only the meridional wind from these tabulations is used here since CIRA-72 superseded the zonal winds but did not include meridional wind.

Rocketsonde data from the Meteorological Rocket Network (MRN) were obtained from the NASA/Wallops database, which is similar to the World Data Center format available from the National Climate Data Center at Asheville, NC. The data cover the time period from 1969 to 1991 and were separated into falling sphere data [Schmidlin, 1985], which make useful measurements to nearly 100 km, and parachute/datasonde measurements which were limited to 75 km. Based on the available time period, only slight overlap is possible with CIRA-72. The MRN concentrated on taking data near local noon, but data are available for all parts of the day for most stations. For each station, the data at two kilometer intervals were separated into two hour local time groups. Monthly averages, determined by summing over all available years, were formed separately for the twelve local time groups. These averages, which provide as equitable a local time coverage as possible, were used as the rocketsonde input to the model and data comparisons in order to minimize tidal bias from this source.

The rocket grenade data from 1960-1972 were partly included in GROVES-69 and CIRA-72, but are not included in the rocketsonde data.

The more recent MF and Meteor radar data included here were not available for CIRA-72 and are presented only as supplementary data for CIRA 1986 [Manson, 1990].

3. Model Formulation

The HWM93 model is an extension of the HWM87 and HWM90 wind models [Hedin et al., 1988; 1991] summarizing wind measurements in the thermosphere. Spatial (latitude and longitude) variations in the horizontal wind vector are represented by an expansion in vector spherical harmonics [Morse and Feshbach, 1953] with each expansion coefficient represented by a Fourier series in day of year for annual and semiannual variations. The expansion involves two orthogonal vector fields, the divergence B field and the rotational C field. Solar activity and magnetic activity variations are not included below 100 km. Hemispheric differences are allowed but are very limited. This report will treat only non-tidal variations, although tidal and non-tidal variations were fit in an iterative fashion to produce as self-consistent an overall model as possible. Quasi-biennial variations are not included. Zonally averaged meridional winds were not modelled below 45 km. Stationary wave 1 longitude variations were limited to 7 to 90 km. Only the rotational (C) field was used to represent longitude variations since the winds are nearly geostrophic, and thus nearly non-divergent, and it seemed unlikely that departures from a curl field could be extracted from the current limited data.

Below 100 km the wind profiles are represented by a cubic spline, defined by cubic polynomials between specified nodes with first and second derivatives continuous across interior nodes. The nodes were chosen to be at 100, 90, 82.5, 75, 67.5, 60, 52.5, 45, 37.5, 30, 22.5, 15, 7.5, and 0 km providing a convenient division into intervals of approximately one scale height. The wind magnitude and altitude gradient are matched at 100 km with the thermosphere values, and in addition the altitude gradient is specified (fit) at 100 km.

The harmonic expansion at each altitude node is limited to low order terms as summarized in Tables 2a and 2b, thus smoothing the model output in space and time. The classification into symmetrical and asymmetrical is with respect to reflection about the equator with symmetrical meaning the vector spherical harmonic term provides zonal winds which have the same direction across the equator while the meridional wind changes direction. The column value 'm' refers to the longitudinal (or local time) harmonic content (0 means no longitudinal variation, 1 the first harmonic, etc.). The 'n' value is the latitude harmonic order and is always equal to or larger than 'm'. If the n-m value is even, then the B field term is symmetric and the C field term is asymmetric. The higher the order 'n' the greater the latitude variability that can be represented. Terms of order higher than those in the table were not found to be significant in fitting the present data set. In Table 2 a dash (-) means this term is not included for this node.

The determination of the harmonic coefficients for the various nodes of the wind profile is accomplished by a least squares fit to selected subsets of the data. The node to node variations of the harmonic coefficients were smoothed by refitting with the sum of the

4

squares of the differences between adjacent node coefficients (multiplied by a constant) added to the usual sums of squares of data minus model differences. The multiplicative (tension) constant was chosen so that the sums of squares of the data residuals increased by no more than one percent.

Root mean square deviations of the data from the model in different altitude regions are given in Tables 3a and 3b. The grenade and incoherent scatter data tend to have the largest average departures because they were not smoothed or based on monthly averages. Natural variability is also high in the lower thermosphere where tides and electrodynamic effects are important. The differences between the model and rocket and incoherent scatter data also reflect possible mismodeling of the tidal variations (model described in a separate report), although this is not a major factor below 100 km.

4.   Model Examples/Comparisons/Discussion

4.1   Yearly Average Latitude Variations of Zonal Wind

The zonal and annual average zonal winds from the model are illustrated in Fig. 1. The mostly eastward flow in both hemispheres peaks at 30 m/s at mid-latitudes in the southern hemisphere stratosphere (15 m/s in northern hemisphere). An equatorial zone of westward flow peaks near 15 m/s in the stratosphere with small zones near the surface and upper mesosphere. Eastward winds in the lower thermosphere are not as large as in CIRA-86.

Further examples of model winds and comparisons with data are shown in Figs. 2 and 3. Here data have been selected for rather broad altitude or latitude intervals and the model wind plotted vs latitude or altitude for the midpoint of the selected intervals. The example model plot will represent the model prediction at the exact altitude or latitude of individual measurements with a degree of faithfulness that depends on how rapidly the model varies with altitude, latitude, etc. The difference between the plotted points and the model line represents the average difference of each measurement, separated by source as specified in Table 1, from the model (calculated exactly for that location) and the error bars represent the one standard deviation scatter of this difference within the plot bin limits. There are up to three plots for each situation, separating data into three groups: gradient winds, one as published in CIRA-86 and one as derived form MSISE-90; rocket data, CIRA-72, and CAO-83 (primarily stratosphere/mesosphere) and incoherent scatter data (thermosphere); and meteor and MF radars (monthly averages).

In the stratosphere the winds are well defined by gradient winds, rocket data, CIRA-72 and CAO-83 (Figs. 2 and 3). The gradient winds are in good agreement with each other except at the equator, thus confirming the representation of temperature and density gradients in MSISE-90. At low latitudes (Figs. 2a and 2b) the gradient winds may differ by 5-10 m/s, but neither is systematically in better agreement with the rocket data. Equatorial differences are not surprising given

5

the dependence of the derived zonal wind on the second derivative of pressure as a function of latitude, rather than the first, and the small magnitudes of the terms involved [Fleming and Chandra, 1989]. The quasi-biennial variation near the equator will also introduce some scatter. At high latitudes there is a systematic tendency for the rocket data, CIRA-72, and CAO-83 to be higher than the gradient winds in the southern hemisphere by 5 to 10 m/s and similarly lower than the gradient winds in the northern hemisphere.

In the mesosphere the winds are fairly well defined by gradient winds, rocket data, CIRA-72, CAO-83, and Meteor/MF radars, but with increasing scatter and discrepancies toward higher altitudes and at lower latitudes. The Meteor and MF radar values generally differ from the model by less than 5 m/s. At low latitudes, CIRA-86 is fairly close to the model but MSISE-90 is higher by 10 m/s (Fig. 3b). Rocket data show stronger eastward flow than the model in the lower mesosphere (closer to MSISE-90) and stronger westward flow than the model in the upper mesosphere (closer to CIRA-86). At midlatitudes, the rocket data, CIRA-72, and CAO-83 show stronger eastward flow by 5 to 10 m/s than the gradient or meteor and MF winds (Fig. 2c).

In the lower thermosphere there is considerable scatter between data points and sets such that consistency is often poor. The spread between gradient winds is the order of 10-20 m/s. They follow the model in only a very rough way. The Meteor and MF radar data are generally clustered about the model within 5 m/s. At low latitudes, rocket data, CIRA-72, and IS radar are mostly less than model while the gradient winds are much above (Fig. 2d). At high latitudes, the IS radar tends to be above the model while the Meteor/MF radar tends to be below model.

4.2 Yearly Average Latitude Variations of Meridional Wind

The zonal and annual average meridional winds (Fig. 1) are mostly northward in the northern hemisphere and southward in the southern hemisphere peaking near 3 m/s in the mesosphere and 6 m/s in the lower thermosphere with small regions of reverse flow near the mesopause at lower latitudes and the stratopause at high latitudes. The model uses only the two lowest symmetric harmonics so there is no hemispheric difference except in direction of flow.

Model and data comparison plots similar to those for zonal winds are shown in Figs. 4 and 5, except there is no plot for gradient winds and the only rocket model is GROVES-69.

There is considerable scatter among data points and data sets (Figs. 4 and 5). Consistency is often poor, arguing against the use of higher harmonics for a more complicated pattern. However, the rocket data (Fig. 5b) suggest that an alternating pattern of north/south cells near 75 km in equatorial latitudes should probably be stronger than modeled. While the rocket data is fairly consistent in the lower mesosphere, Groves-69 is inconsistent with meteor and MF radar in the southern hemisphere. Meteor and MF radar data generally cluster about

6

the model within 5 m/s. There is up to 10 m/s differences among incoherent scatter data in the lower thermosphere.

4.3 Annual and Semiannual Variations of Zonal Wind

The annual variation of the zonal wind has a winter eastward maximum phase (Fig. 6) peaking at midlatitudes just above the stratopause with amplitudes of 70 m/s (southern hemisphere) and 60 m/s (northern). An annual variation with a summer eastward maximum phase exists near the mesopause with an amplitude of 10 m/s. The semiannual variation (Fig. 7) has an equinox eastward maximum at low latitudes with an amplitude of 20 m/s in upper stratosphere and a westward maximum at the equinoxes in upper mesosphere with an amplitude of 15 m/s. These features have been well documented in the literature (e.g. Angell and Korshover [1970]; Groves, 1972b; Belmont [1985] and references therein). Example latitudinal cross-sections are shown in Fig. 8 for four different months.

In the stratosphere the annual and semiannual variations are rather well defined by gradient winds, rocket data, CIRA-72, and CAO-83. Comparison plots versus day of year for six broad latitude groupings are shown in Fig. 9. There are sometimes considerable differences such as at high southern latitudes where CIRA-72 and CAO-83 winds are well above the model and gradient winds during the September equinox (Fig. 9a).

In the mesosphere the annual and semiannual variations are fairly well defined by gradient wind, rocket data, CIRA-72, and CAO-83, as well as meteor and MF radar data. However, at low latitudes the gradient wind variation is qualitatively different from rocket and radar in the upper mesosphere. Recently reported equatorial data [Vincent and Lesicar, 1991; Fritts and Isler, 1992] support a strong westward wind in the spring equinox which is quite different from the gradient winds (Figs. 9l and 9m). The model semiannual amplitude reaches a deeper minimum near 65 km which is more in accord with rocket data than with the amplitude suggested by gradient winds [Fleming and Chandra, 1989]. At northern mid-latitudes near 80 km (Fig. 9n), there are small but striking differences in the annual variation observed by different techniques. Meteor radars have a weaker annual variation than either rocket or gradient winds, while the MF radars in this grouping (Saskatoon and Urbana) have an annual variation similar to the gradient winds and larger than the variation described by rocket data. The small average eastward flow in December from the meteor radars leads to an extremely weak (compared to the southern hemisphere winter) eastward mesospheric jet during northern winter in the Miyahara et al. [1991] model based only on radar data. Differences in the height of the summer reversal from westward to eastward flow [Manson et al., 1990] also contribute to differences in the annual variation in the 80 to 90 km region. For example, Saskatoon has a reversal height near 90 km and Atlanta and Kyoto have a reversal height near 80 km. In the lower mesosphere there is considerable separation between CIRA-72 and CAO-83 at high southern latitudes (Figs. 9a and 9b) where data has always been sparse.

7

In the lower thermosphere there are considerable differences between the gradient winds. Consistency is often poor between data sets. The gradient winds are closer to each other and the model during solstices than equinoxes (e.g. figs. 9f and 9p). The relatively large eastward winds of CIRA-86 relative to radar data have been discussed by Manson et al. [1991]. Here the temperature and pressure gradients in the revised MSISE-90 appear to be an improvement over CIRA-86/MSIS-86. At low latitudes, CIRA-86 is particularly high relative to rocket, meteor, and MF radar during equinoxes (Figs. 9i and 9m). At high latitudes, incoherent scatter shows larger annual variations in the northern hemisphere (June maximum) than meteor and MF radar or gradient winds (Fig. 9r). This may be due in part to limited data or biasing by magnetic disturbances when data yield is best.

4.4 Annual and Semiannual Variations of Meridional Wind

The annual variation of the meridional wind (Fig. 6) has a January northward maximum peaking at 8 m/s near the equator in the mesosphere and reversing to a July maximum in the lower thermosphere above 105 km. Only the lowest harmonic in latitude is used below the thermosphere, given the large data scatter, producing meridional winds of the same direction in both hemispheres. The semiannual variation is very small (Fig. 7) with an equinox poleward maximum at midlatitudes of 2 m/s in upper mesosphere and equatorward maximum of 1 m/s in lower mesosphere. Only the lowest harmonic in latitude is used providing winds of opposite direction in each hemisphere. Example latitudinal cross-sections are shown in Fig. 8 for four different months.

Data comparison plots are shown in Fig. 10. There is considerable scatter among data points and data sets. Consistency is often poor between data sets. Overall model trends are clearly present in the data, but details are not particularly robust. While fluctuations in meridional and zonal wind measurements are similar (Table 3), the desired average signal is much smaller relative to the fluctuations for the meridional wind and thus incomplete coverage in the rocket and incoherent scatter data is more noticeable. Seasonal patterns are often similar to Groves [1969] but of lesser magnitude (e.g. Fig. 10a). Sometimes higher amplitudes would be consistent with limited radar data (Fig. 10c) but not so obviously consistent with similar data in the other hemisphere (Fig. 10i). Latitudinal patterns are also similar to those of Maiyahara et al. [1991], although less detailed. In particular, our analysis did not find a region of winter to summer flow near 80 km at equatorial latitudes (imbedded in the more typical summer to winter flow). The characteristics of the summer to winter flow as found in radar data and the relation to measured momentum deposition by gravity waves has been discussed by Manson et al. [1991]. The reversal to a winter to summer flow in the lower thermosphere is clearly present in the MF/Meteor radar data, as it was in the incoherent scatter data [Hedin et al., 1991], but again with station to station differences in reversal height as in the zonal wind.

8

4.5 Longitude Variations

The stationary wave 1 (first harmonic in longitude) amplitudes are illustrated in Figs. 11 and 12. The zonal variations peak in the upper stratosphere at northern winter mid-latitudes with an amplitude of 30 m/s (zonal) and again at the pole with an amplitude of 35 m/s (zonal and meridional). Meridional wind variations peak at the pole with the same amplitude. Southern hemisphere amplitudes are less than 10 m/s. Annual and semiannual variation in wave amplitude are included in the model. Longitude variations related to planetary waves are not carried above 90 km for lack of defining data (but longitude variations are present in thermosphere above 130 km because of physical processes tied to the magnetic field geometry) or below 15 km (limited by the CIRA tabulations).

The longitude variations are derived almost entirely from gradient wind data. Comparisons of the gradient winds from remote satellite data [Fleming et al., 1988] and from MSISE-90 with the HWM93 model are shown in Figs. 13 and 14. The two gradient wind estimates are generally similar with each other except near the poles where there was difficulty in performing the numerical differentiation from the tabulated satellite data and near the equator where, as for zonal averages, the wind depends on a second derivative of pressure. The month to month variability is remarkably well represented by a sum of annual and semiannual variations in the longitudinal harmonic coefficients. Other data are nominally consistent, but are insufficient in longitude coverage to define the variation. In particular, the CIRA-72 tables, separated by American and European longitudes, are reasonably consistent with the satellite data. An example comparing gradient winds with other data is shown in Fig. 15. Systematic differences are noticed between gradient and radar winds as seen also in the zonal average plots (Fig. 9n).

Second harmonic (wave 2) variations are present [Barnett and Labitzke, 1990; Fleming et al., 1988] in the stratosphere and mesosphere but, unlike the wave 1 variations, their month to month variability is more random and not as usefully represented in terms of a mean and annual and semiannual variations and is thus not included in this model.

5. Summary

Reference winds from CIRA-86 combined with rocket soundings, incoherent scatter, MF radar, meteor radar, and older reference tabulations have been used to extend the HWM90 spherical harmonic wind model into the lower atmosphere providing a unified description of zonal and meridional prevailing winds from the surface to the exosphere. While month to month details cannot be completely represented, mesospheric data are fit with an overall rms error of approximately 15 m/s and considerably better in the stratosphere. Comparison with rocket and radar data indicates that the model represents current knowledge of climatology reasonably well.

References

Angell, J. K., and J. Korshover, Quasi-bienniel, annual, and
semi-annual zonal wind and temperature harmonic amplitudes and phases
in the stratosphere and lower mesosphere of the northern hemisphere,
J. Geophys. Res., 75, 543-550, 1970.

Avery, S. K., A. C. Riddle, B. B. Balsley, The Poker Flat, Alaska,
MST radar as a meteor radar, Radio Sci., 18, 1021-1027, 1983.

Avery, S. K., J. P. Avery, T. A. Valentic, S. E. Palo, M. J. Leary,
and R. L. Obert, A new meteor echo detection and collection system:
Christmas Island mesospheric wind measurements, Radio Sci., 25,
657-669, 1990.

Barnett, J. J., and M. Corney, Middle atmosphere reference model from
satellite data, Handb. MAP, 16, edited by K. Labitzke, J. J.
Barnett, and B. Edwards, pp. 47-85, SCOSTEP, Urbana, Ill., 1985.

Barnett, J. J., and K. Labitzke, Climatological distribution of
planetary waves in the middle atmosphere, Adv. Space Res., 10(12),
63-91, 1990.

Belmont, A. D., Comparisons of time-periodic variations in
temperature and wind from meteorological rockets and satellites,
Adv. Space Res., 5(7), 115-123, 1985.

Bernard, R., Tides in the E-region observed by incoherent scatter
over Saint Santin, J. Atmos. Terr. Phys., 36, 1105-1120, 1974.

Clark, R. R., Upper atmosphere wind observations of waves and tides
with the UNH Meteor Radar System at Durham 43N (1977, 1978 and 1979),
J. Atmos. Terr. Phys., 45, 621-627, 1983.

Fleming, E. L., and S. Chandra, Equatorial zonal wind in the middle
atmosphere derived from geopotential height and temperature data,
J. Atmos. Sci., 46, 860-866, 1989.

Fleming, E. L., S. Chandra, M. R. Schoeberl, and J. J. Barnett,
Monthly mean global climatology of temperature, wind, geopotential
height, and pressure for 0 - 120 km, NASA Tech. Mem., NASA 100697,
1988.

Fleming, E. L., S. Chandra, J. J. Barnett, and M. Corney, Zonal mean
temperature, pressure, zonal wind and geopotential height as functions
of latitude, Adv. Space Res., 10(12), 11-59, 1990.

Franke, S. J., and D. Thorsen, Mean winds and tides in the upper
middle atmosphere at Urbana (40N,88W) during 1991-1992, submitted to
J. Geophys. Res, 1993.

Fritts, D. C., and J. R. Isler, First observations of mesospheric
dynamics with a partial reflection radar in Hawaii (22N, 160W),
Geophys. Res. Lett., 19, 409-412, 1992.

Groves, G. V., Wind models from 60 to 130 km altitude for different
months and latitudes, J. Brit. Interplanet. Soc., 22, 285-307,
1969.

Groves, G. V., Atmospheric structure and its variations in the region
from 25 to 120 km, in CIRA 1972, pp. 33-224, Akademie, Berlin,
1972a.

Groves, G. V., Annual and semi-annual zonal wind components and
corresponding temperature and density variations, 60-130 km,

Planet. Space Sci., 20, 2099-2112, 1972b.

Harper, R. M., Tidal winds in the 100- to 200-km region at Arecibo, J. Geophys. Res., 82, 3243-3250, 1977.

Harper, R. M., R. H. Wand, C. J. Zamlutti, and D. T. Farley, E region ion drifts and winds from incoherent scatter measurements at Arecibo, J. Geophys. Res., 81, 25-37, 1976.

Hedin, A. E., A revised thermospheric model based on mass spectrometer and incoherent scatter data: MSIS-83, J. Geophys. Res., 88, 10,170-10,188, 1983.

Hedin, A. E., MSIS-86 thermospheric model, J. Geophys. Res., 92, 4649-4662, 1987.

Hedin, A. E., The atmospheric model in the region 90 to 2000 km, Adv. Space Res., 8(5), 9-25, 1988.

Hedin, A. E., Extension of the MSIS thermosphere model into the middle and lower atmosphere, J. Geophys. Res., 96, 1159-1172, 1991.

Hedin, A. E., N. W. Spencer, and T. L. Killeen, Empirical global model of upper thermosphere winds based on Atmosphere and Dynamics Explorer satellite data, J. Geophys. Res., 93, 9959-9989, 1988.

Hedin, A. E., M. A. Biondi, R. G. Burnside, G. Hernandez, R. M. Johnson, T. L. Killeen, C. Mazaudier, J. W. Meriwether, J. E. Salah, R. J. Sica, R. W. Smith, N. W. Spencer, V. B. Wickwar, and T. S. Virdi, Revised global model of thermosphere winds using satellite and ground-based observations, J. Geophys. Res., 96, 7657-7688, 1991.

Johnson, R. M., V. B. Wickwar, R. G. Roble, and J. G. Luhmann, Lower-thermosphere winds at high latitude: Chatanika radar observations, Annales Geophys., 5A, 383-404, 1987.

Koshelkov, Y. P., Proposal for a reference model of the middle atmosphere of the southern hemisphere, Adv. Space Res., 3(1), 3-16, 1983.

Koshellkov, U. P., Southern hemisphere reference middle atmosphere, Adv. Space Res., 10(12), 245-263, 1990.

MacLeod, R., and R. A. Vincent, Observations of winds in the Antarctic summer mesosphere using the spaced antenna technique, J. Atmos. Terr. Phys., 47, 567-574, 1985.

Manson, A. H., and C. E. Meek, Climatologies of mean winds and tides observed by medium frequency radars at Tromso (70N) and Saskatoon (52N) during 1987-1989, Can. J. Phys., 69, 1991.

Manson, A. H., C. E. Meek, J. B. Gregory, Winds and waves (10 min - 30 days) in the mesosphere and lower thermosphere at Saskatoon (52N, 107W, 1-4.3) during the year, October 1979 to July 1980, J. Geophys. Res., 86, 9615, 1981.

Manson, A. H., C. E. Meek, M. Massebeuf, J. L. Fellous, W. G. Elford, R. A. Vincent, R. L. Craig, R. G. Roper, S. Avery, B. B. Balsley, G. J. Fraser, M. J. Smith, R. R. Clark, S. Kato, T. Tsuda, and E. Ebel, Mean winds of the upper middle atmosphere (60-110 km): A global distribution from radar systems (M.F., Meteor, VHF), Handbook for MAP, 16, Eds. K. Labitzke, J. J. Barnett, and B. Edwards, Urbana, IL, 239-268, 1985.

Manson, A. H., C. E. Meek, M. Massebeuf, J. L. Fellous, W. G. Elford, R. A. Vincent, R. L. Craig, A. Phillips, R. G. Roper, G. J. Fraser, M. J. Smith, S. Avery, B. B. Balsley, R. R. Clark, S. Kato, T. Tsuda, R. Schminder, and D. Kuerschner, Description and presentation of

reference atmosphere radar winds (80-110 km), Adv. Space Res., 10(12), 267-315, 1990.

Manson, A. H., C. E. Meek, E. Fleming, S. Chandra, R. A. Vincent, A. Phillips, S. K. Avery, G. J. Fraser, M. J. Smith, J. L. Fellous, and M. Massebeuf, Comparisons between satellite-derived gradient winds and radar-derived winds from the CIRA-86, J. Atmos. Sci., 48, 411-428, 1991

Massebeuf, M., R. Bernard, J. L. Fellous, and M. Glass, The mean zonal circulation in the meteor zone above Garchy (France) and Kiruna (Sweden), J. Atmos. Terr. Phys., 41, 647-655, 1979.

Massebeuf, M, R. Bernard, J. L. Fellous, and M. Glass, Simultaneous meteor radar observations at Monpazier (France, 44N) and Punta Borinquen (Puerto-Rico, 18N). II - Mean zonal wind and long period waves, J. Atmos. Terr. Phys., 43, 525-533, 1981.

Miyahara, S., Y. I. Portnyagin, J. M. Forbes, and T. V. Solovjeva, Mean zonal acceleration and heating of the 70- to 100-km region, J. Geophys. Res., 96, 1225-1238, 1991.

Morse, P. M., and H. Feshbach, Methods of Theoretical Physics, McGraw-Hill, New York, 1953.

Oort, A. H., Global atmospheric circulation statistics, 1958-1983, NOAA Professional Paper 14, National Oceanic and Atmospheric Admin., p. 180, U.S. Government Printing Office, Washington, DC 20402, 1983.

Salby, M. L., and R. G. Roper, Long-period oscillations in the meteor region, J. Atmos. Sci., 37, 237-244, 1980.

Schmidlin, F. J., Rocket techniques used to measure the neutral atmosphere, Handbook for Map, 19, Ed. R. A. Goldberg, Urbana, IL, 1-28, 1986.

Schmidlin, F. J., M. Carlson, D. Rees, D. Offermann, C. R. Philbrick, H. U. Widdel, Wind structure and variability in the middle atmosphere during the November 1980 Energy Budget Campaign, J. Atmos. Terr. Phys., 47, 183-193, 1985.

Theon, J. S., W. S. Smith, J. F. Casey, and B. R. Kirkwood, The mean observed meteorological structure and circulation of the stratosphere and mesosphere, NASA Tech. Rep., NASA TR R-375, 1972.

Tsuda, T., T. Nakamura, and S. Kato, Mean winds observed by the Kyoto meteor radar in 1983-1985, J. Atmos. Terr. Phys., 49, 461-466, 1987.

Vincent, R. A., and T. J. Stubs, A study of motions in the winter mesosphere using the partial reflection drift technique, Planet. Space Sci., 25, 441-445, 1977.

Vincent, R. A., and S. M. Ball, Mesospheric winds at low- and mid-latitudes in the southern hemisphere, J. Geophys. Res., 86, 9159-9169, 1981.

Vincent, R. A., and D. Lesicar, Dynamics of the equatorial mesosphere: First results with a new generation partial reflection radar, Geophys. Res. Lett., 18, 825-828, 1991.

Virdi, T. S., and P. J. S. Williams, Observations of tidal modes in the lower thermosphere using EISCAT, Adv. Space Res., 9(5), 83-86, 1989.

Wand, R. H., Seasonal variations of lower thermospheric winds from the Millstone Hill incoherent scatter radar, J. Geophys. Res., 88, 9227-9241, 1983.

Tables

TABLE 1. Wind Data Summary

Station	Wind Component	Latitude	Longitude	Years	Altitude	Plot Sym	Reference
Incoherent Scatter							
EISCAT							
Chatanika	M&Z	69.6N	19.2E	85-87	100-120	B	[Virdi and Williams, 1989][3]
St. Santin	M&Z	85.1N	147.4W	76-82	90-130	1	[Johnson et al., 1987][3]
Millstone	M	44.6N	2.2E	73-85	90-170	5	[Bernard, 1974][3]
Arecibo	M&Z	42.5N	71.5W	76-77	105-135	3	[Wand, 1983]
Arecibo	M	18.3N	66.6W	74-77	100-170	6	[Harper et al., 1976][3]
	Z			74-75	100-130	6	[Harper, 1977][1]
MF radar, monthly averages							
Tromso	M&Z	70.N	20.E	87-89	87-112	M	[Manson & Meek, 1991][2]
Saskatoon	M&Z	52.N	107.W	79-82	61-111	F	[Manson et al., 1981; Magson et al., 1990][1]
Urbana	M&Z	40.N	88.W	91-92	86-111	T	[Franke & Thorsen, 1993][3]
Townsville	M&Z	20.S	147.E	78-80	78-100	K	[Vincent and Ball, 1981; Manson et al., 1990][1]
Adelaid	M&Z	35.S	138.E	78-86	78-100	J	[Vincent & Stubbs, 1977; Manson et al., 1990][1]
Christchurch	Z	44.S	173.E	78-86	65-102	I	[Manson et al., 1990][1]
Mawson	M&Z	67.6S	62.9E	84-86	76-100	O	[MacLeod and Vincent, 1985; Manson et al., 1981][1]
Meteor radar, monthly averages							
Poker Flat	M&Z	65.N	147.W	83-84	75-106	W	[Avery et al., 1983; Mangon et al., 1990][1]
Garchy	Z	47.N	3.E	76-76	78-102	+	[Massebeuf et al., 1979][2]
Monpazier	Z	44.N	1.E	79-80	76-104	L	[Massebeuf et al., 1981; Manson et al., 1990][1]
Durham	M&Z	43.N	71.W	78-84	77-110	V	[Clark, 1983; Manson et al., 1990][1]
Kyoto	M&Z	35.N	136.E	83-84	82-106	G	[Tsuda et al., 1987; Manson et al., 1985][1]
Atlanta	M&Z	34.N	84.W	74-77	80-100	H	[Salby & Roper, 1980; Manson et al., 1990][1]
Punta Borinquen	Z	18.N	67.W	77-78	80-100	R	[Massebeuf et al., 1981; Manson et al., 1990][1]
Christmas Is.	M&Z	2.N	158.W	88-91	80-100	S	[Avery et al., 1990][3]
Rocket data							
Grenade	M&Z			60-72	30-100	N	[Theon et al., 1972][1]
Falling sphere	M&Z			69-91	25-100	P	[Schmidlin, 1985][3]
Datasonde	M&Z			69-91	20-75	C	[Schmidlin, 1986][3]
Model tabulations							
CIRA-86 gradient wind							
wave 1	Z				0-120	B	[Fleming et al., 1990][1]
MSISE-90 gradient wind	M&Z				15-82	B	[Fleming et al., 1988][3]
wave 1	Z				0-120	A	[Hedin, 1991]
CIRA-72	M&Z				0-120	A	[Hedin, 1991]
Groves-69,	Z				25-130	9	[Groves, 1972a][1]
CAO southern hemisphere	M				60-130	E	[Groves, 1969][1]
	Z				20-80	7	[Koshelkov, 1983][1]

Wind component is M, Z, or M&Z for meridional, zonal, or both.
[1] Data from published tabulations or plots.
[2] Data from MLT radar database
[3] Data from other original databases

14

Table 2a.   Maximum B Field Spherical Harmonic Order (n)

Term	m	100	90	82	75	67	60	52	45	37	30	22	15	7	0	grad 100
Symmetrical																
Time Indep.	0	4	4	4	4	4	2	2	2	–	–	–	–	–	–	2
Semiannual	0	–	2	2	2	2	2	2	–	–	–	–	–	–	–	–
Asymmetrical																
Annual	0	3	1	1	1	1	–	–	–	–	–	–	–	–	–	1

Table 2b.   Maximum C Field Spherical Harmonic Order (n)

Term	m	100	90	82	75	67	60	52	45	37	30	22	15	7	0	grad 100
Symmetrical																
Time Indep.	0	5	5	5	5	5	5	5	5	5	5	5	5	5	5	5
Annual	0	–	1	1	1	1	1	1	1	1	1	1	1	–	–	–
Semiannual	0	3	5	5	5	5	5	5	5	5	5	3	3	–	–	3
Longitude	1	–	–	6	6	6	6	6	6	6	6	6	6	–	–	–
Longitude–annual	1	–	–	6	6	6	6	6	6	6	6	6	6	–	–	–
Longitude–semiannual	1	–	–	6	6	6	6	6	6	6	6	6	6	–	–	–
Asymmetrical																
Time Indep.	0	–	–	–	2	2	2	2	2	2	2	2	2	2	2	–
Annual	0	4	6	6	6	6	6	6	6	6	6	6	6	6	6	2
Semiannual	0	–	4	4	4	4	4	4	4	4	4	–	–	–	–	–
Longitude	1	–	–	5	5	5	5	5	5	5	5	5	5	–	–	–
Longitude–annual	1	–	–	5	5	5	5	5	5	5	5	5	5	–	–	–
Longitude–semiannual	1	–	–	5	5	5	5	5	5	5	5	5	5	–	–	–

15

TABLE 3a. RMS Zonal Wind Differences from HWM92

Data Set	15-60 km		60-90 km		90-120 km	
	rms	pts	rms	pts	rms	pts
MSIS Gradient	8	1428	12	1020	15	1020
CIRA-86	8	2521	13	1973	21	1825
Datasonde	7	4949	13	1694		
Falling Sphere	10	1550	13	1336	32	135
Grenade	16	771	18	973	55	146
CIRA-72	16	1655	18	1225	22	744
CAO-83	10	768	12	480		
MF radar			6	1029	6	896
Meteor radar			11	776	8	866
IS radar					47	1329

TABLE 3b. RMS Meridional Wind Differences from HWM92

Data Set	15-60 km		60-90 km		90-120 km	
	rms	pts	rms	pts	rms	pts
Datasonde	4	4949	9	1684		
Falling Sphere	4	1551	9	1368	27	138
Grenade	10	772	16	973	50	147
GROVES-69	5	204	8	1260	12	972
MF radar			5	1028	5	896
Meteor radar			9	394	6	487
IS radar					34	2064

Here rms is root mean square difference between data and model, pts is number of sample points, MF is medium frequency, and IS is incoherent scatter.

Figures

SDL AVERAGE ZONAL WIND

SDL AVERAGE MERIDIONAL WIND
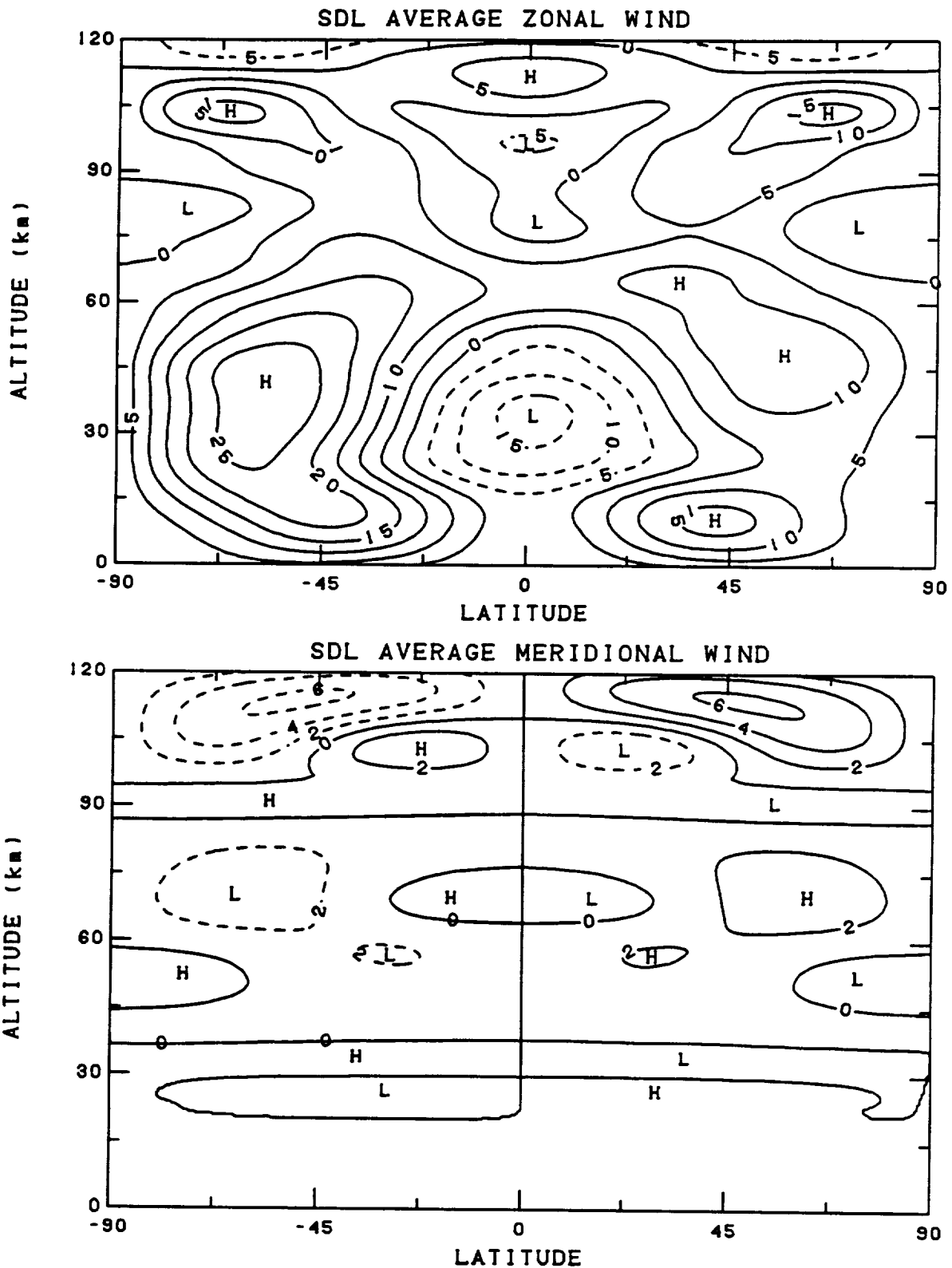
Fig. 1. Contour plots in altitude versus latitude of the seasonal, diurnal, and longitudinal (SDL) average zonal wind (upper panel) and meridional wind (lower panel). Positive is eastward and northward (negative dashed). H and L indicate relative highs and lows.

18
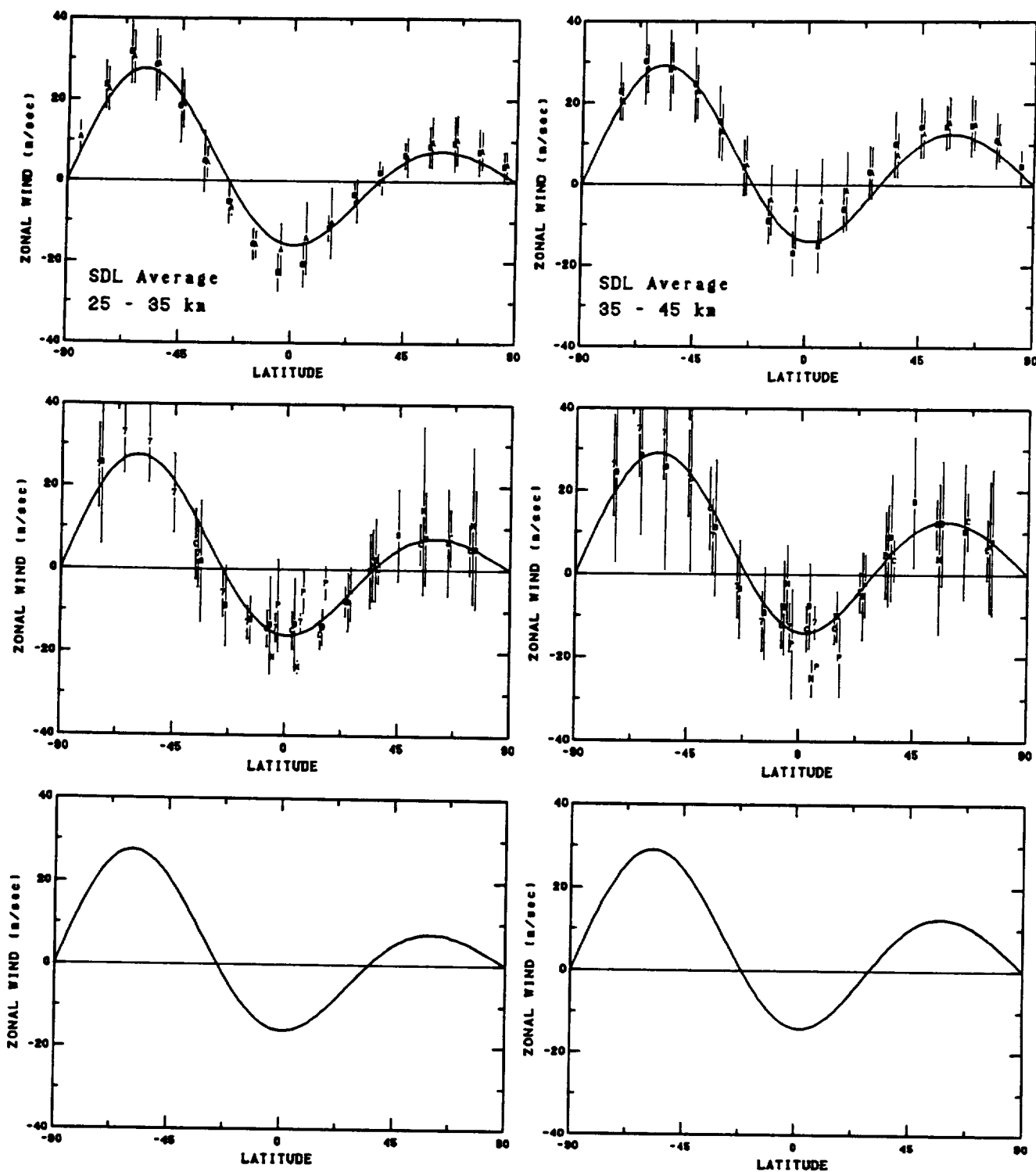
Fig. 2a. SDL average zonal wind versus latitude for 25 to 35 and 35 to 45 km. The HWM93 wind (solid line) shown for mid-range conditions. Plot symbols indicate data source as given in Table 1. Top row of plots contain gradient winds, middle row rocket data, and bottom row MF/Meteor radar data. See text for further description.
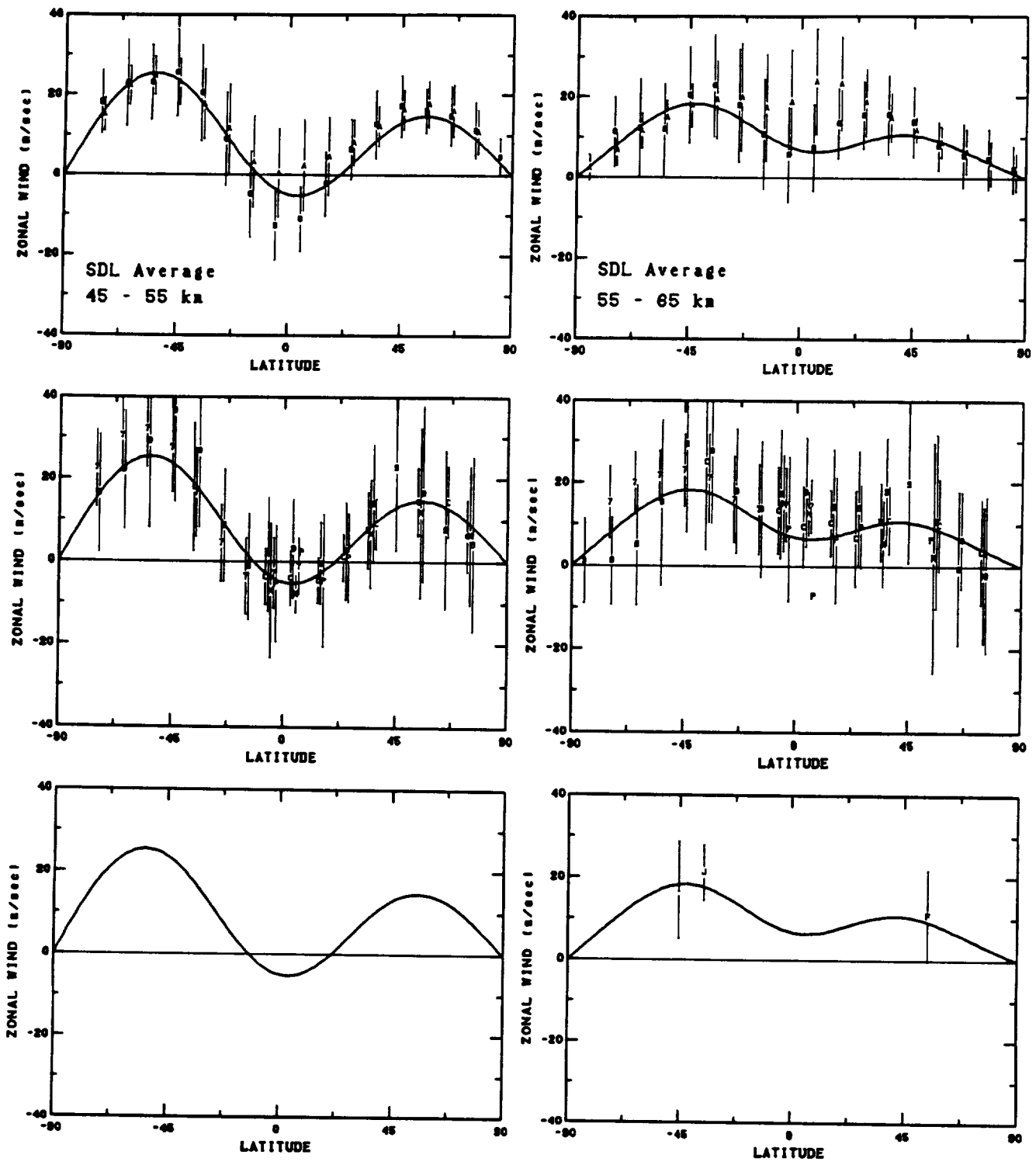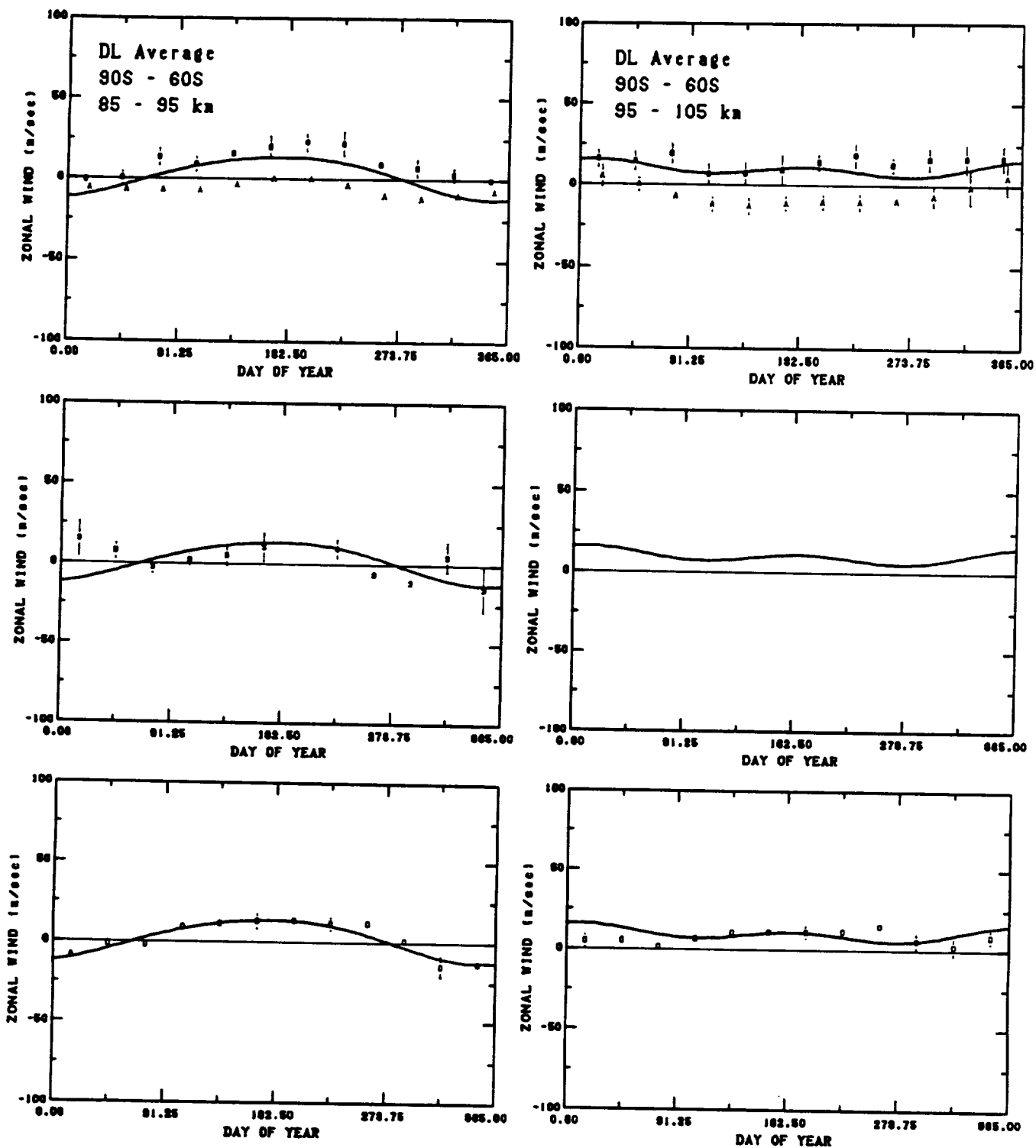
Fig. 2b. SDL average zonal wind versus latitude for 45 to 55 and 55 to 65 km. The HWM93 wind (solid line) shown for mid-range conditions. Plot symbols indicate data source as given in Table 1. Top row of plots contain gradient winds, middle row rocket data, and bottom row MF/Meteor radar data. See text for further description.
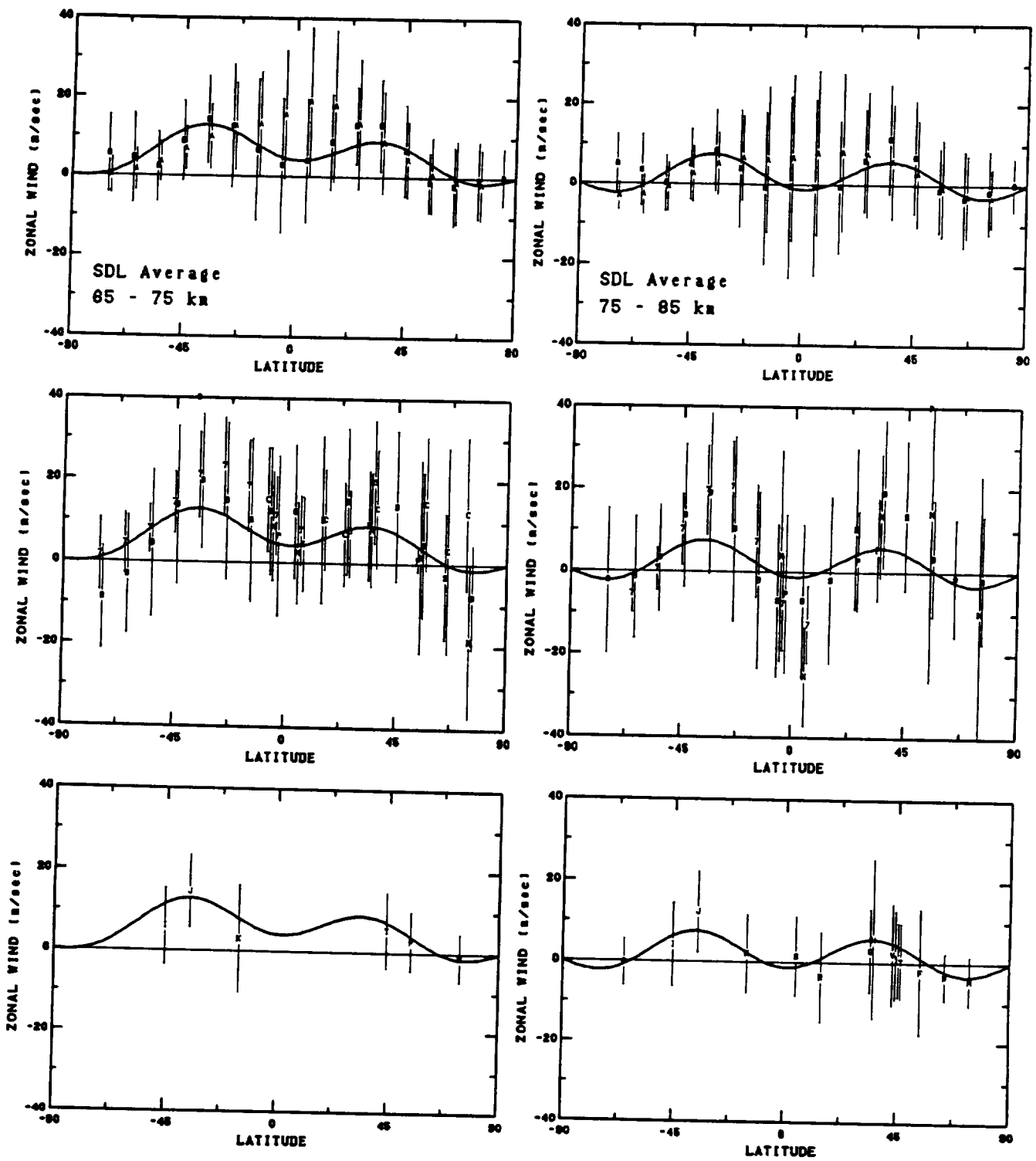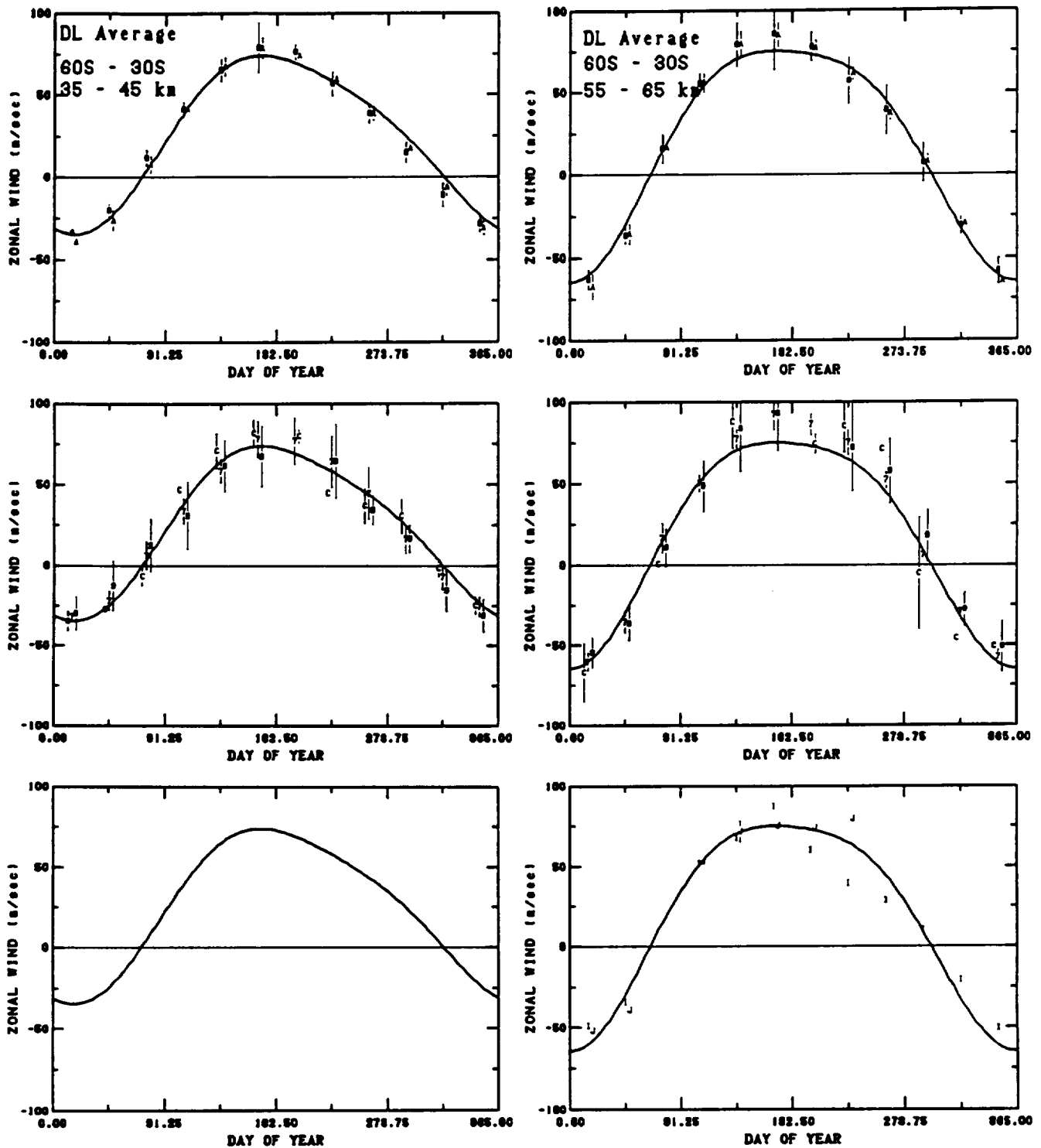
Fig. 2c. SDL average zonal wind versus latitude for 65 to 75 and 75 to 85 km. The HWM93 wind (solid line) shown for mid-range conditions. Plot symbols indicate data source as given in Table 1. Top row of plots contain gradient winds, middle row rocket data, and bottom row MF/Meteor radar data. See text for further description.
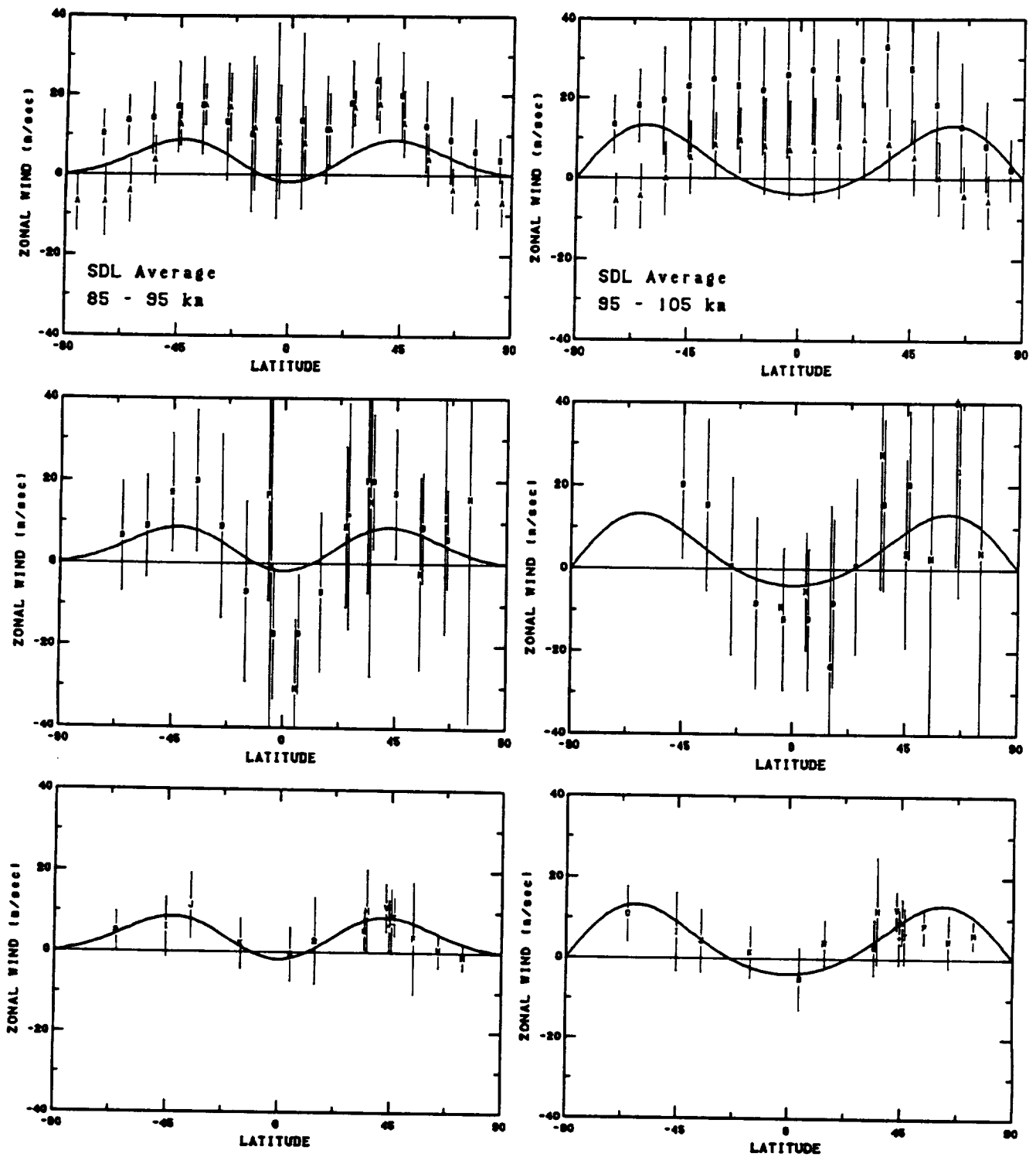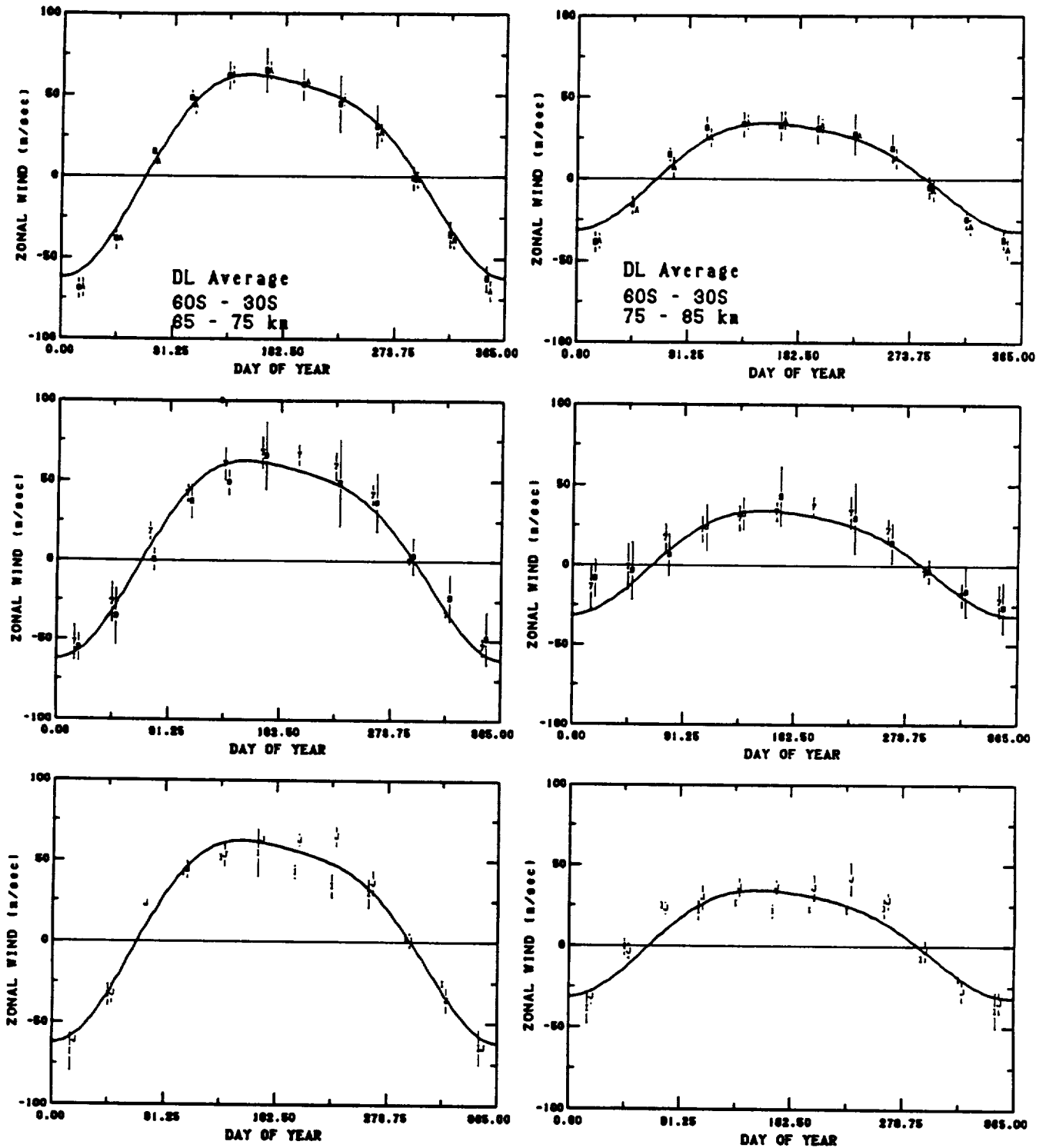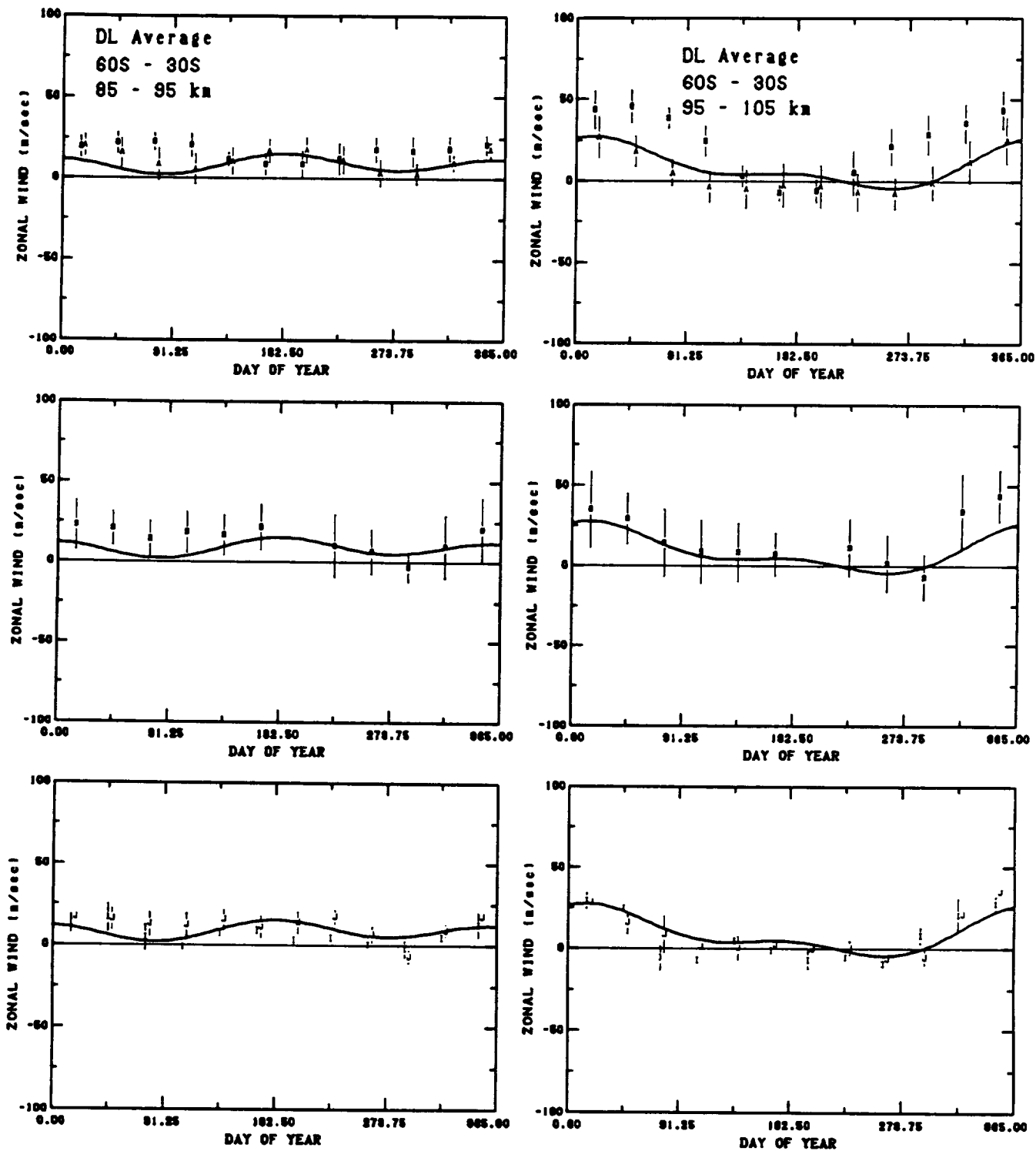
Fig. 2d. SDL average zonal wind versus latitude for 85 to 95 and 95 to 105 km. The HWM93 wind (solid line) shown for mid-range conditions. Plot symbols indicate data source as given in Table 1. Top row of plots contain gradient winds, middle row rocket and IS data, and bottom row MF/Meteor radar data. See text for further description.
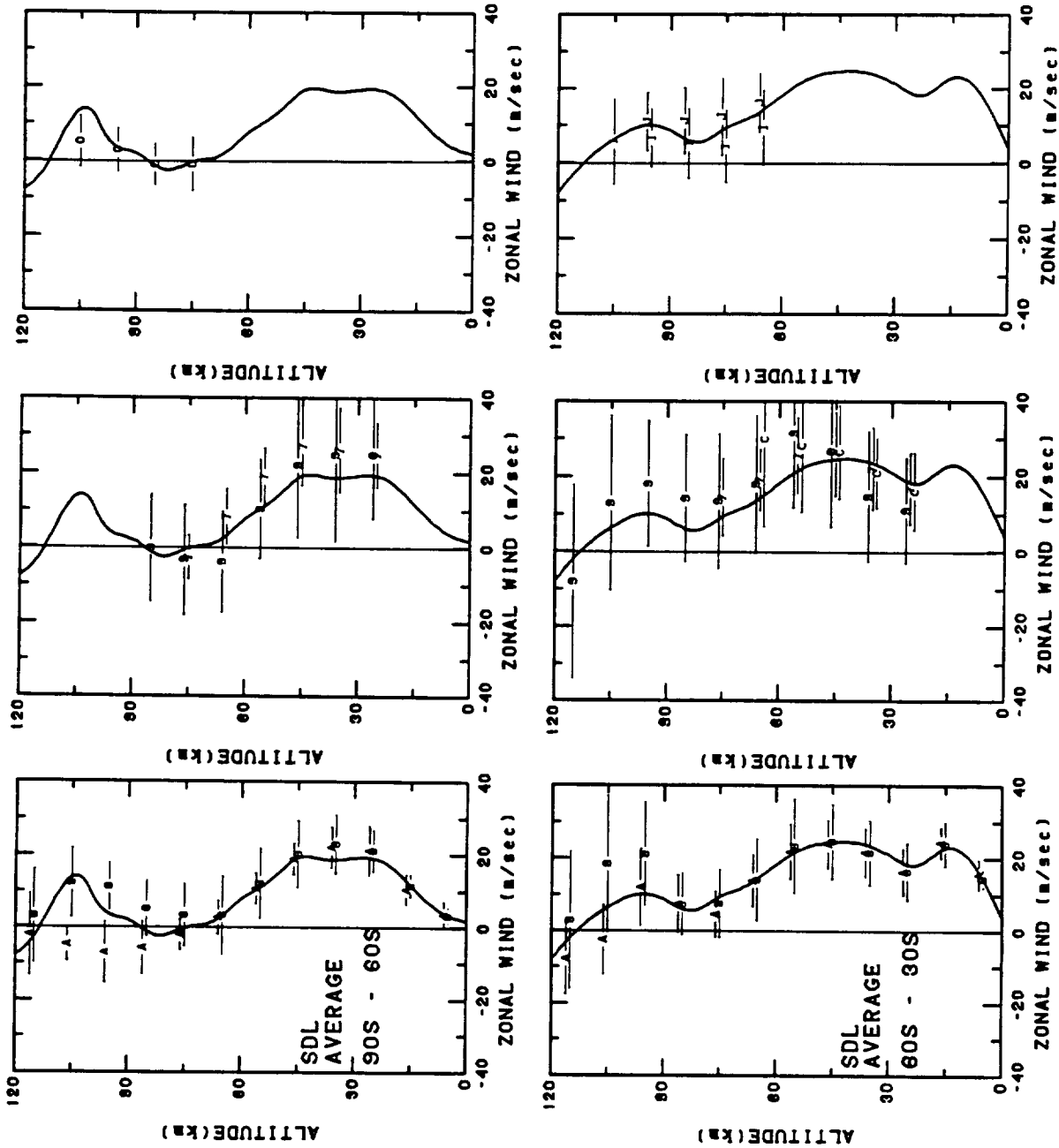
Fig. 3a. SDL average zonal wind versus altitude for southern high and middle latitudes. The HWM93 wind (solid line) shown for mid-range conditions. Plot symbols indicate data source as given in Table 1. Left column of plots contain gradient winds, middle column rocket data, and right column MF/Meteor radar data.
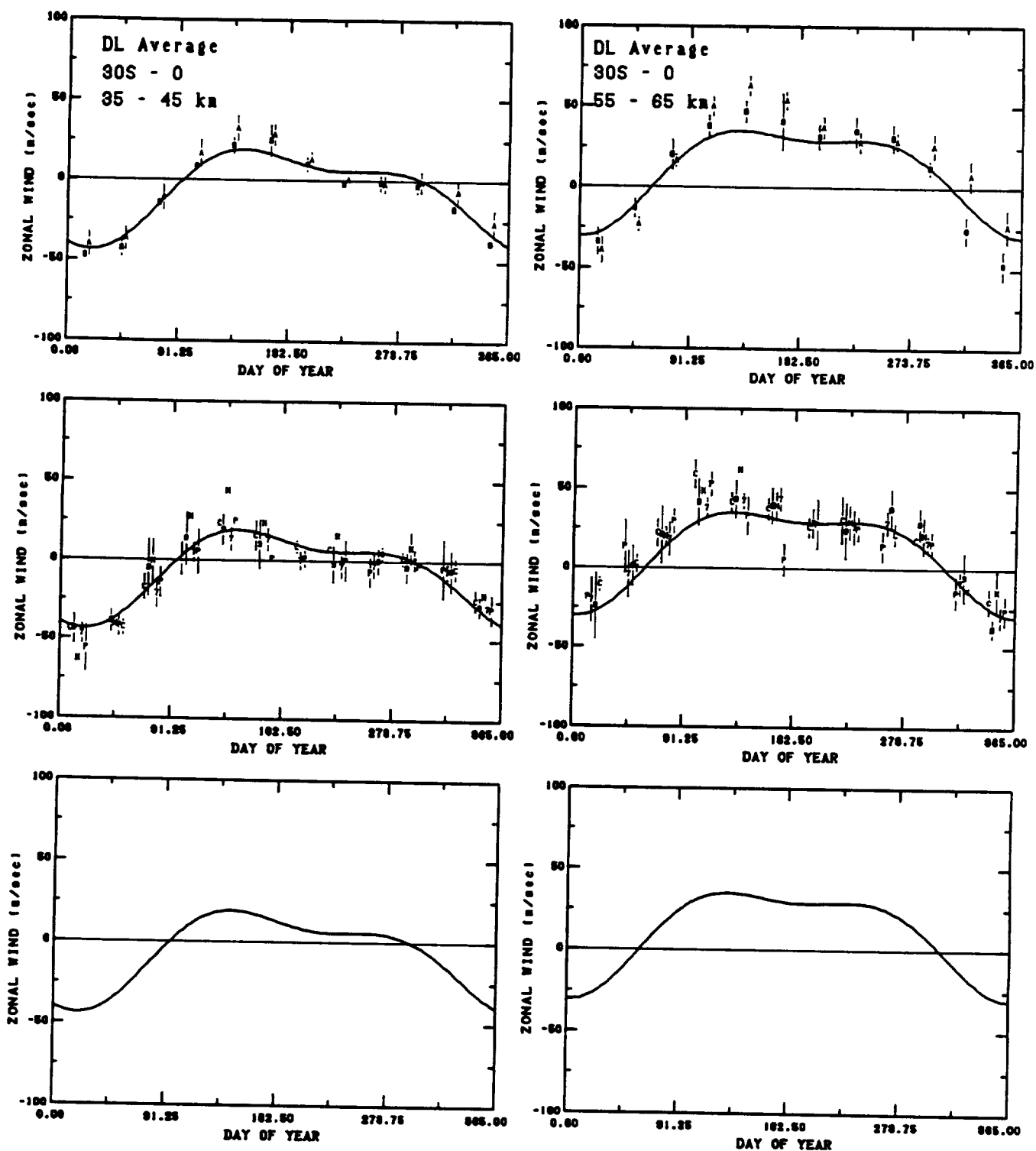
23
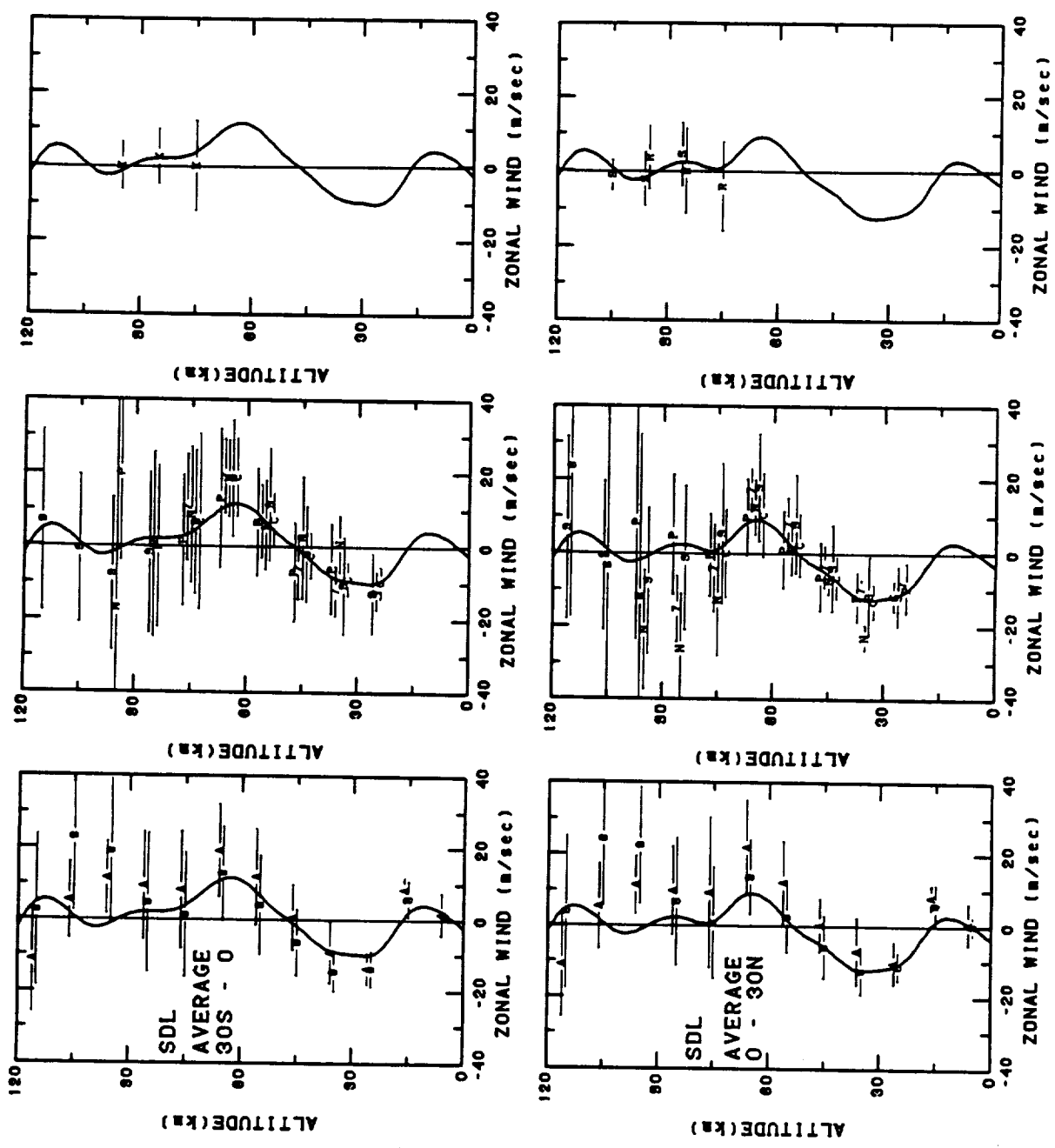
Fig. 3b. SDL average zonal wind versus altitude for equatorial latitudes. The HWM93 wind (solid line) shown for mid-range conditions. Plot symbols indicate data source as given in Table 1. Left column of plots contain gradient winds, middle column rocket and IS data, and right column MF/Meteor radar data.

Fig. 3c. SDL average zonal wind versus altitude for northern high and middle latitudes. The HWM93 wind (solid line) shown for mid-range conditions. Plot symbols indicate data source as given in Table 1. Left column of plots contain gradient winds, middle column rocket and IS data, and right column MF/Meteor radar data.

25
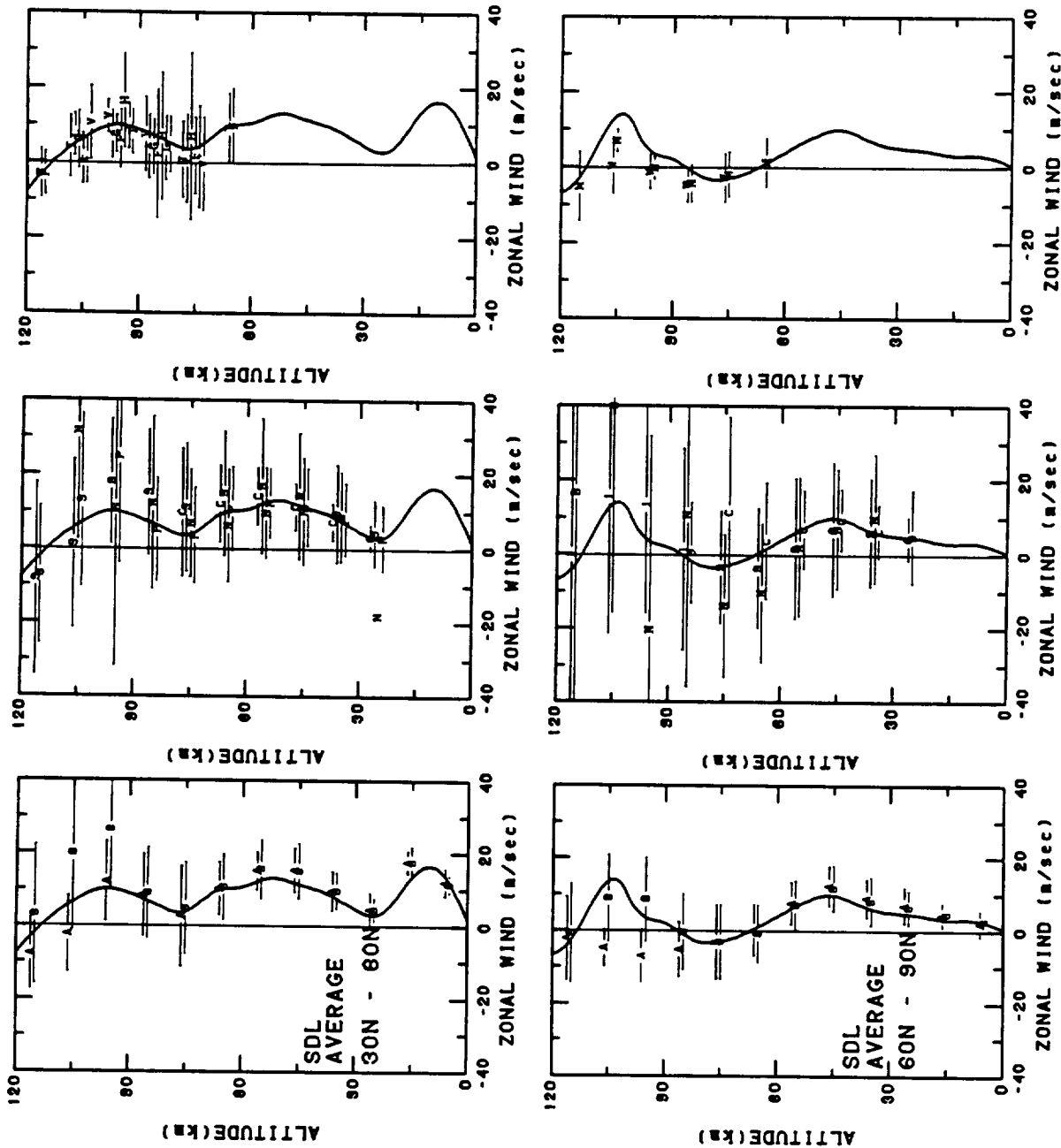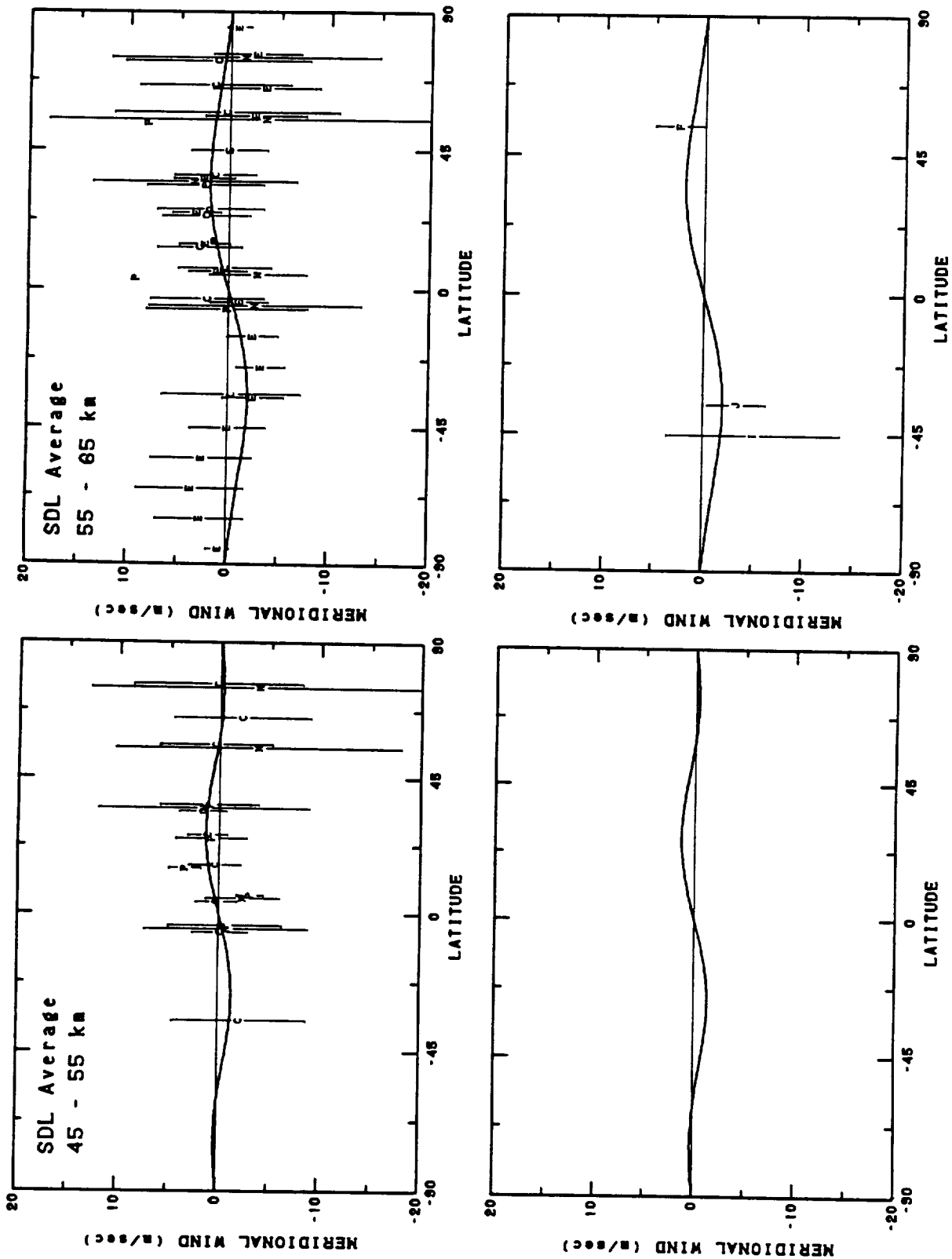
Fig. 4a. SDL average meridional wind versus latitude for 45 to 55 and 55 to 65 km. The HWM93 wind (solid line) shown for mid-range conditions. Plot symbols indicate data source as given in Table 1. Top row of plots contains rocket data and bottom row MF/Meteor radar data.

26

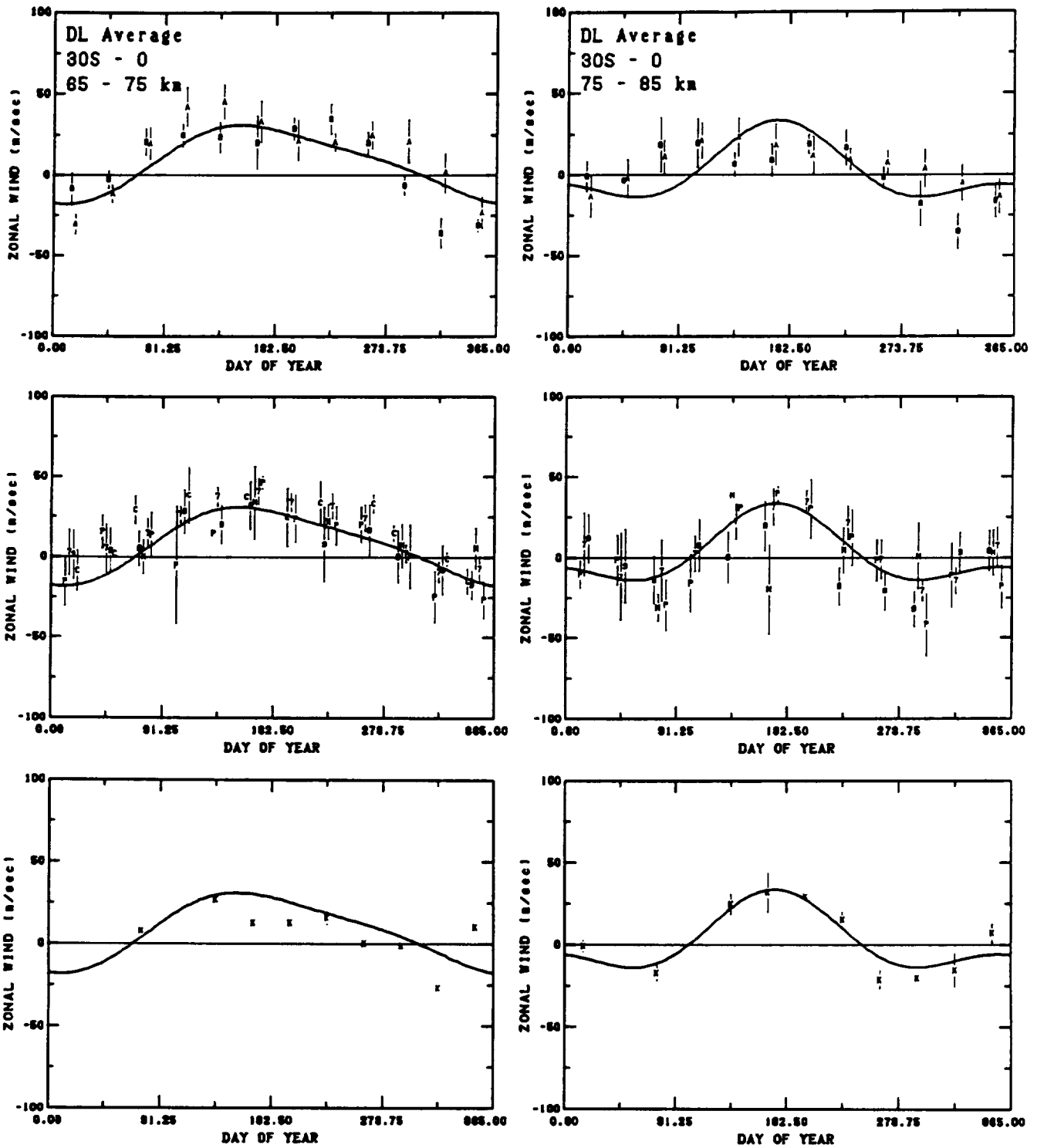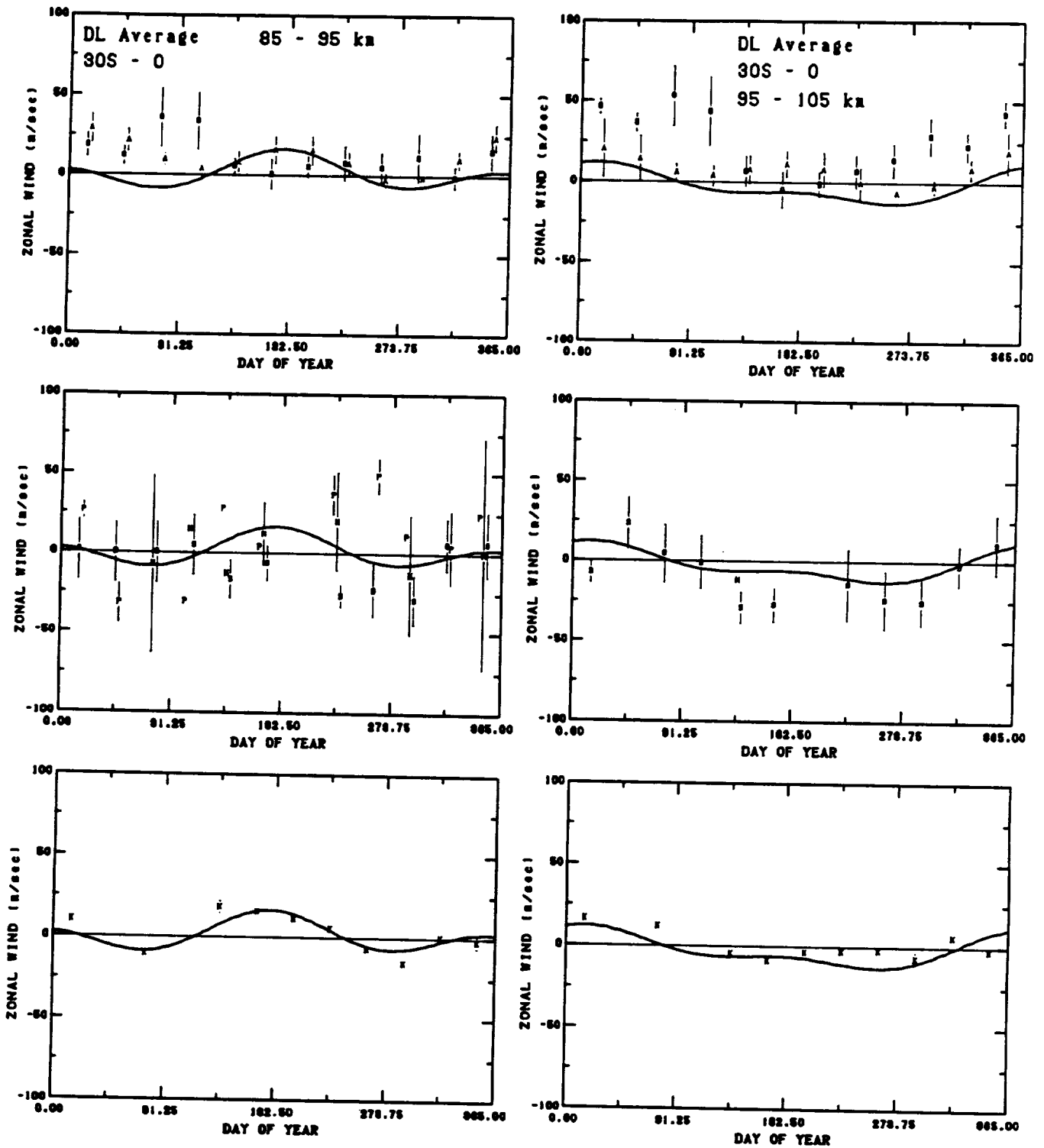Fig. 4b. SDL average meridional wind versus latitude for 65 to 75 and 75 to 85 km. The HWM93 wind (solid line) shown for mid-range conditions. Plot symbols indicate data source as given in Table 1. Top row of plots contains rocket data and bottom row MF/Meteor radar data.

27
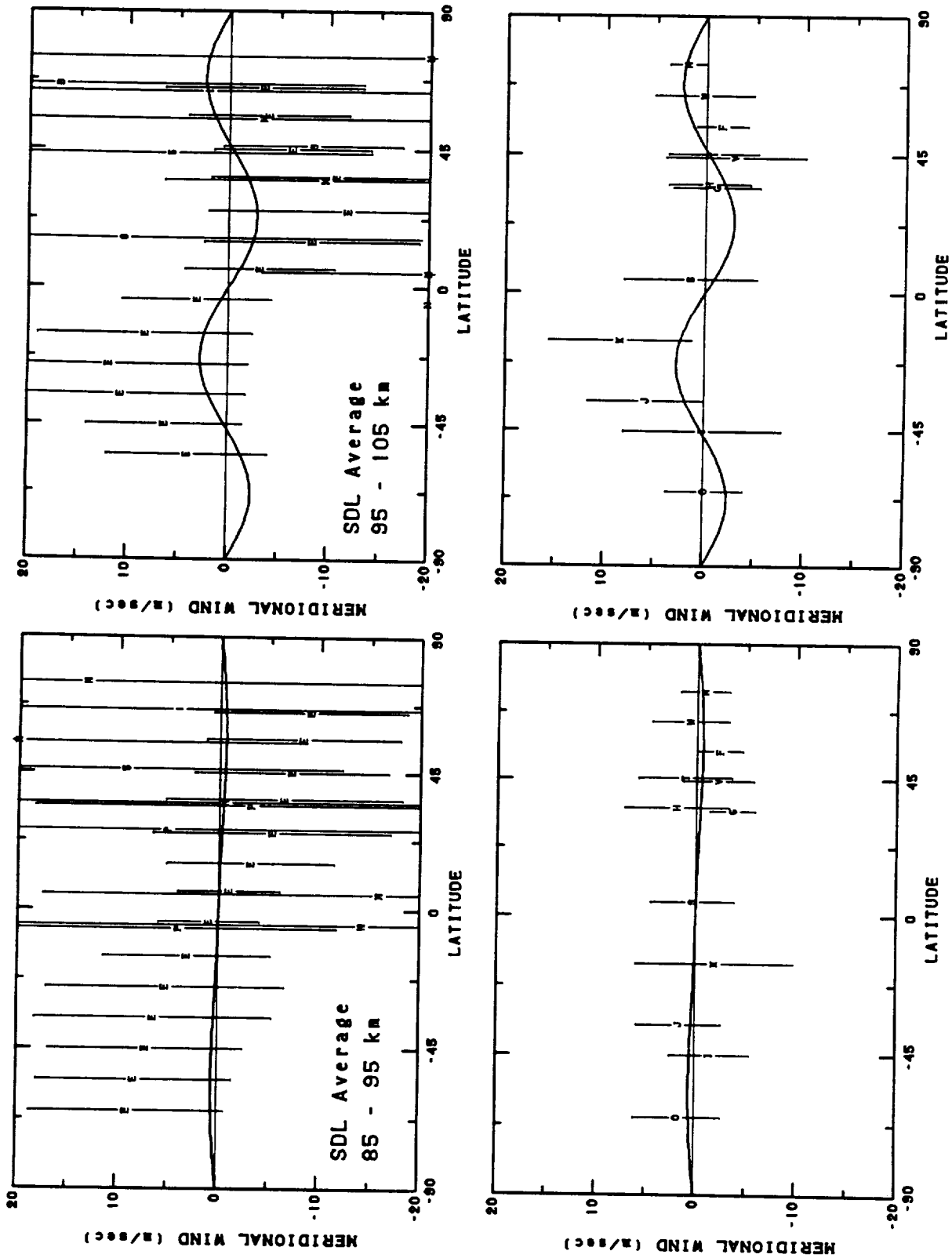
Fig. 4c. SDL average meridional wind versus latitude for 85 to 95 and 95 to 105 km. The HWM93 wind (solid line) shown for mid-range conditions. Plot symbols indicate data source as given in Table 1. Top row of plots contains rocket and IS data and bottom row MF/Meteor radar data.
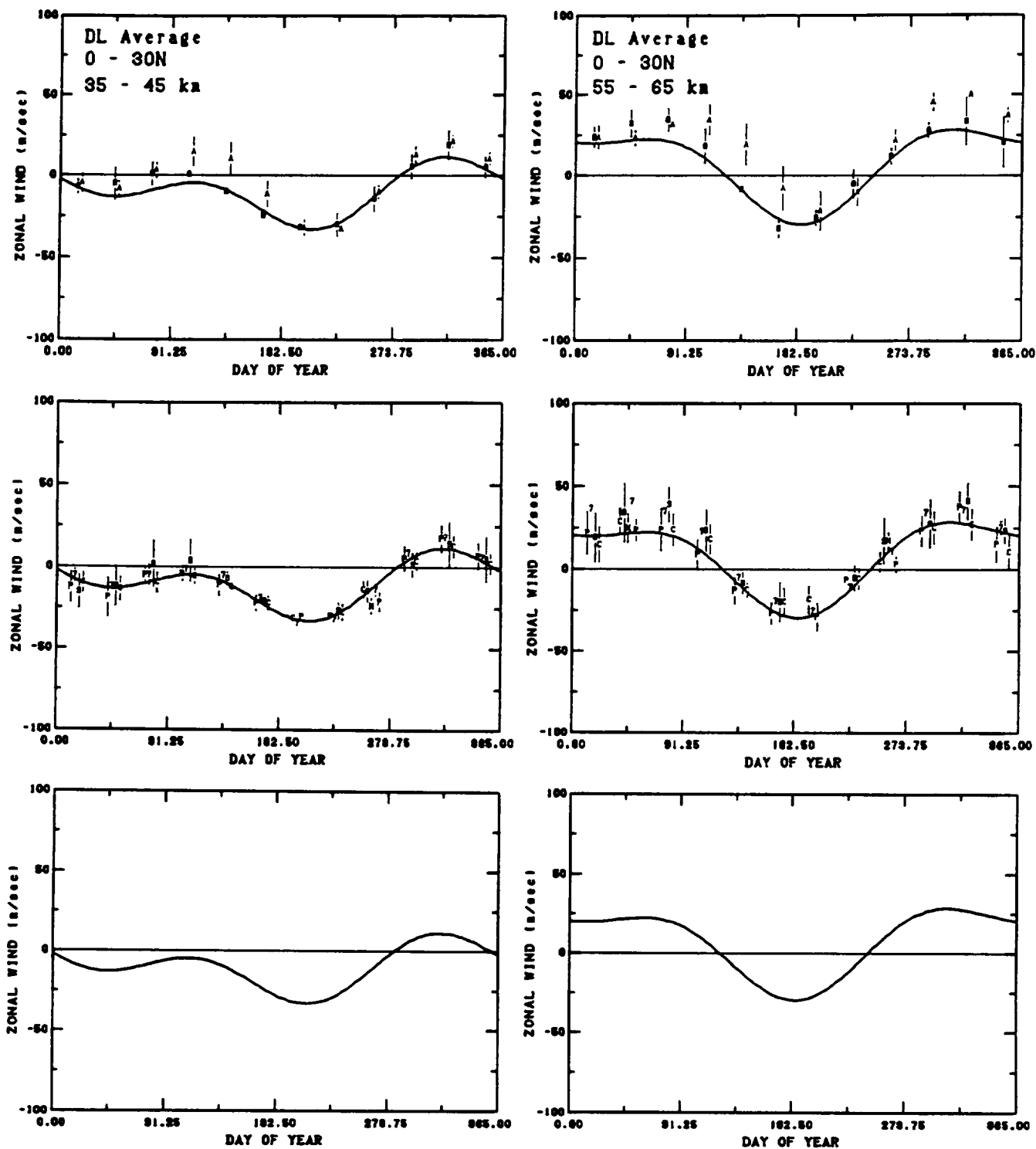
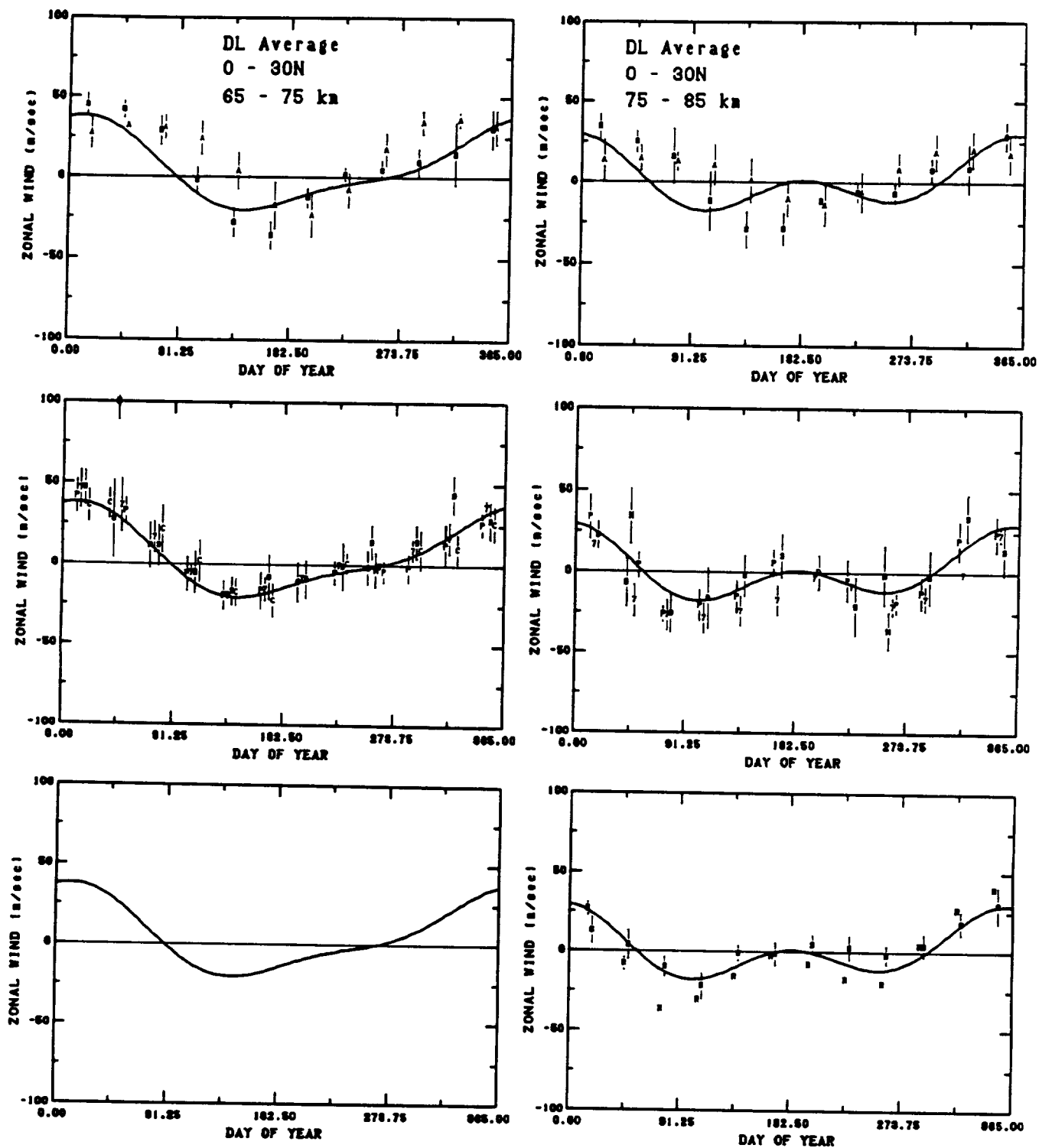Fig. 5a. SDL average meridional wind versus altitude for southern high and middle latitudes. The HWM93 wind (solid line) shown for mid-range conditions. Plot symbols indicate data source as given in Table 1. Left column of plots contains rocket data and right column MF/Meteor radar data.

Fig. 5b. SDL average meridional wind versus altitude for equatorial latitudes. The HWM93 wind (solid line) shown for mid-range conditions. Plot symbols indicate data source as given in Table 1. Left column of plots contains rocket and IS data data and right column MF/Meteor radar data.
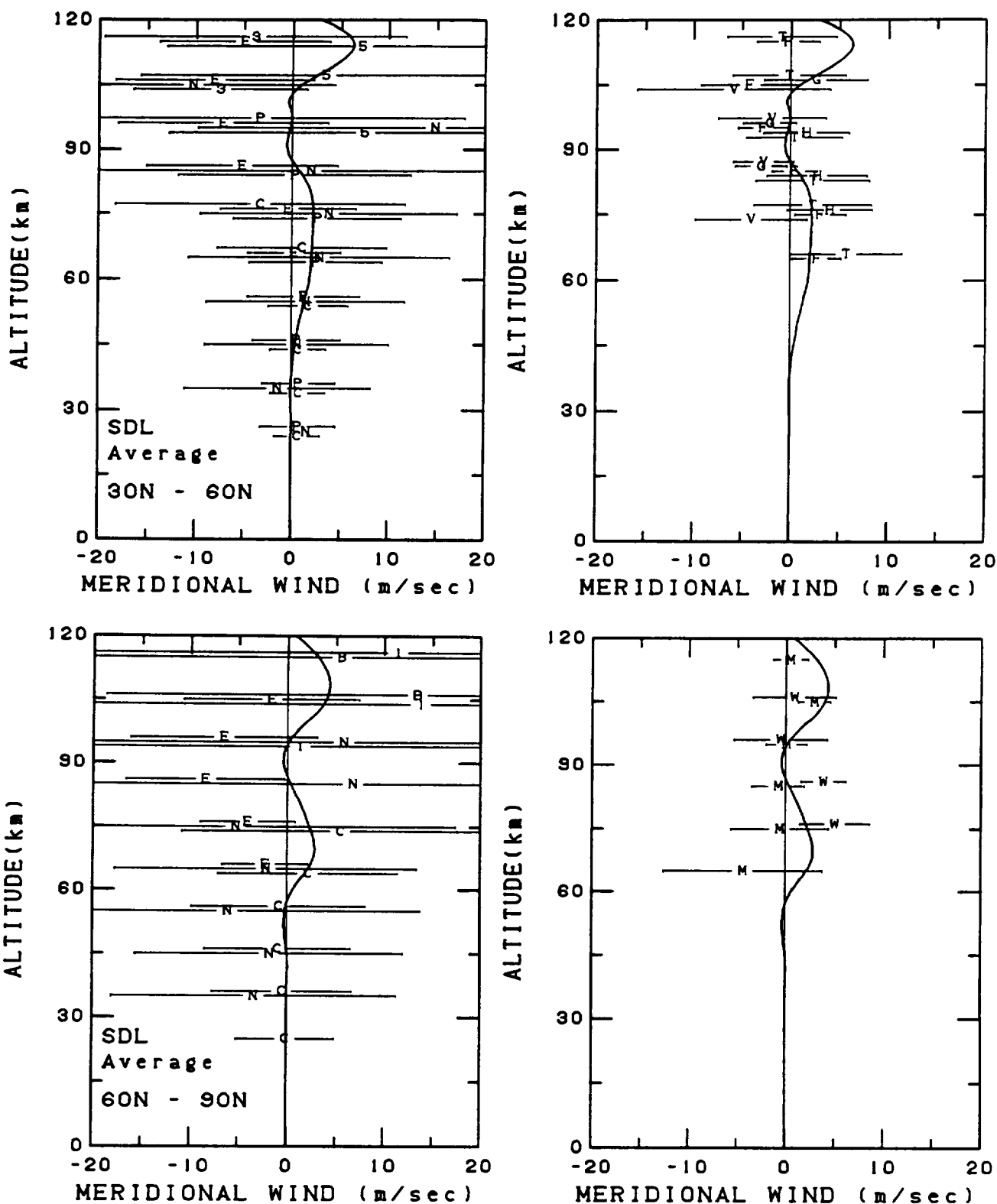
Fig. 5c. SDL average meridional wind versus altitude for northern high and middle latitudes. The HWM93 wind (solid line) shown for mid-range conditions. Plot symbols indicate data source as given in Table 1. Left column of plots contains rocket and IS data and right column MF/Meteor radar data.
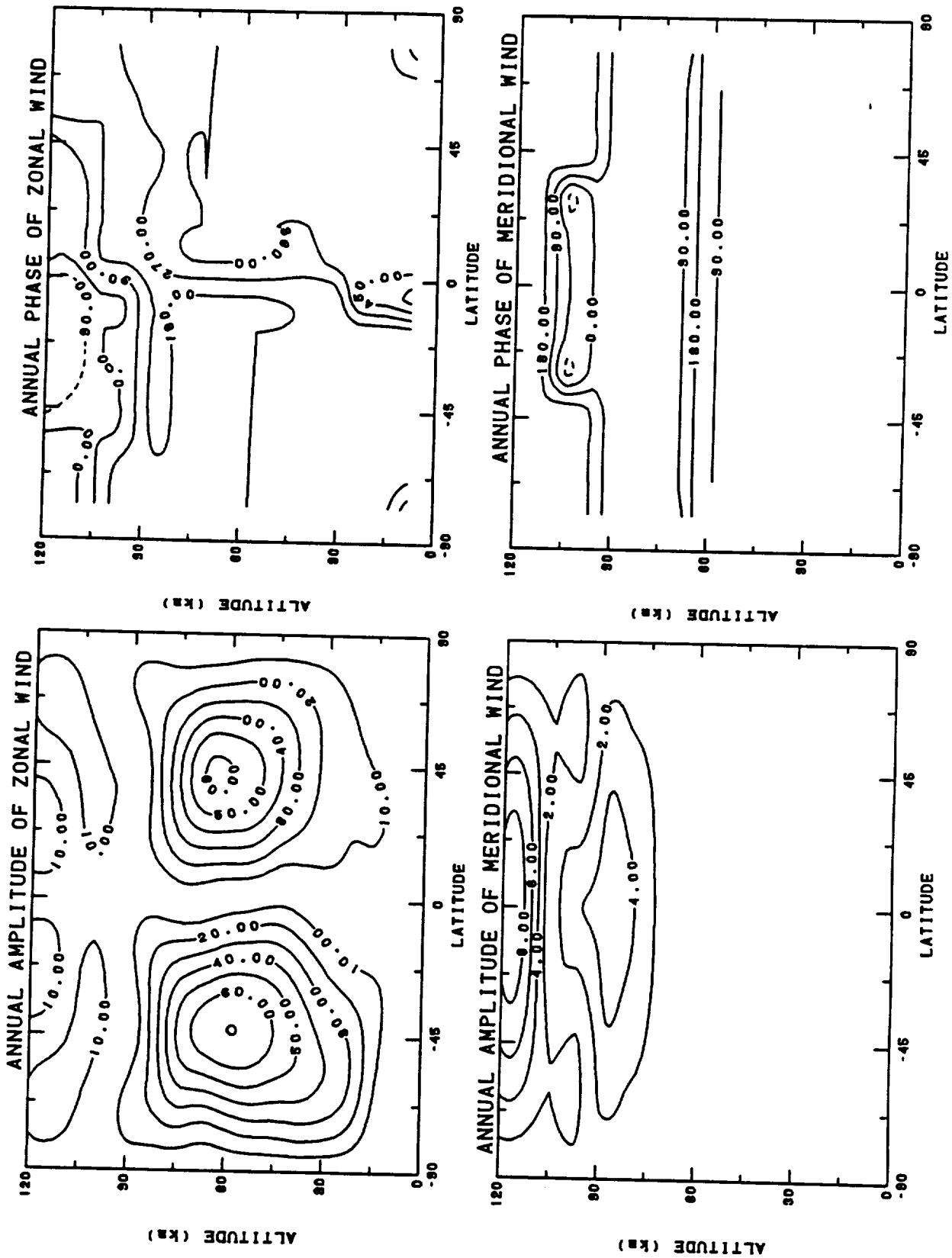
Fig. 8. Contour plots in altitude versus latitude of the diurnal and longitudinal (DL) average annual amplitude and phase (day of year) of the zonal and meridional wind.

32
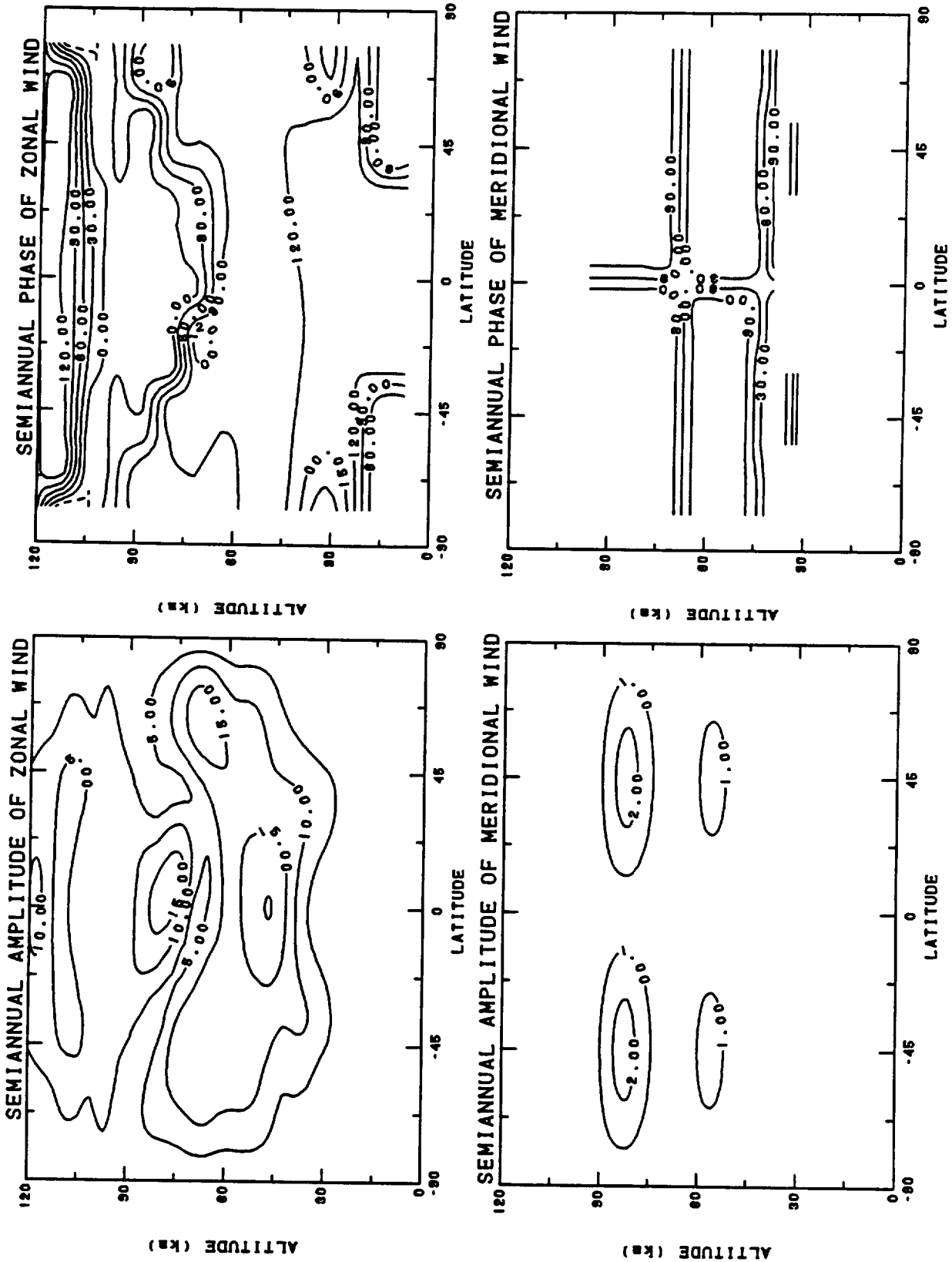
Fig. 7. Contour plots in altitude versus latitude of the DL average semiannual amplitude and phase (day of year) of the zonal and meridional wind.

33
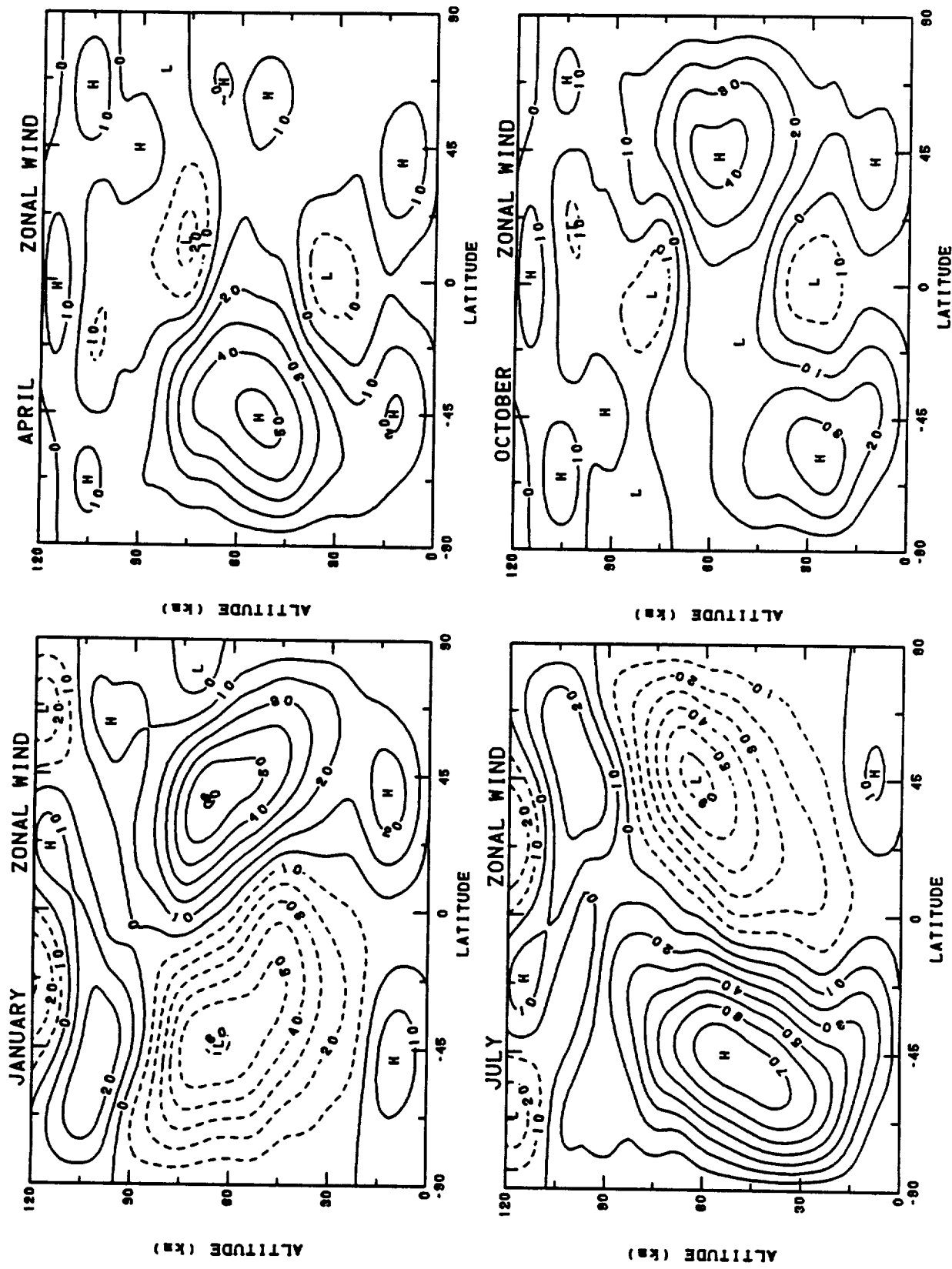
Fig. 8a. Contour plots in altitude versus latitude of the DL average zonal wind for four indicated months (mid-month).

34
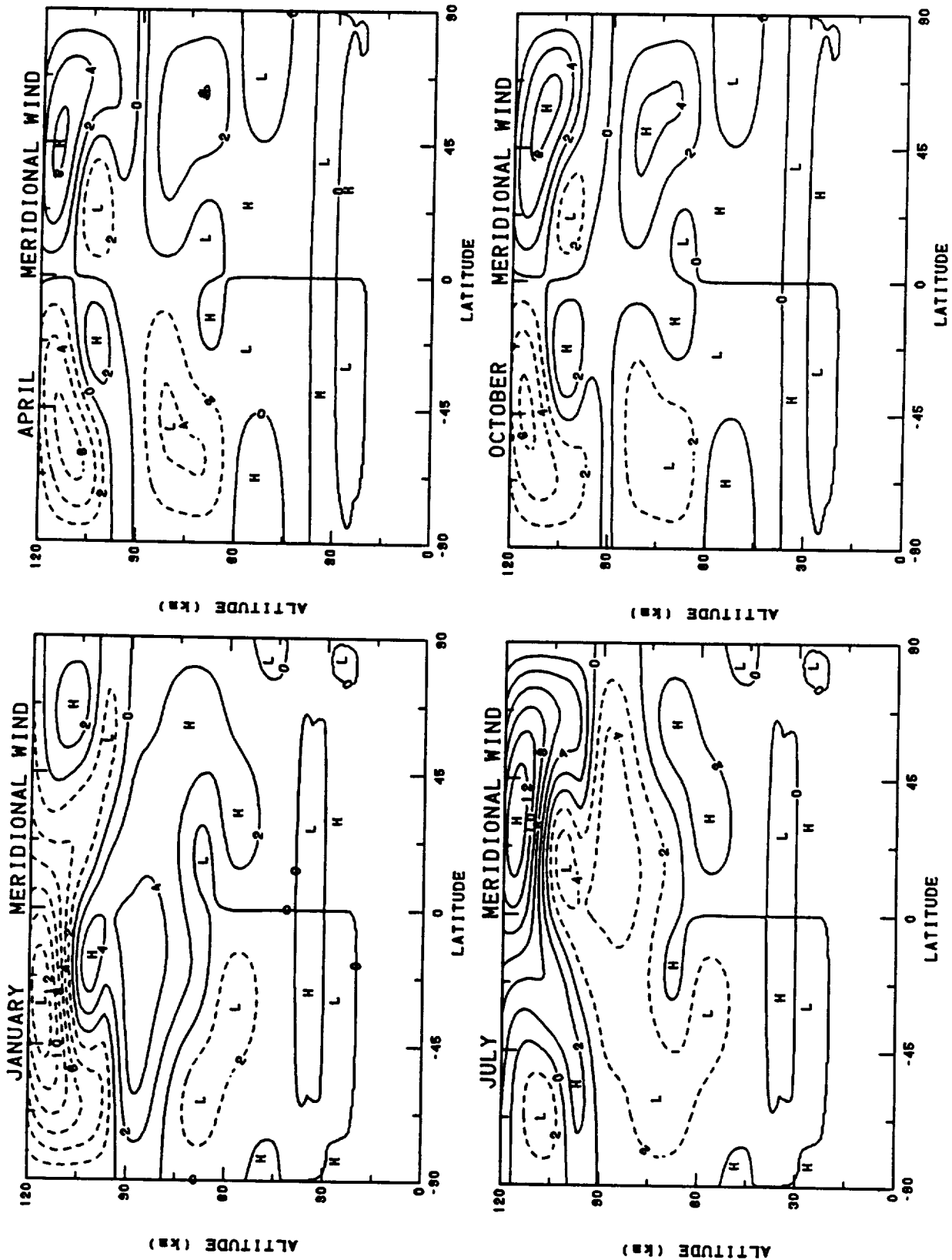
Fig. 8b. Contour plots in altitude versus latitude of the DL average meridional wind for four indicated months (mid-month).
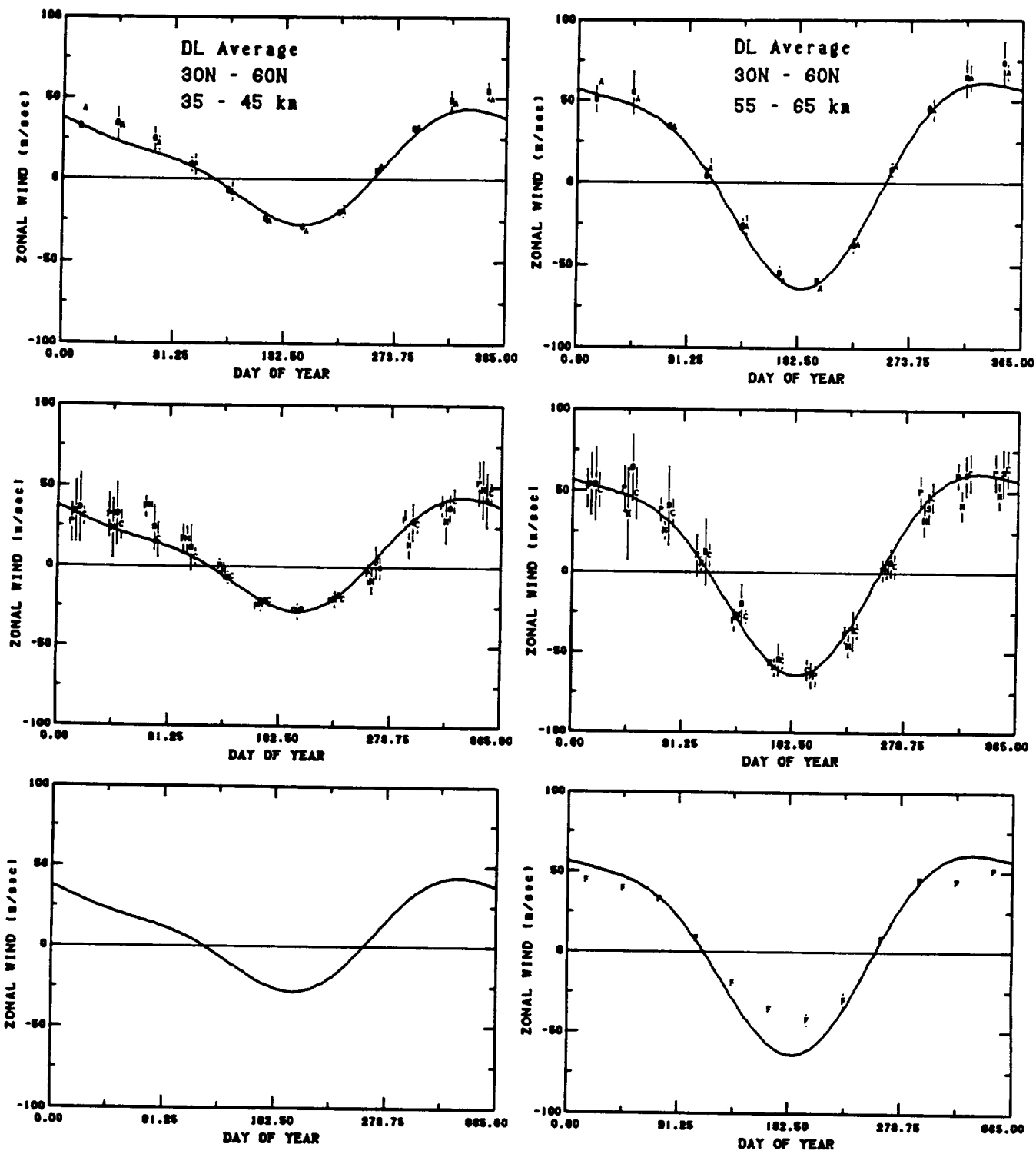
35
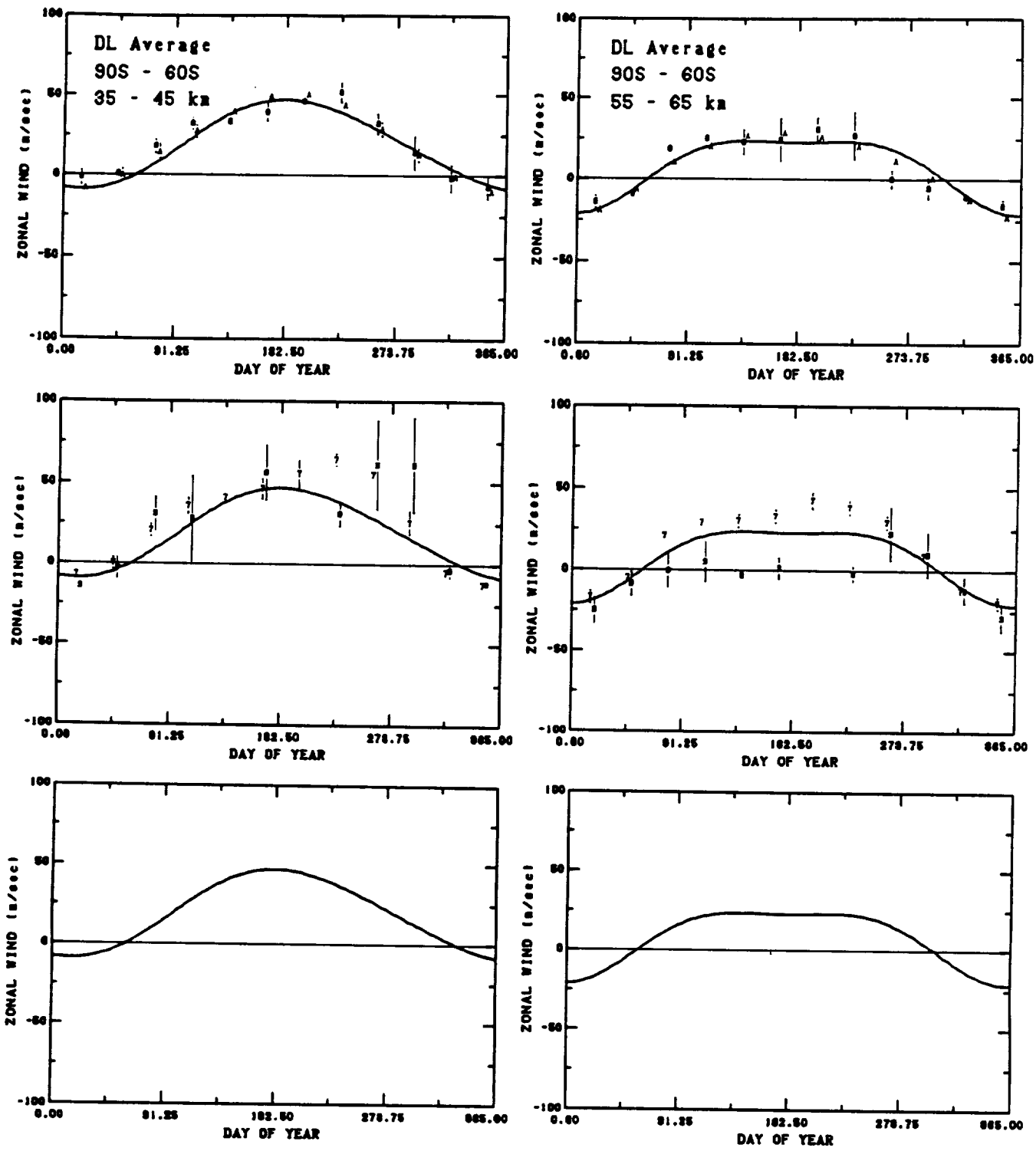
Fig. 9a.   DL average zonal wind versus day of year for 35 to 45 and 55 to 65 km at southern high latitudes. The HWM93 wind (solid line) shown for mid-range conditions.   Plot symbols indicate data source as given in Table 1.   Top row of plots contain gradient winds, middle row rocket data, and bottom row MF/Meteor radar data.
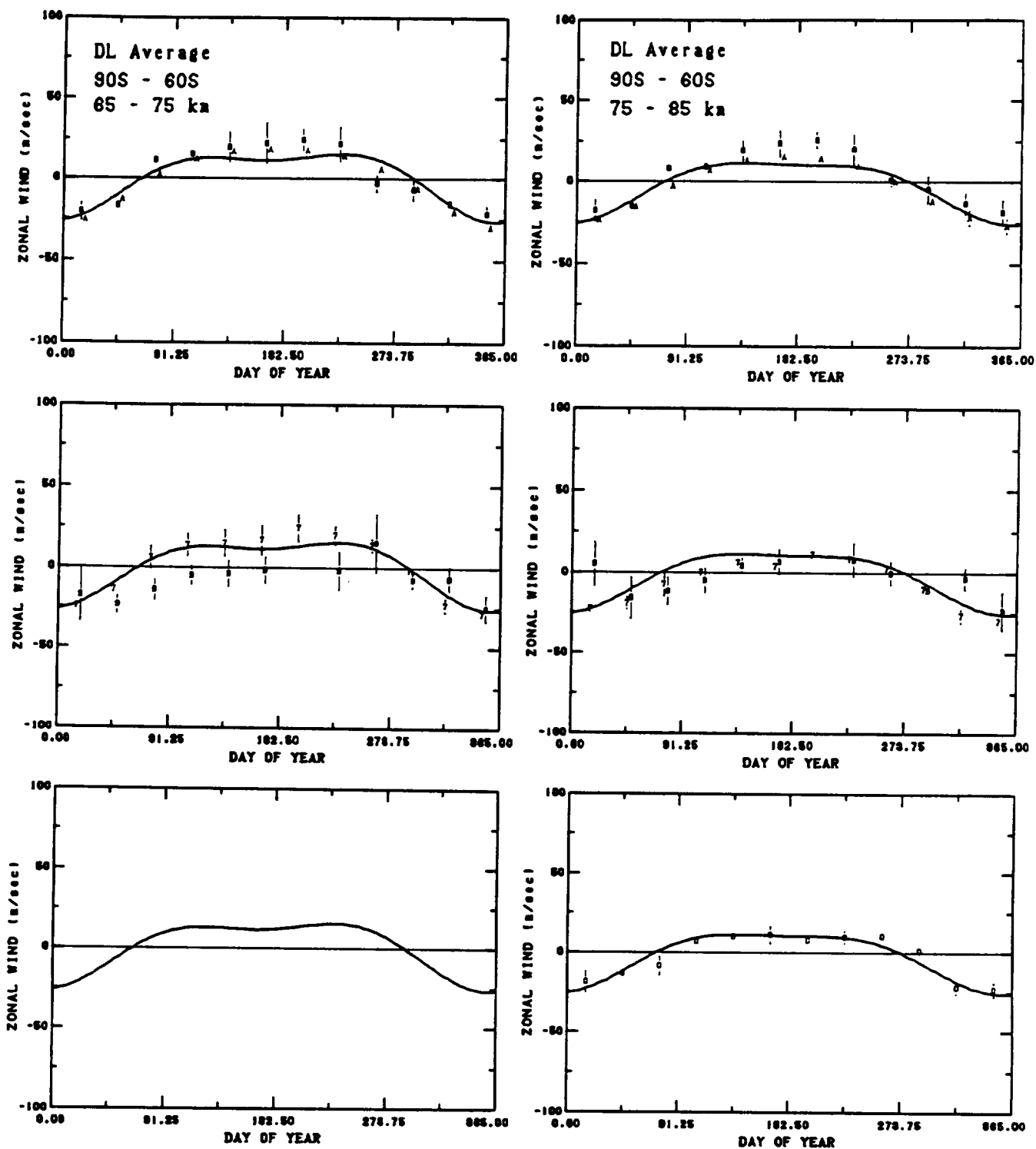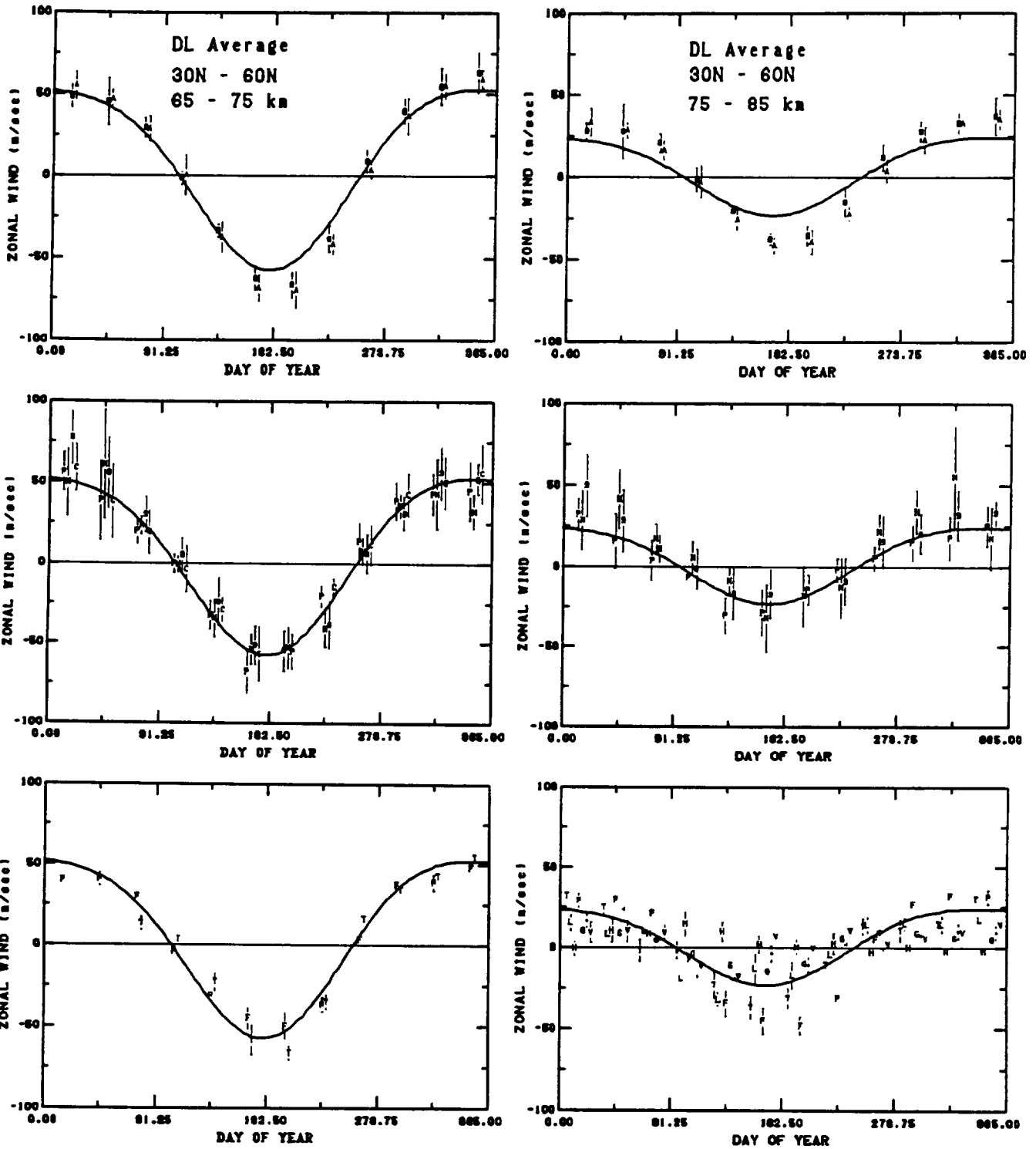
Fig. 9b. DL average zonal wind versus day of year for 65 to 75 and 75 to 85 km at southern high latitudes. The HWM93 wind (solid line) shown for mid-range conditions. Plot symbols indicate data source as given in Table 1. Top row of plots contain gradient winds, middle row rocket data, and bottom row MF/Meteor radar data.
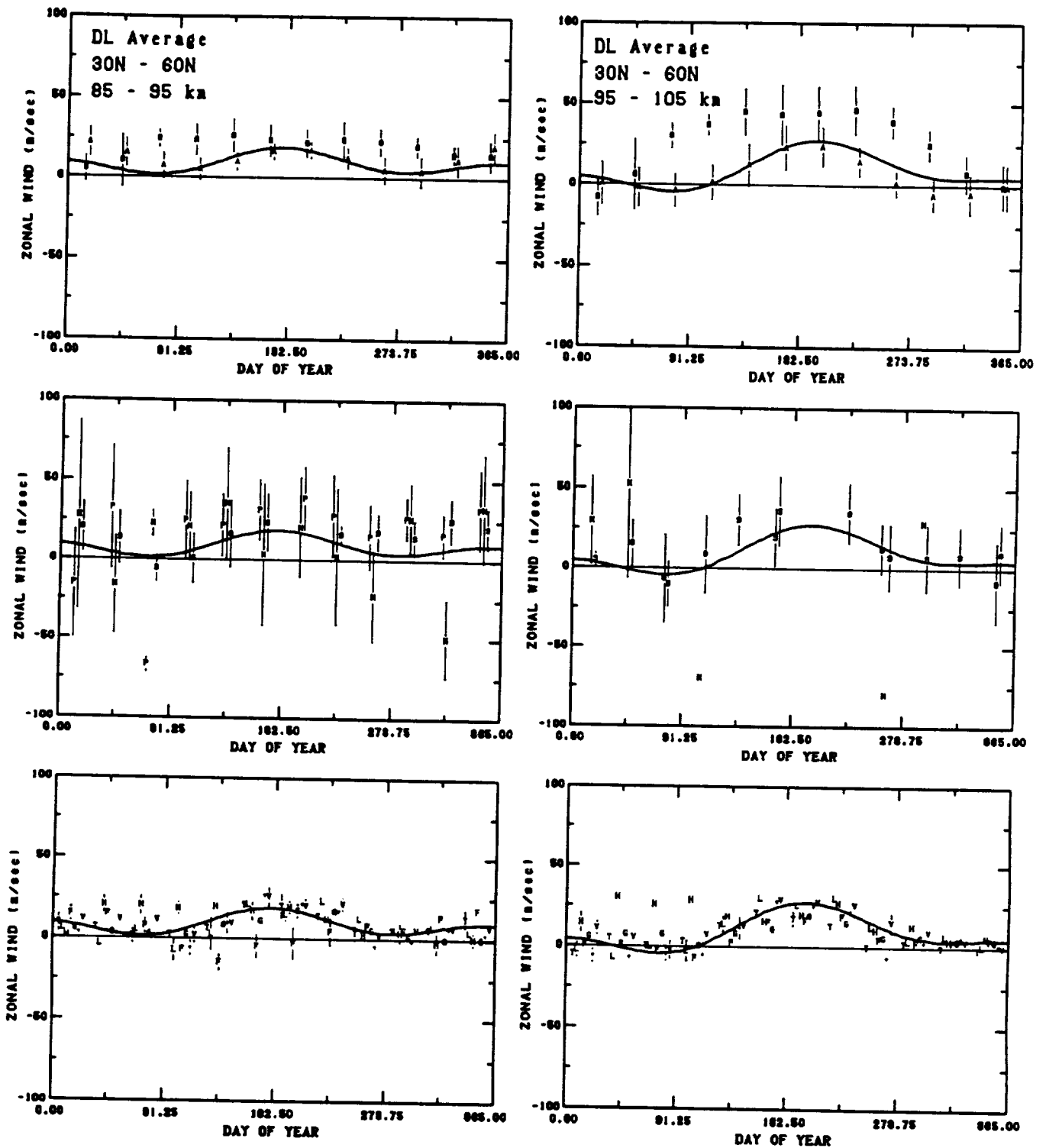
37

Fig. 9c. DL average zonal wind versus day of year for 85 to 95 and 95 to 105 km at southern high latitudes. The HWM93 wind (solid line) shown for mid-range conditions. Plot symbols indicate data source as given in Table 1. Top row of plots contain gradient winds, middle row rocket data, and bottom row MF/Meteor radar data.
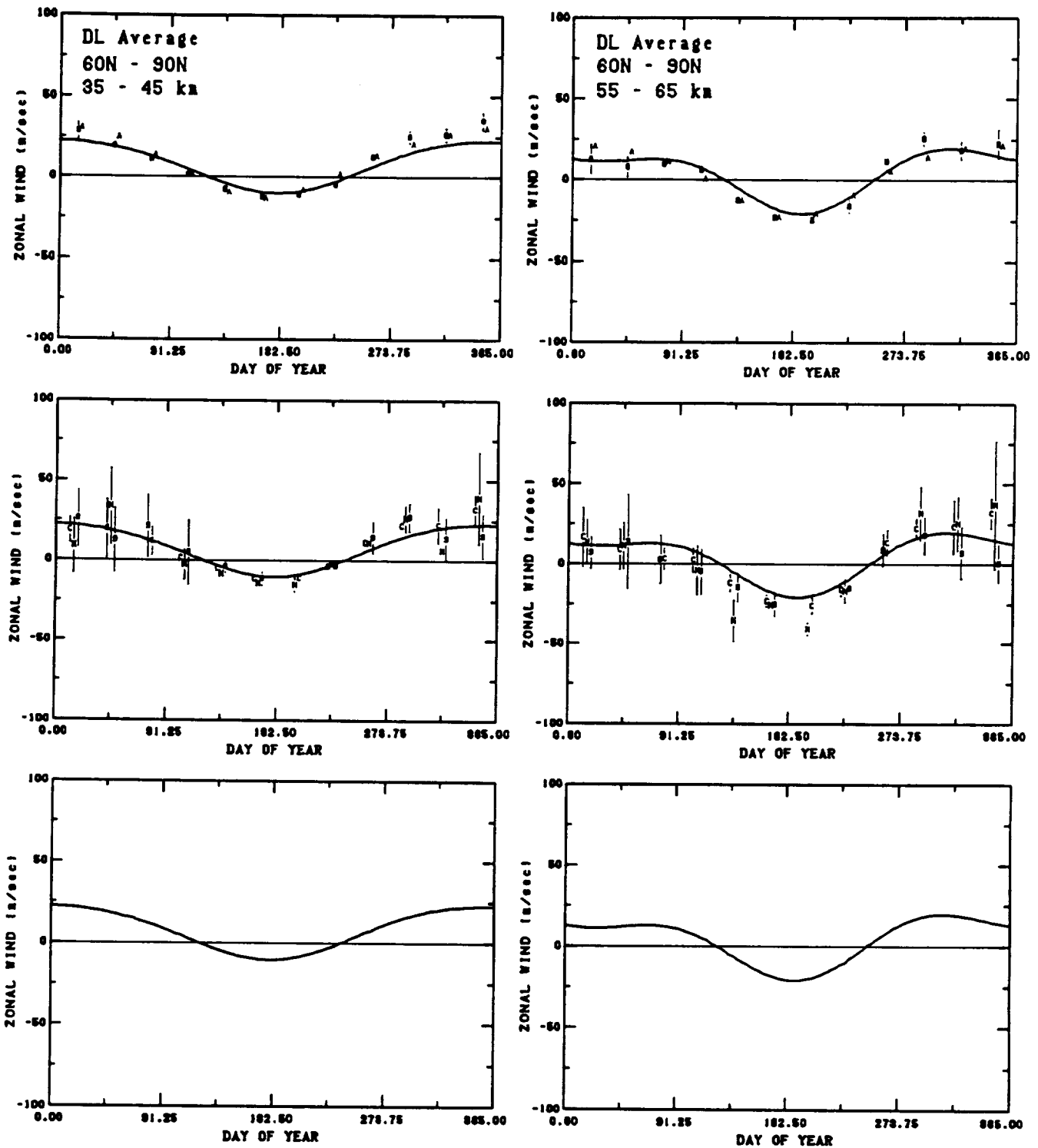
38

Fig. 9d. DL average zonal wind versus day of year for 35 to 45 and 55 to 65 km at southern mid latitudes. The HWM93 wind (solid line) shown for mid-range conditions. Plot symbols indicate data source as given in Table 1. Top row of plots contain gradient winds, middle row rocket data, and bottom row MF/Meteor radar data.

Fig. 9e. DL average zonal wind versus day of year for 65 to 75 and 75 to 85 km at southern mid latitudes. The HWM93 wind (solid line) shown for mid-range conditions. Plot symbols indicate data source as given in Table 1. Top row of plots contain gradient winds, middle row rocket data, and bottom row MF/Meteor radar data.
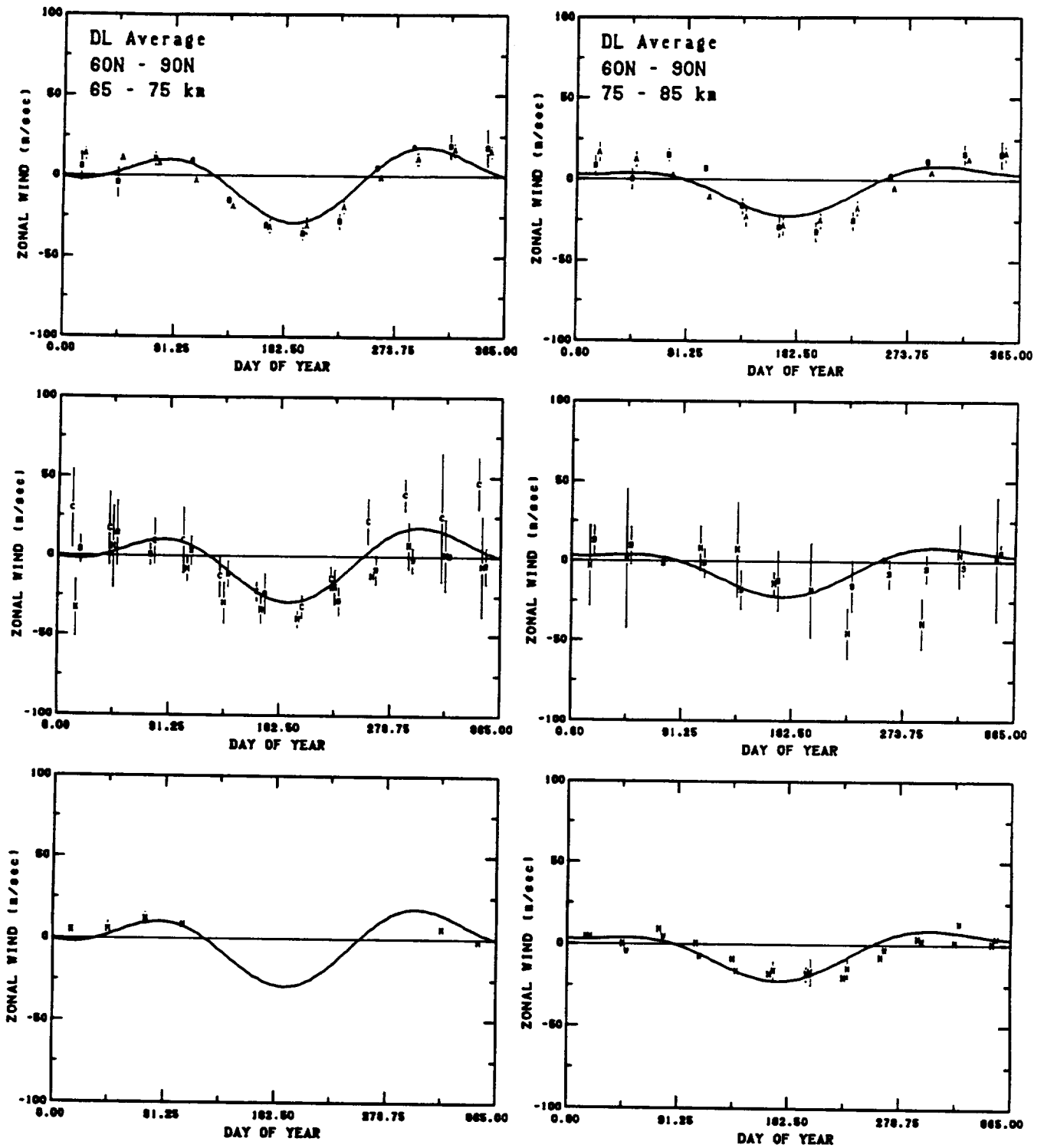
Fig. 9f. DL average zonal wind versus day of year for 85 to 95 and 95 to 105 km at southern mid latitudes. The HWM93 wind (solid line) shown for mid-range conditions. Plot symbols indicate data source as given in Table 1. Top row of plots contain gradient winds, middle row rocket data, and bottom row MF/Meteor radar data.
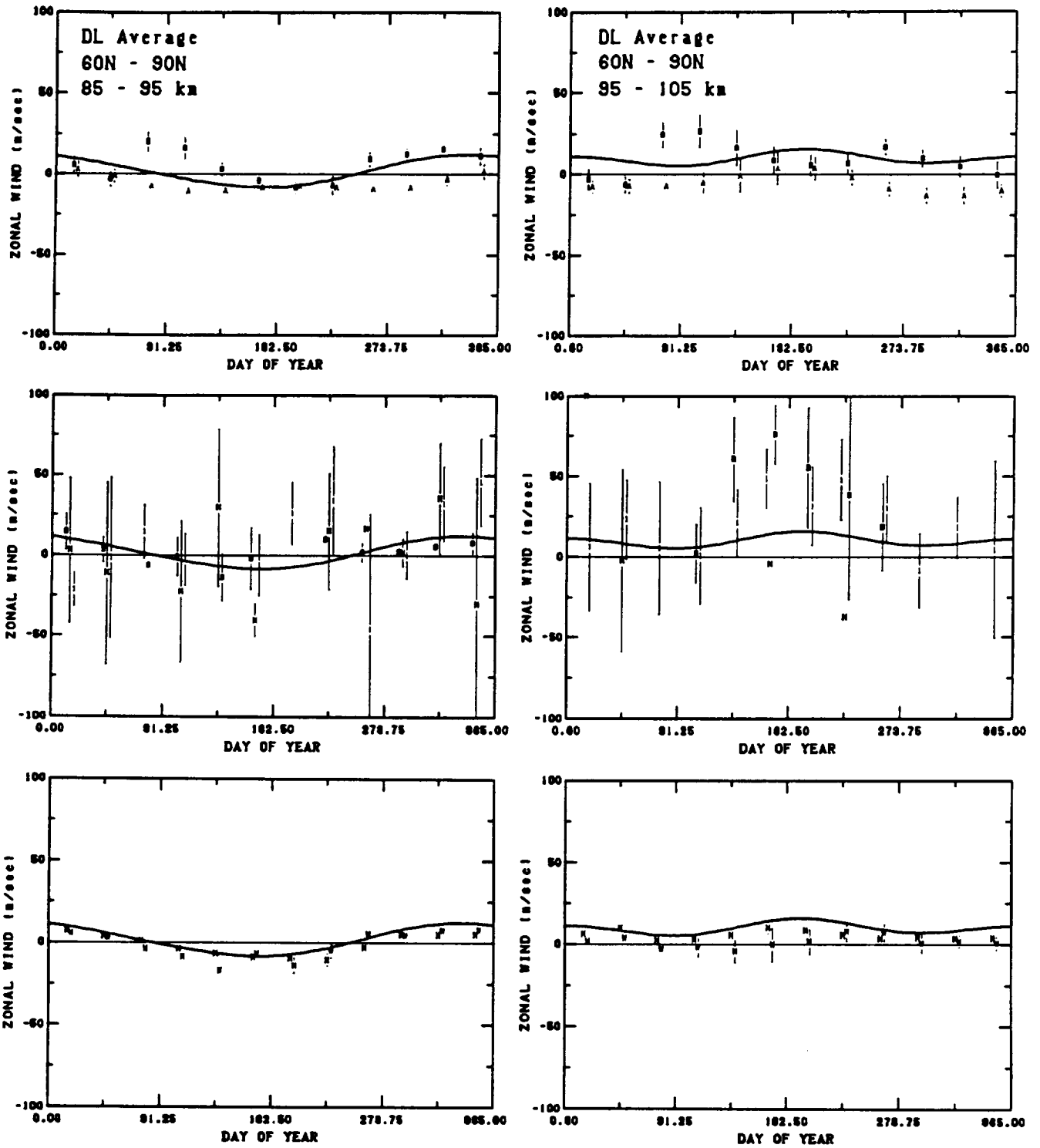
41

Fig. 9g. DL average zonal wind versus day of year for 35 to 45 and 55 to 65 km at southern low latitudes. The HWM93 wind (solid line) shown for mid-range conditions. Plot symbols indicate data source as given in Table 1. Top row of plots contain gradient winds, middle row rocket data, and bottom row MF/Meteor radar data.
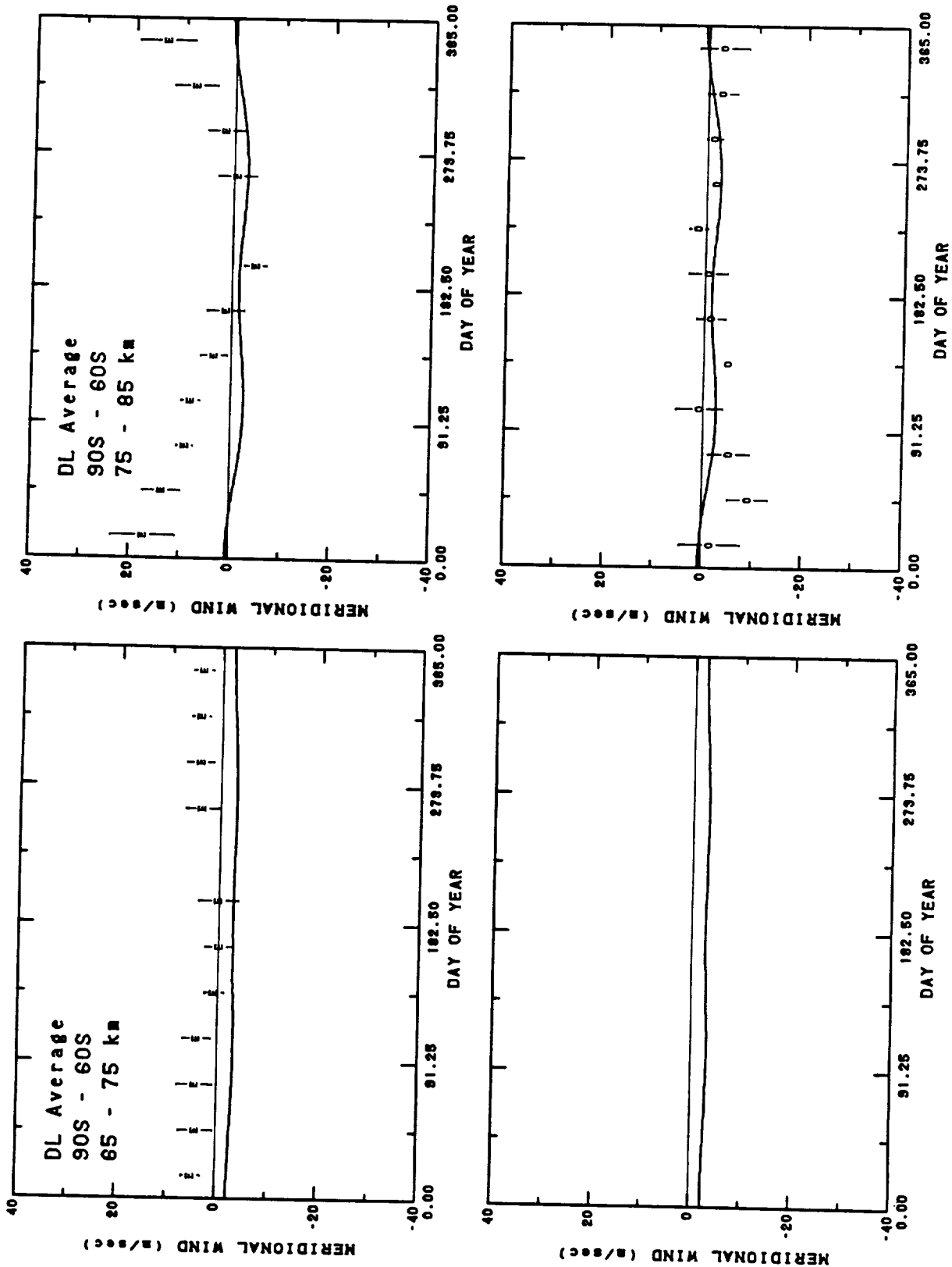
42

Fig. 9h.   DL average zonal wind versus day of year for 65 to 75 and 75 to 85 km at southern low latitudes. The HWM93 wind (solid line) shown for mid-range conditions.   Plot symbols indicate data source as given in Table 1.   Top row of plots contain gradient winds, middle row rocket data, and bottom row MF/Meteor radar data.
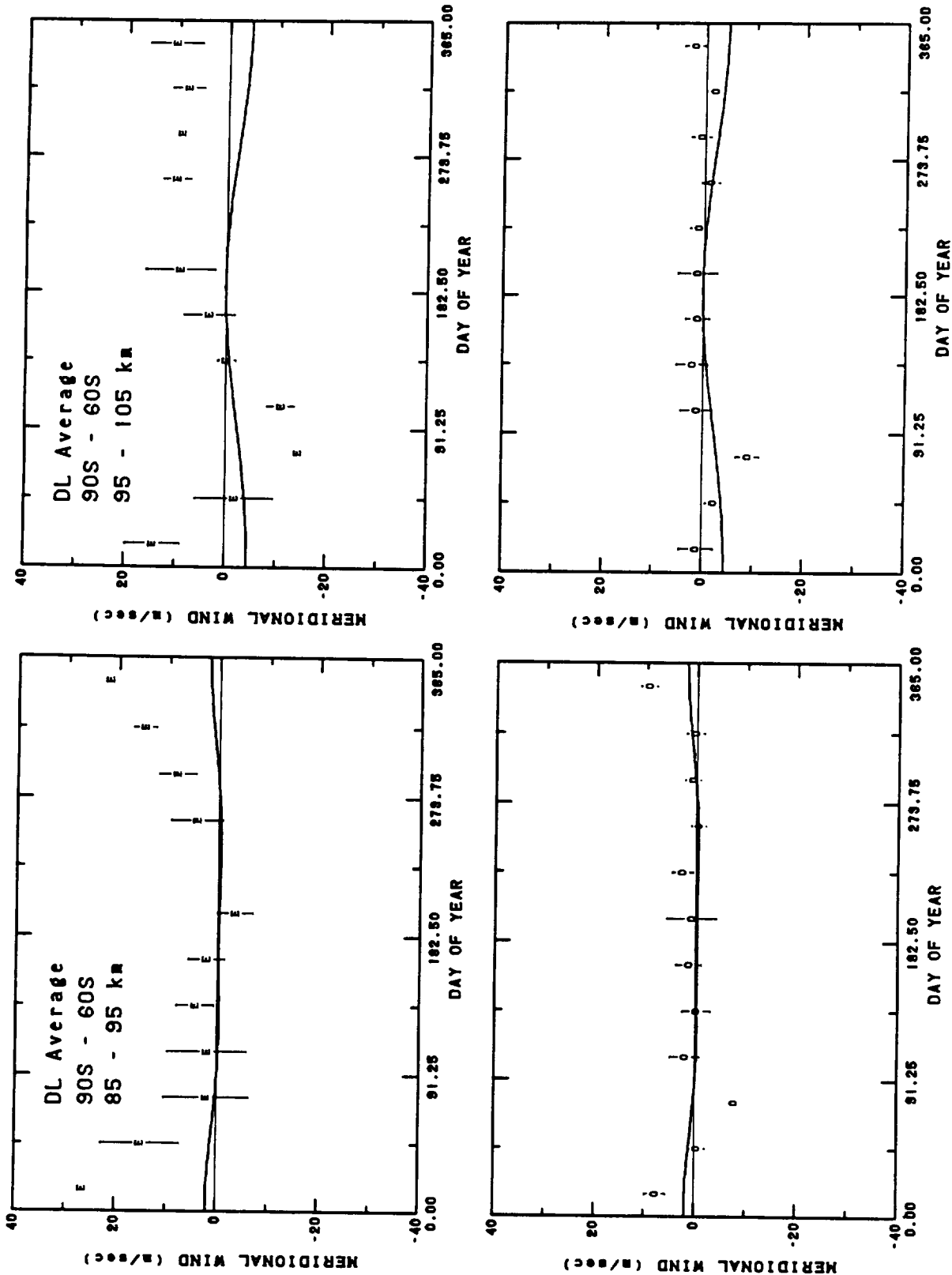
43

Fig. 91. DL average zonal wind versus day of year for 85 to 95 and 95 to 105 km at southern low latitudes. The HWM93 wind (solid line) shown for mid-range conditions. Plot symbols indicate data source as given in Table 1. Top row of plots contain gradient winds, middle row rocket data, and bottom row MF/Meteor radar data.
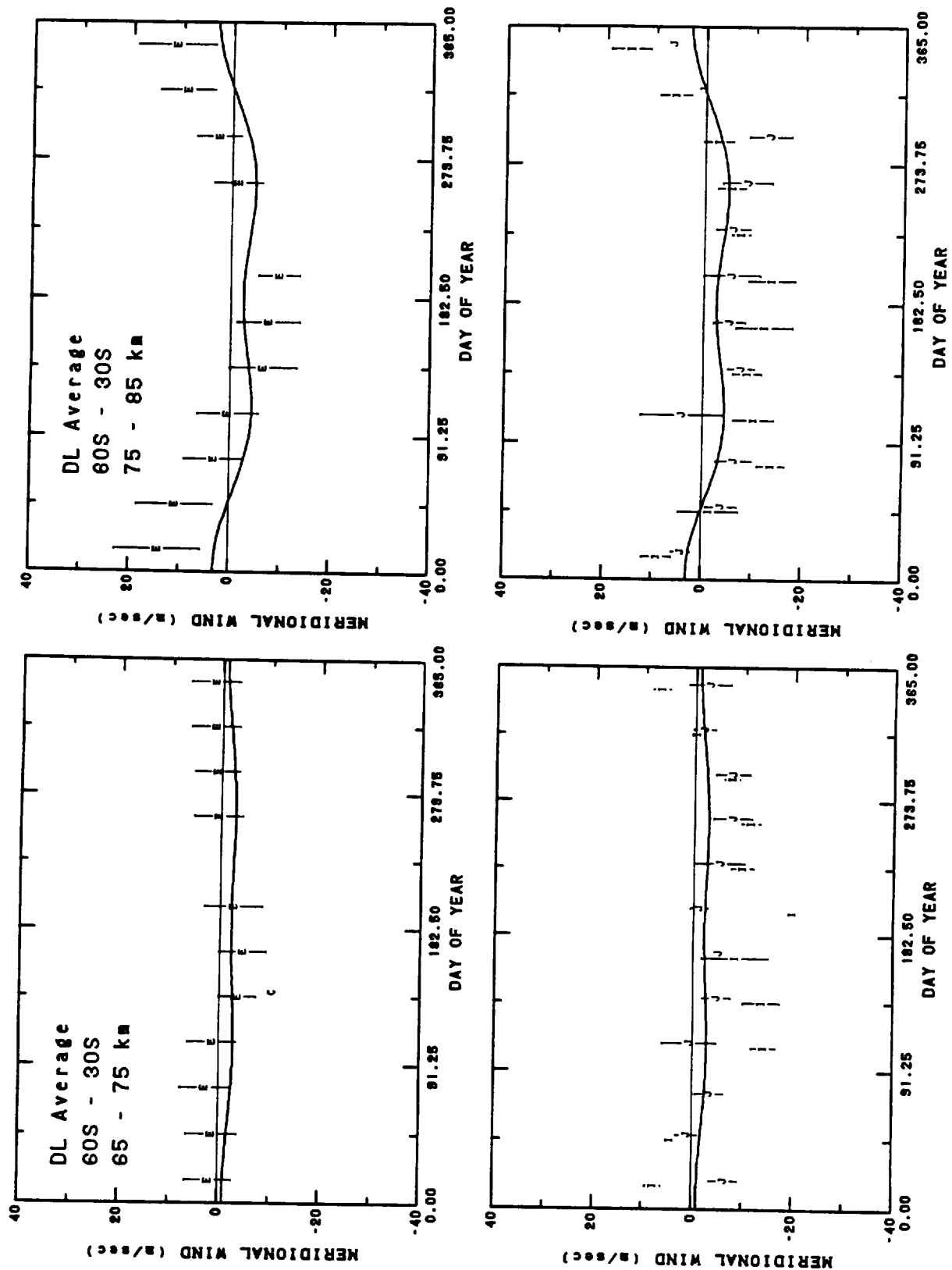
44

Fig. 9j. DL average zonal wind versus day of year for 35 to 45 and 55 to 65 km at northern low latitudes. The HWM93 wind (solid line) shown for mid-range conditions. Plot symbols indicate data source as given in Table 1. Top row of plots contain gradient winds, middle row rocket data, and bottom row MF/Meteor radar data.

45

Fig. 9k. DL average zonal wind versus day of year for 65 to 75 and 75 to 85 km at northern low latitudes. The HWM93 wind (solid line) shown for mid-range conditions. Plot symbols indicate data source as given in Table 1. Top row of plots contain gradient winds, middle row rocket data, and bottom row MF/Meteor radar data.
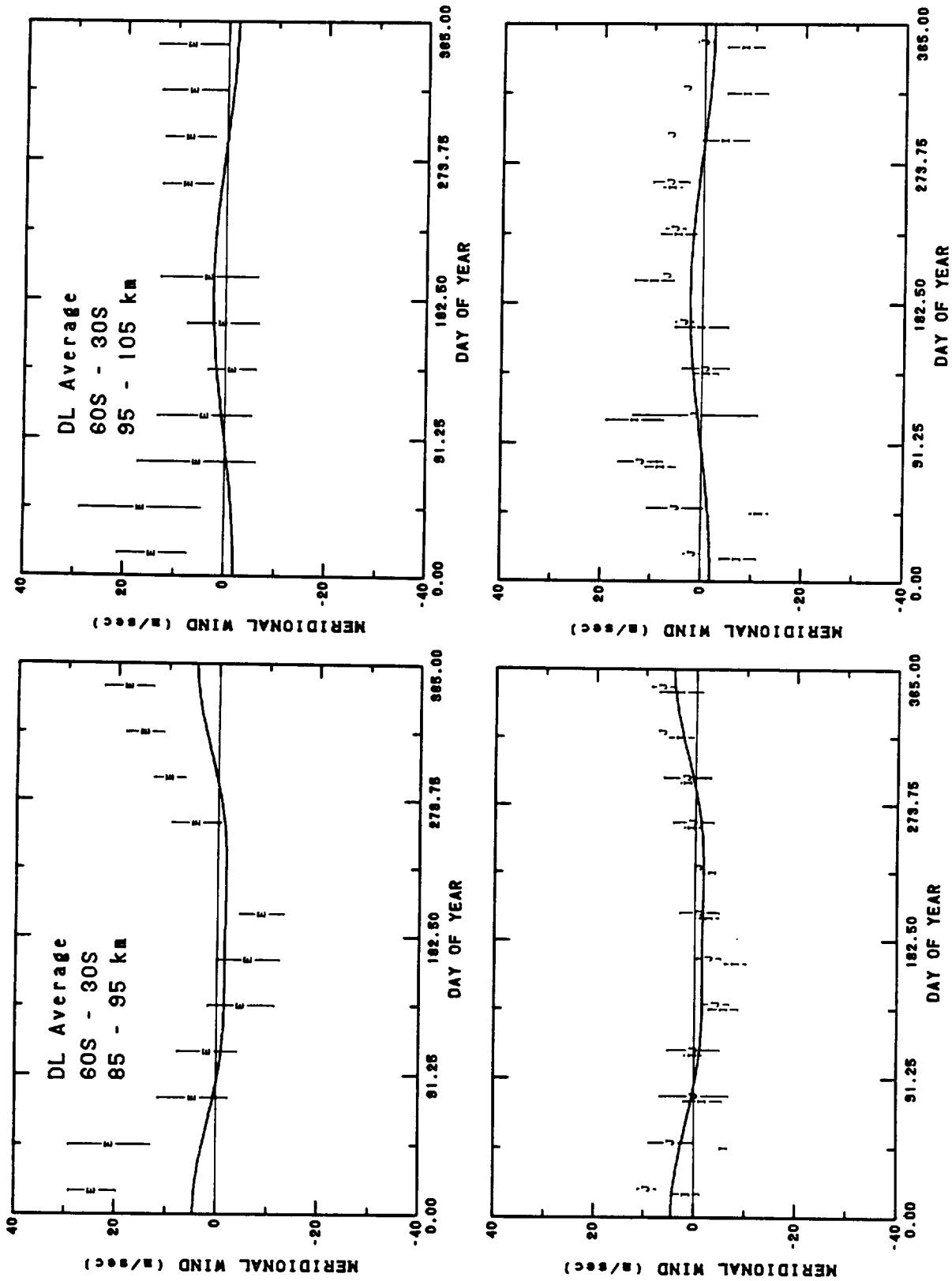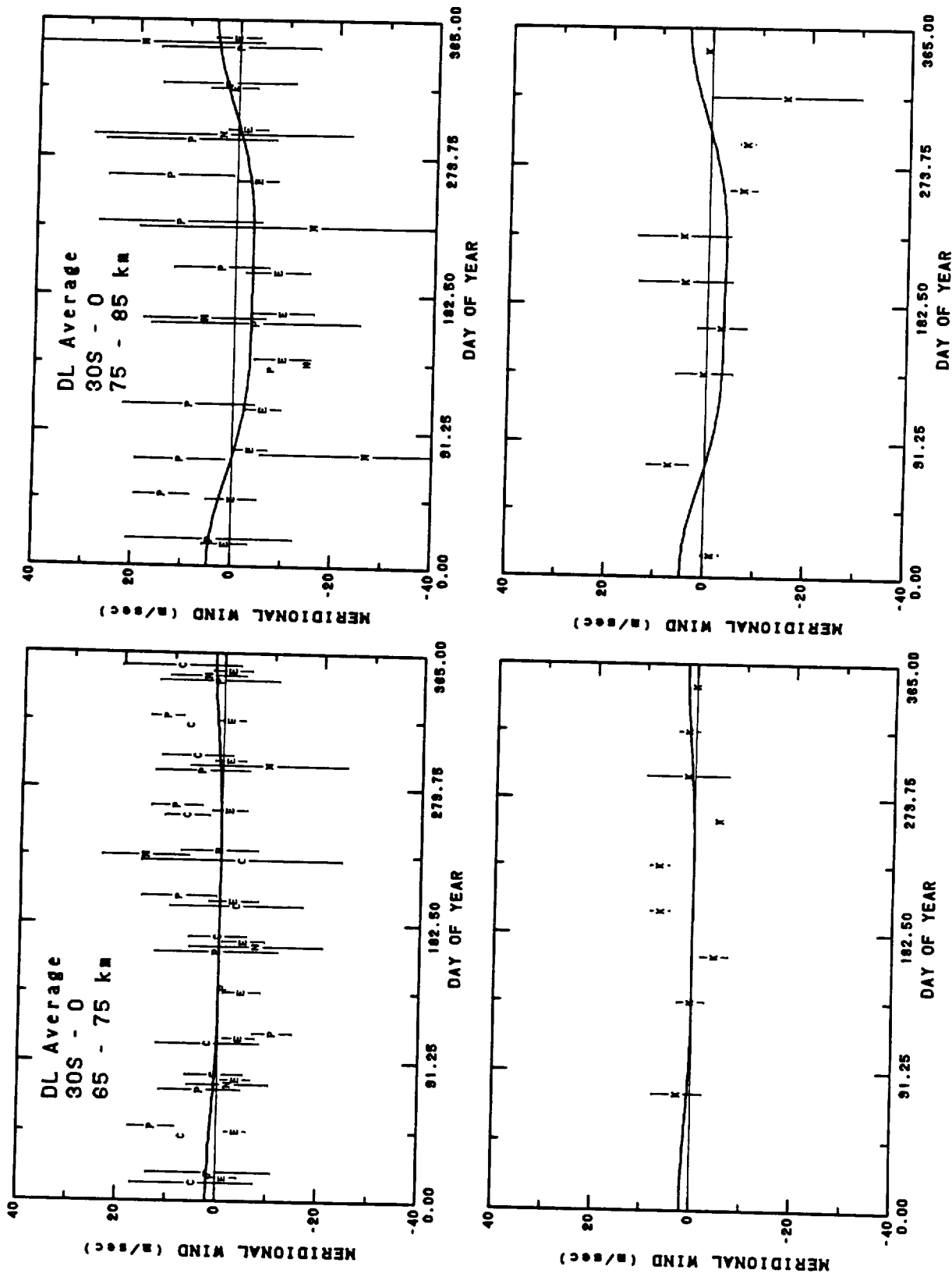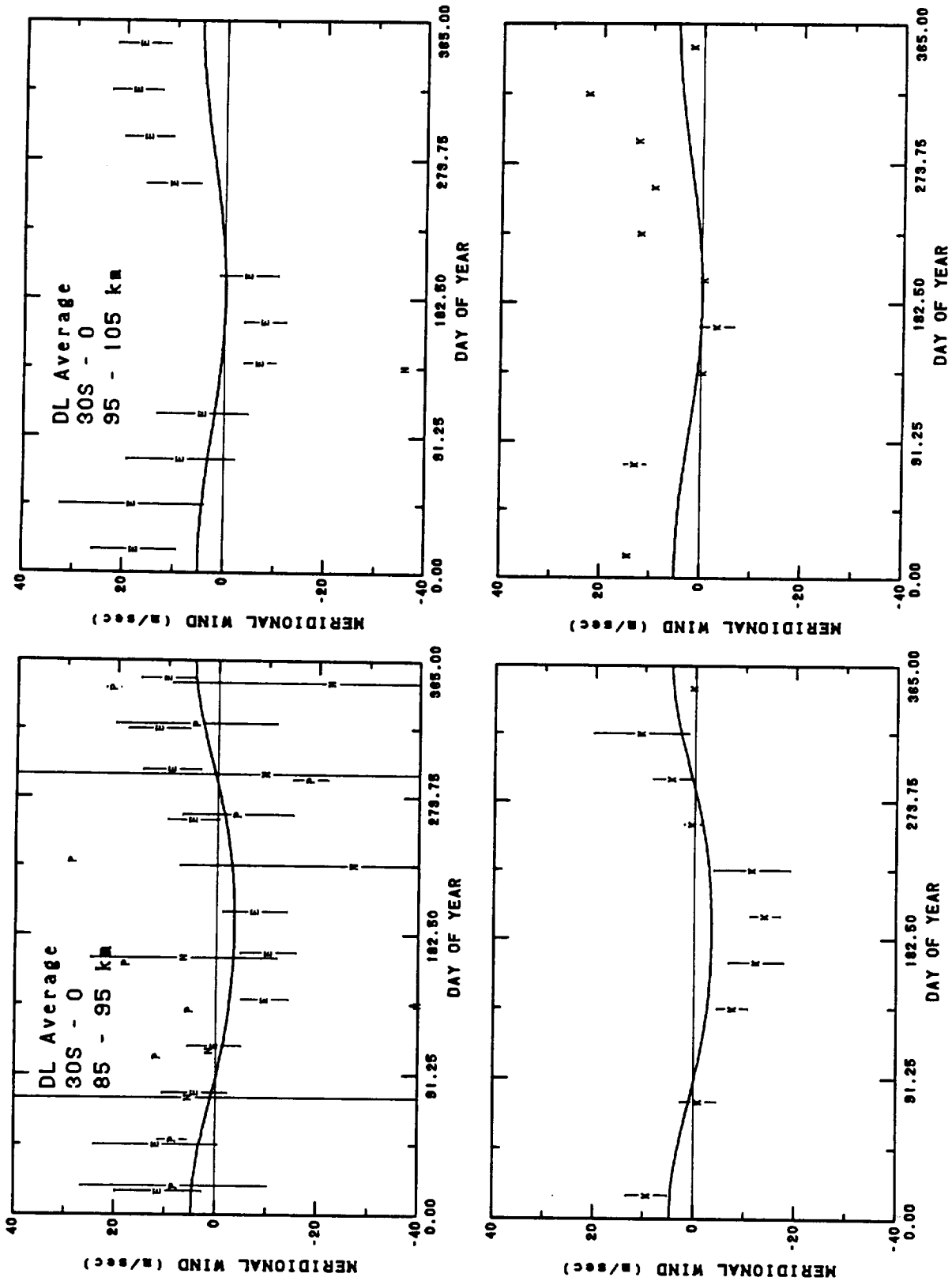
Fig. 91. DL average zonal wind versus day of year for 85 to 95 and 95 to 105 km at northern low latitudes. The HWM93 wind (solid line) shown for mid-range conditions. Plot symbols indicate data source as given in Table 1. Top row of plots contain gradient winds, middle row rocket and IS data, and bottom row MF/Meteor radar data.

47
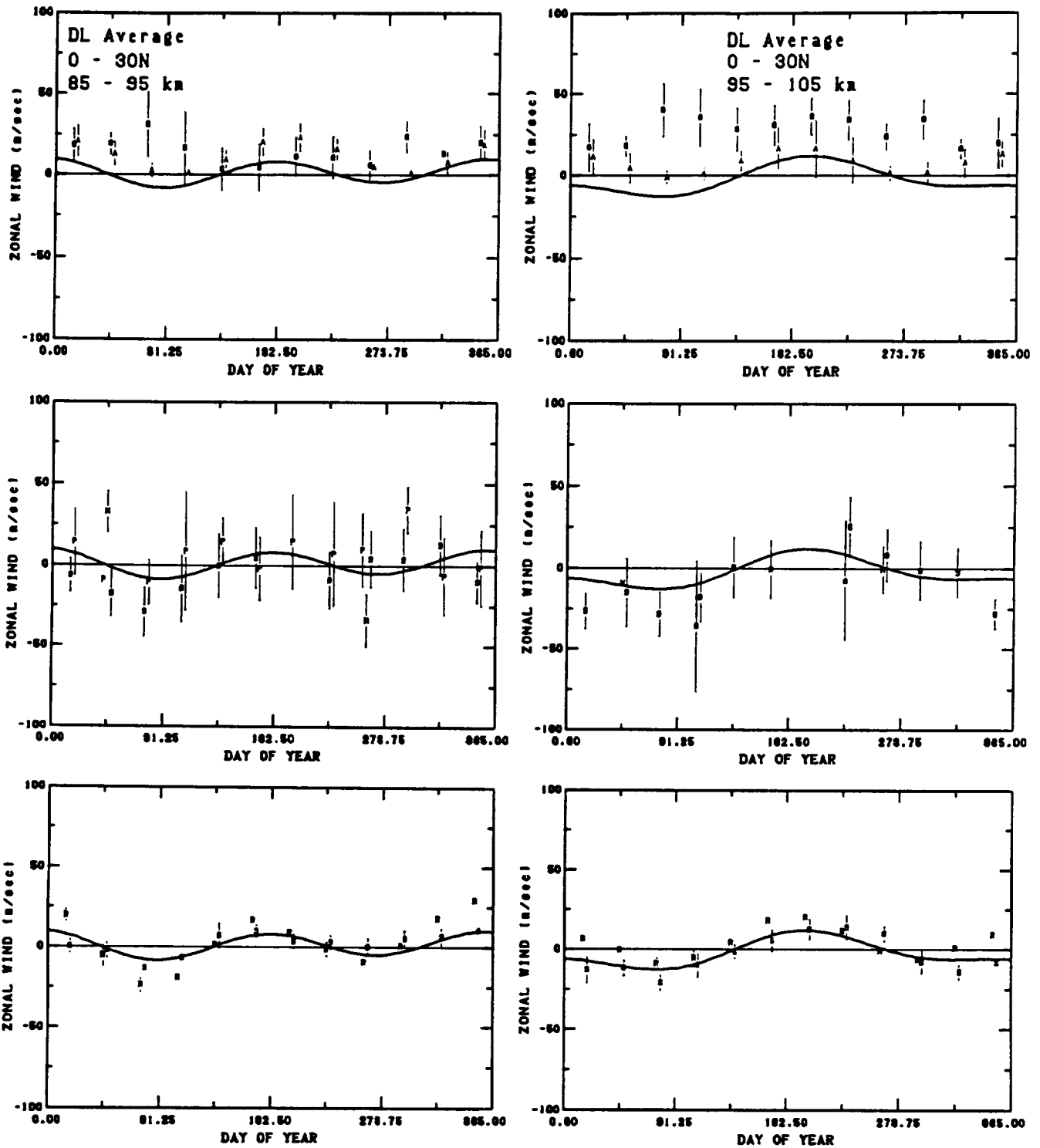
Fig. 9m. DL average zonal wind versus day of year for 35 to 45 and 55 to 65 km at northern mid latitudes. The HWM93 wind (solid line) shown for mid-range conditions. Plot symbols indicate data source as given in Table 1. Top row of plots contain gradient winds, middle row rocket data, and bottom row MF/Meteor radar data.

48

Fig. 9n. DL average zonal wind versus day of year for 65 to 75 and 75 to 85 km at northern mid latitudes. The HWM93 wind (solid line) shown for mid-range conditions. Plot symbols indicate data source as given in Table 1. Top row of plots contain gradient winds, middle row rocket data, and bottom row MF/Meteor radar data.
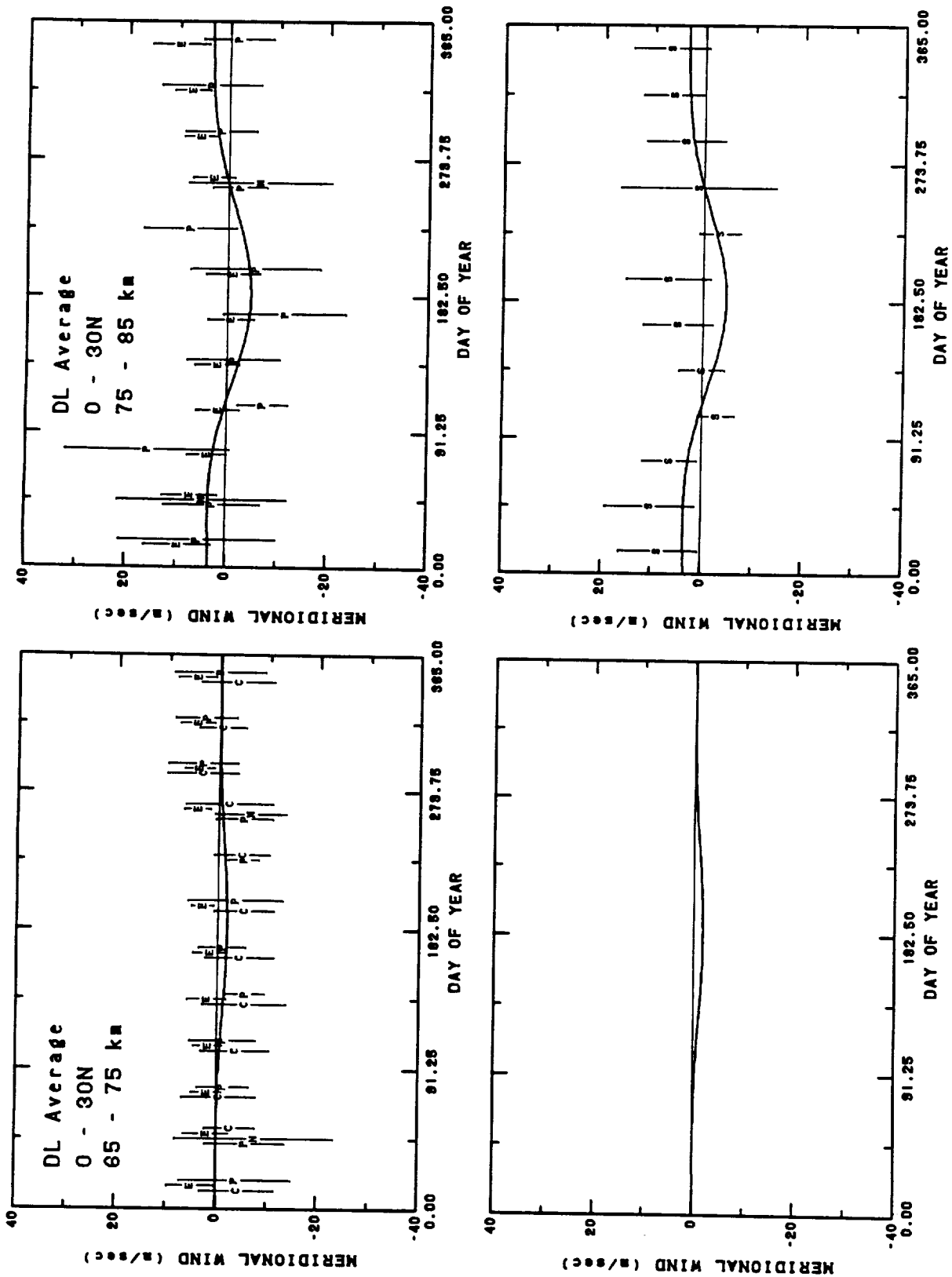
49

Fig. 9o. DL average zonal wind versus day of year for 85 to 95 and 95 to 105 km at northern mid latitudes. The HWM93 wind (solid line) shown for mid-range conditions. Plot symbols indicate data source as given in Table 1. Top row of plots contain gradient winds, middle row rocket data, and bottom row MF/Meteor radar data.

Fig. 9p. DL average zonal wind versus day of year for 35 to 45 and 55 to 65 km at northern high latitudes. The HWM93 wind (solid line) shown for mid-range conditions. Plot symbols indicate data source as given in Table 1. Top row of plots contain gradient winds, middle row rocket data, and bottom row MF/Meteor radar data.
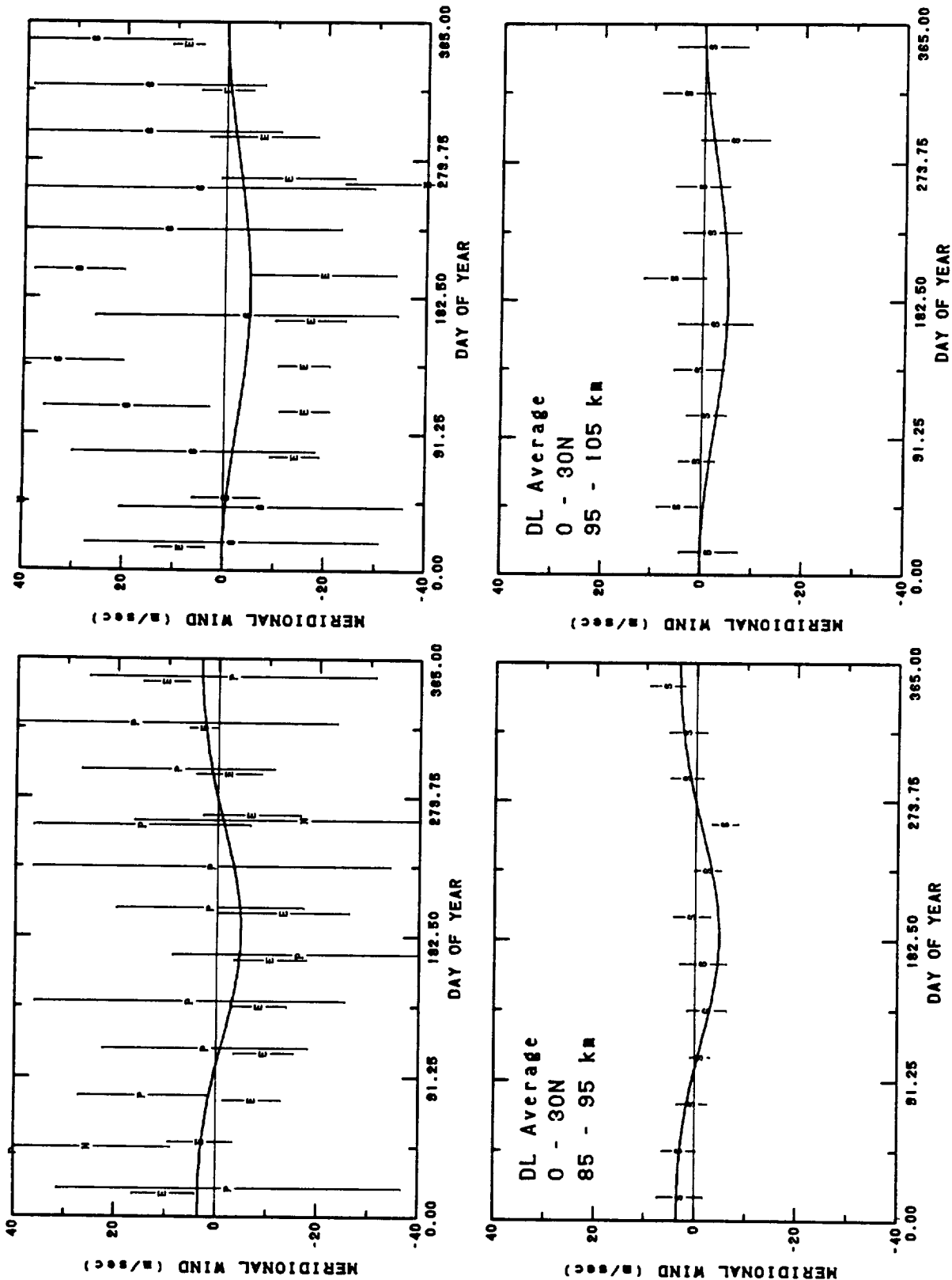
51

Fig. 9q. DL average zonal wind versus day of year for 65 to 75 and 75 to 85 km at northern high latitudes. The HWM93 wind (solid line) shown for mid-range conditions. Plot symbols indicate data source as given in Table 1. Top row of plots contain gradient winds, middle row rocket data, and bottom row MF/Meteor radar data.
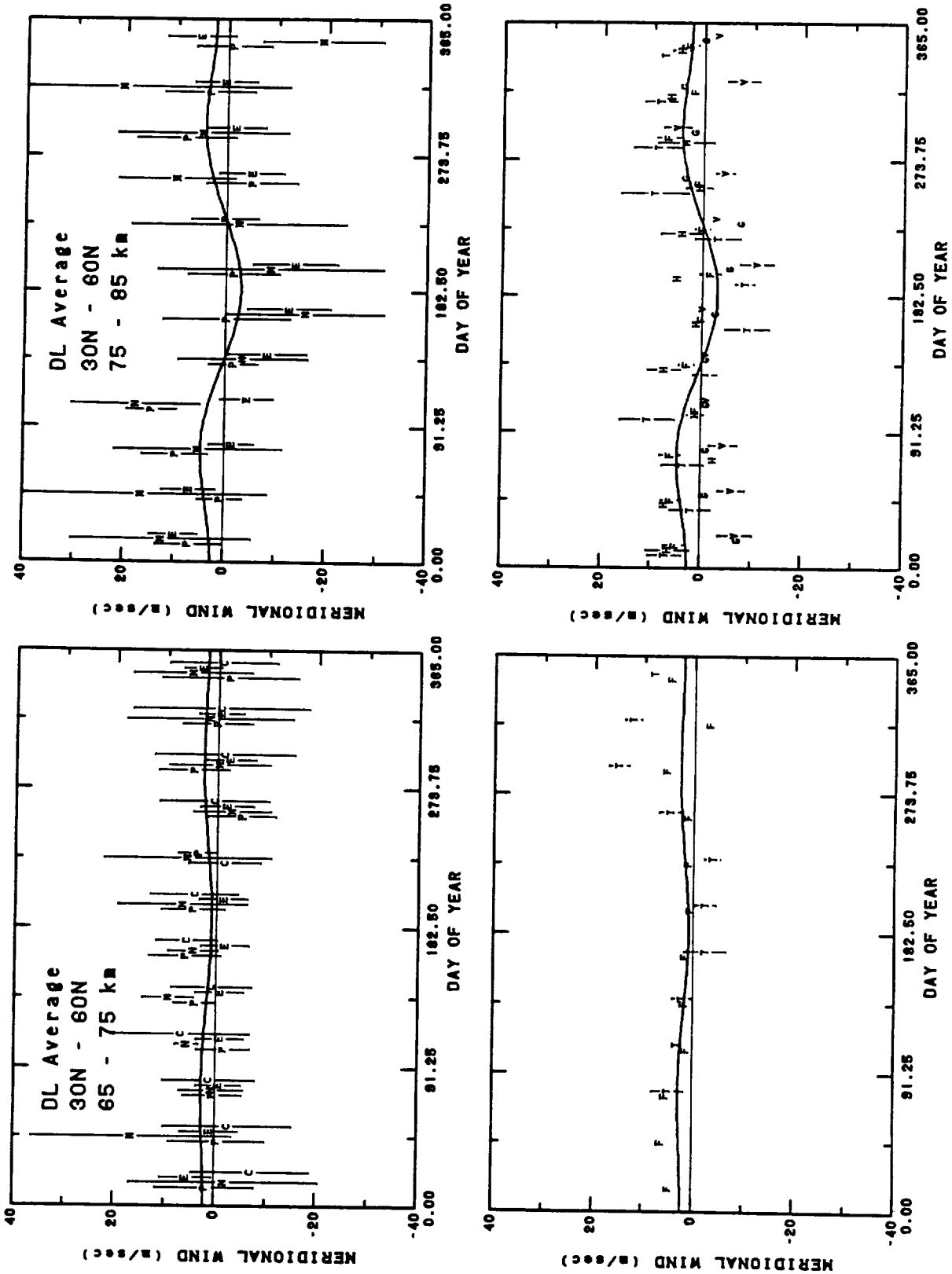
52

Fig. 9r. DL average zonal wind versus day of year for 85 to 95 and 95 to 105 km at northern high latitudes. The HWM93 wind (solid line) shown for mid-range conditions. Plot symbols indicate data source as given in Table 1. Top row of plots contain gradient winds, middle row rocket and IS data, and bottom row MF/Meteor radar data.

53

Fig. 10a. DL average meridional wind versus day of year for 65 to 75 and 75 to 85 km at southern high latitudes. The HWM93 wind (solid line) shown for mid-range conditions. Plot symbols indicate data source as given in Table 1. Top row of plots contains rocket data and bottom row MF/Meteor radar data.
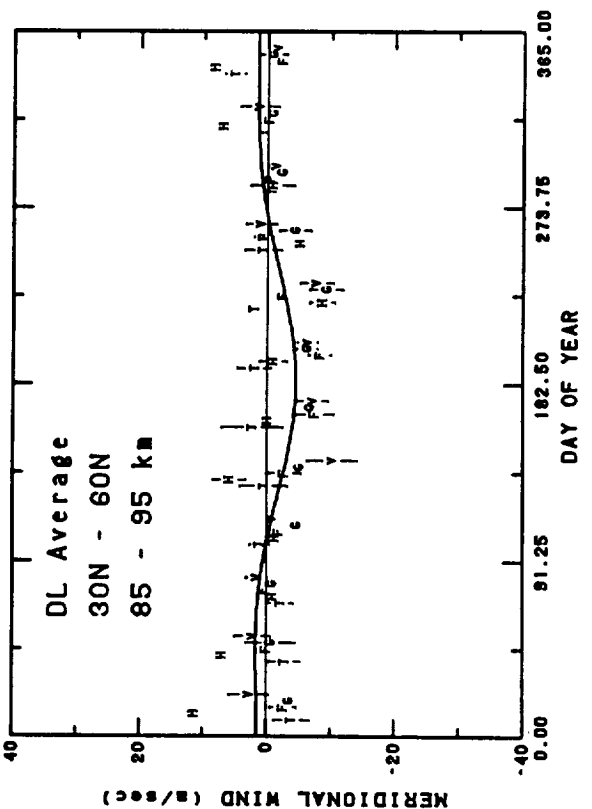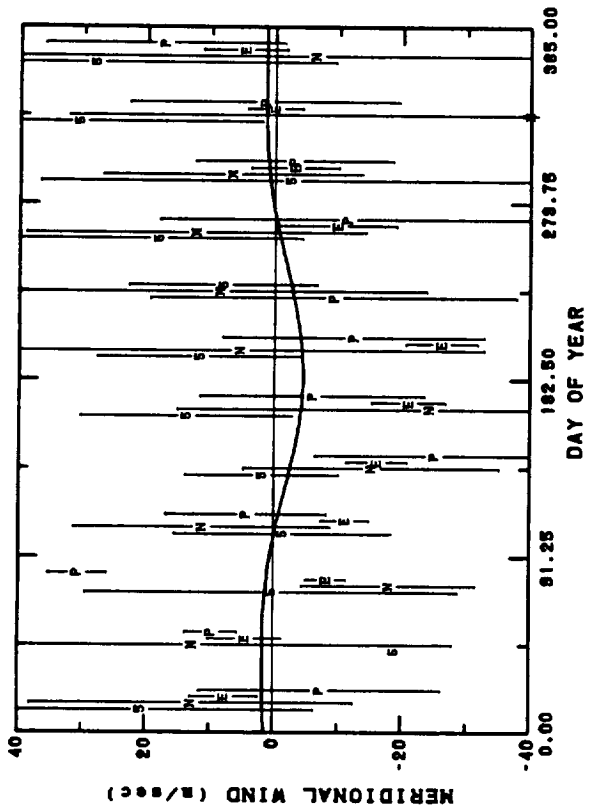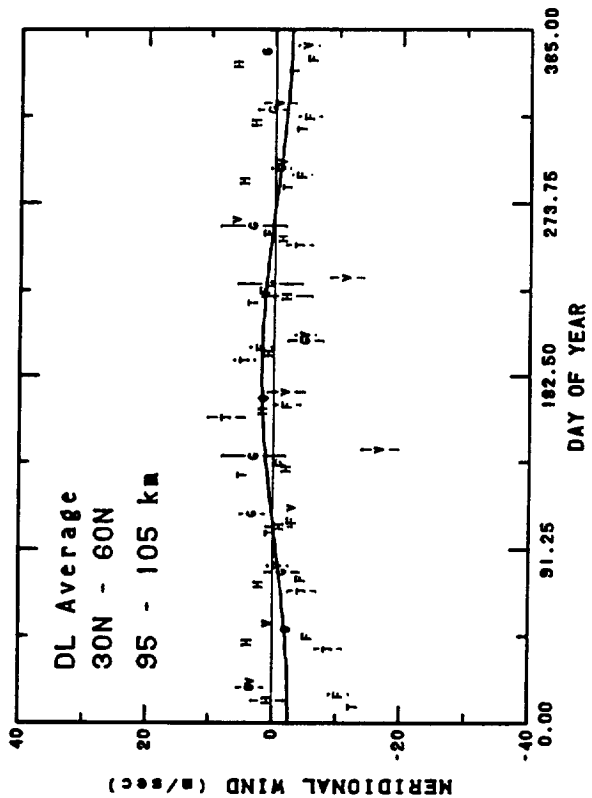
Fig. 10b. DL average meridional wind versus day of year for 85 to 95 and 95 to 105 km at southern high latitudes. The HWM93 wind (solid line) shown for mid-range conditions. Plot symbols indicate data source as given in Table 1. Top row of plots contains rocket data and bottom row MF/Meteor radar data.
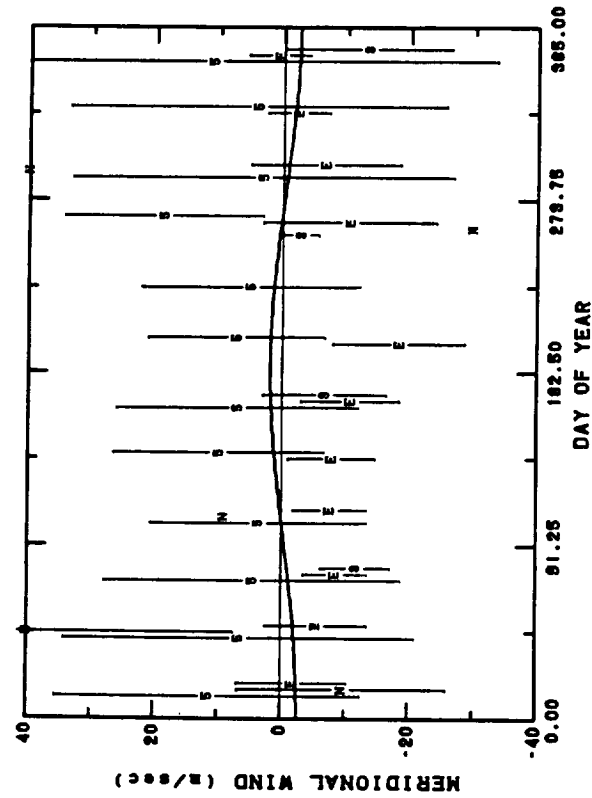
Fig. 10c. DL average meridional wind versus day of year for 65 to 75 and 75 to 85 km at southern middle latitudes. The HWM93 wind (solid line) shown for mid-range conditions. Plot symbols indicate data source as given in Table 1. Top row of plots contains rocket data and bottom row MF/Meteor radar data.
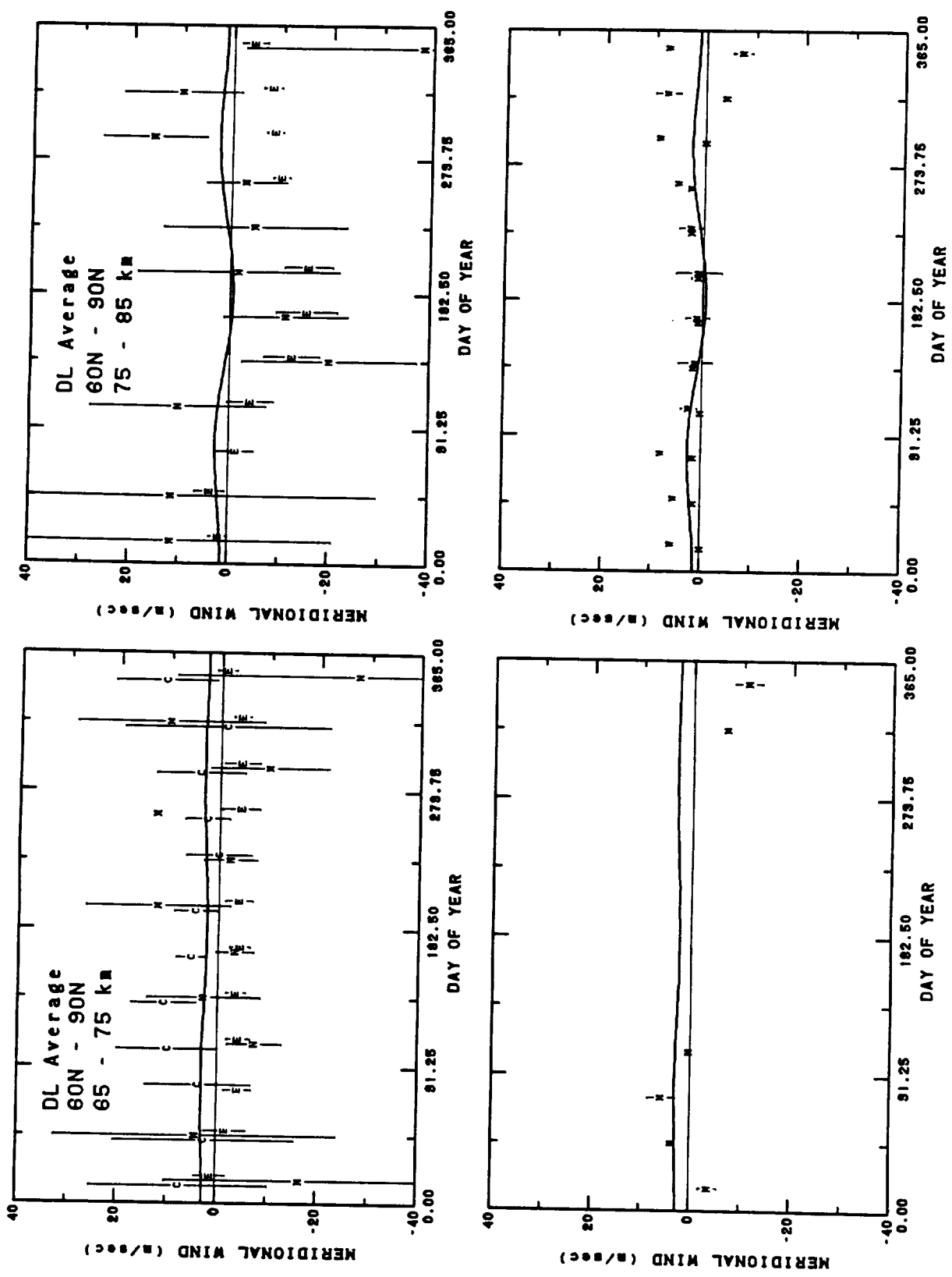
56

Fig. 10d. DL average meridional wind versus day of year for 85 to 95 and 95 to 105 km at southern middle latitudes. The HWM93 wind (solid line) shown for mid-range conditions. Plot symbols indicate data source as given in Table 1. Top row of plots contains rocket data and bottom row MF/Meteor radar data.

57

Fig. 10e. DL average meridional wind versus day of year for 65 to 75 and 75 to 85 km at southern low latitudes. The HWM93 wind (solid line) shown for mid-range conditions. Plot symbols indicate data source as given in Table 1. Top row of plots contains rocket data and bottom row MF/Meteor radar data.
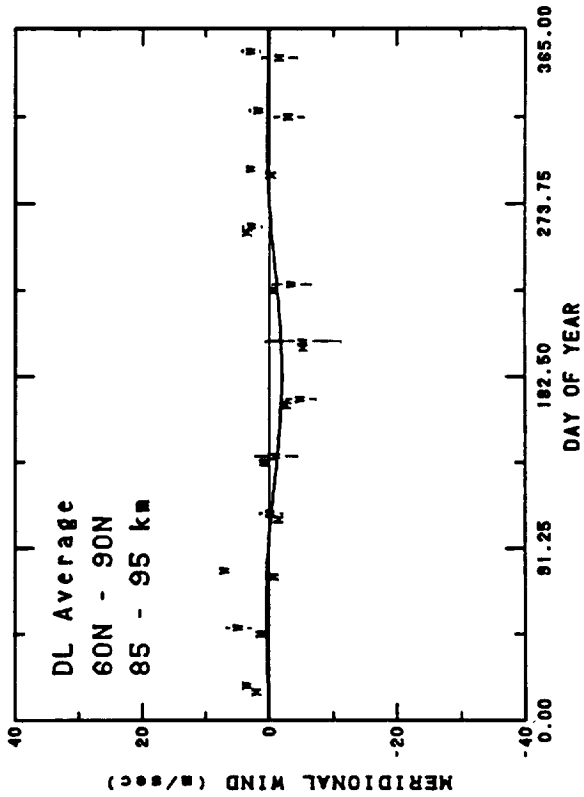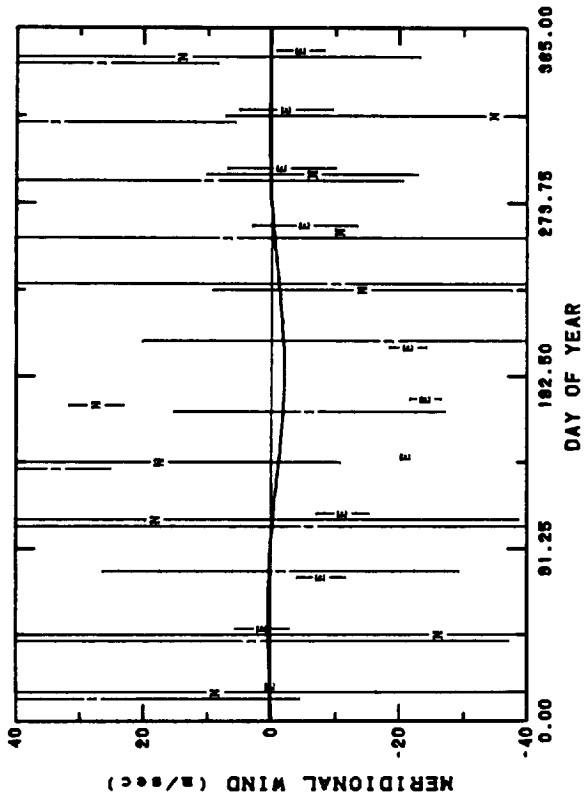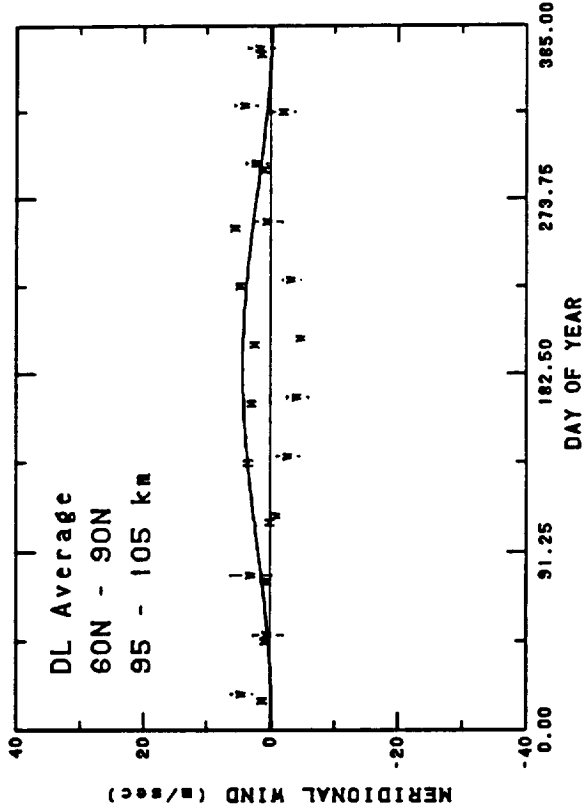
Fig. 10f. DL average meridional wind versus day of year for 85 to 95 and 95 to 105 km at southern low latitudes. The HWM93 wind (solid line) shown for mid-range conditions. Plot symbols indicate data source as given in Table 1. Top row of plots contains rocket data and bottom row MF/Meteor radar data.
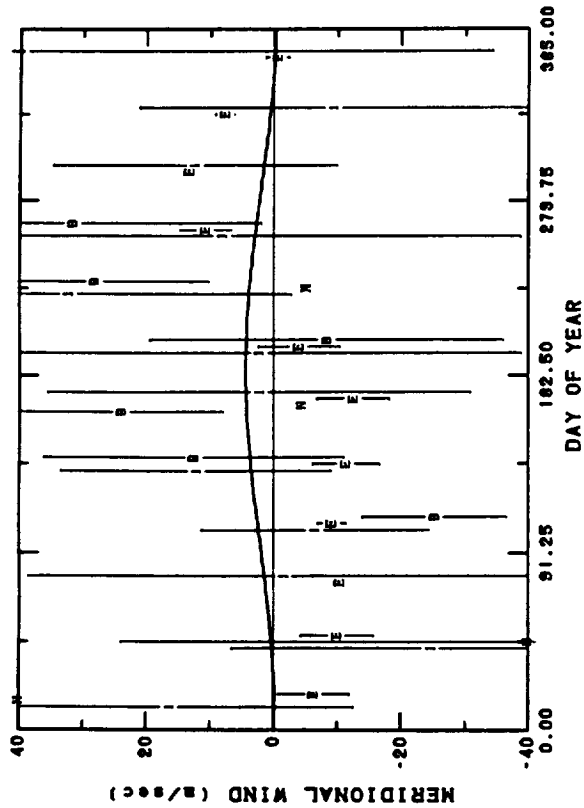
59

Fig. 10g. DL average meridional wind versus day of year for 65 to 75 and 75 to 85 km at northern low latitudes. The HWM93 wind (solid line) shown for mid-range conditions. Plot symbols indicate data source as given in Table 1. Top row of plots contains rocket data and bottom row MF/Meteor radar data.

60

Fig. 10h. DL average meridional wind versus day of year for 85 to 95 and 95 to 105 km at northern low latitudes. The HWM93 wind (solid line) shown for mid-range conditions. Plot symbols indicate data source as given in Table 1. Top row of plots contains rocket and IS data and bottom row MF/Meteor radar data.

61

Fig. 101. DL average meridional wind versus day of year for 65 to 75 and 75 to 85 km at northern middle latitudes. The HWM93 wind (solid line) shown for mid-range conditions. Plot symbols indicate data source as given in Table 1. Top row of plots contains rocket data and bottom row MF/Meteor radar data.

62

Fig. 10j. DL average meridional wind versus day of year for 85 to 95 and 95 to 105 km at northern middle latitudes. The HWM93 wind (solid line) shown for mid-range conditions. Plot symbols indicate data source as given in Table 1. Top row of plots contains rocket and IS data and bottom row MF/Meteor radar data.

Fig. 10k. DL average meridional wind versus day of year for 65 to 75 and 75 to 85 km at northern high latitudes. The HWM93 wind (solid line) shown for mid-range conditions. Plot symbols indicate data source as given in Table 1. Top row of plots contains rocket data and bottom row MF/Meteor radar data.

Fig. 101. DL average meridional wind versus day of year for 85 to 95 and 95 to 105 km at northern high latitudes. The HWM93 wind (solid line) shown for mid-range conditions. Plot symbols indicate data source as given in Table 1. Top row of plots contains rocket and IS data and bottom row MF/Meteor radar data.

65
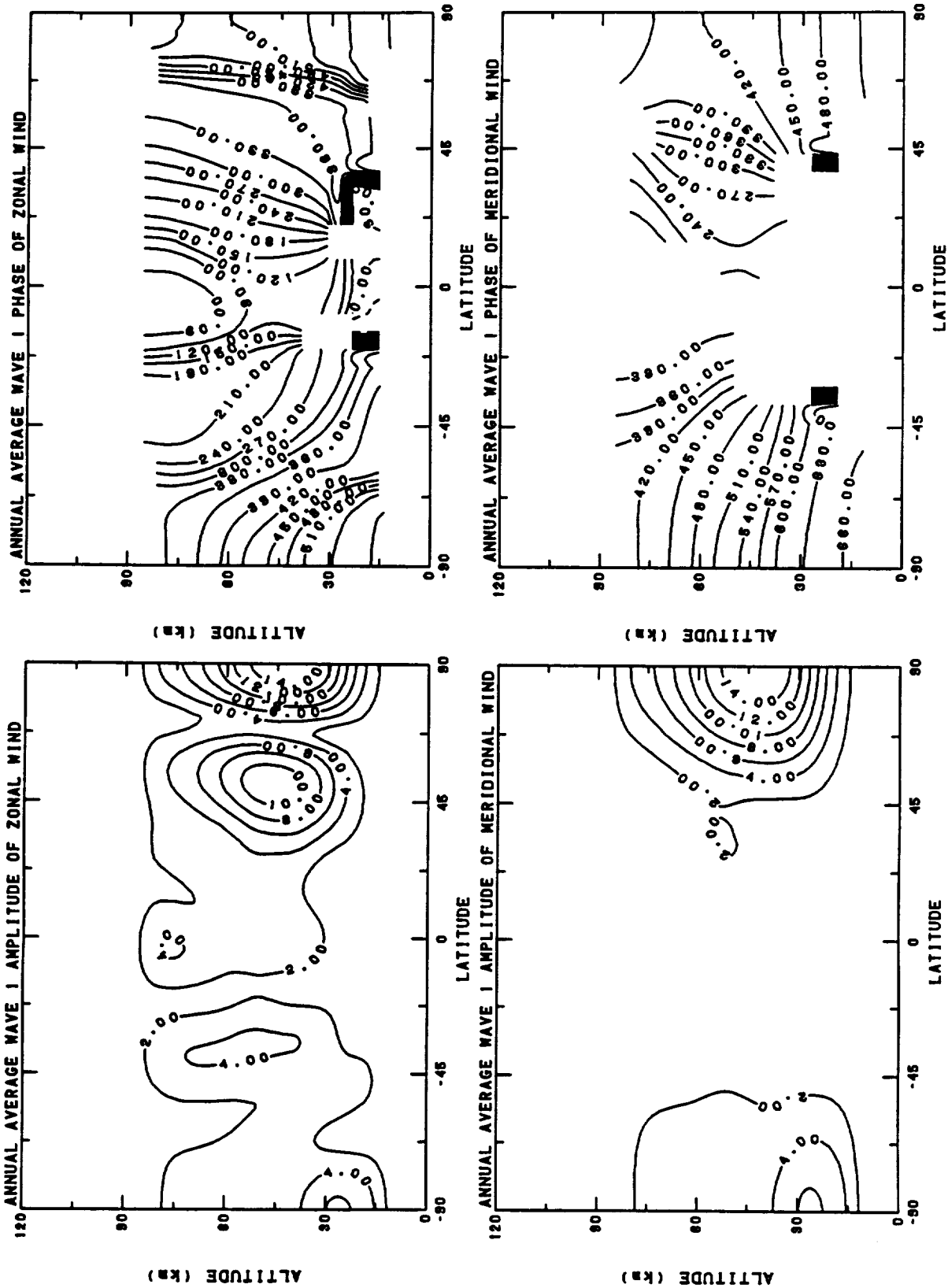
Fig. 11. Contour plots in altitude versus latitude of the seasonal and diurnal (SD) average wave 1 amplitude and phase of the zonal and meridional wind.

66
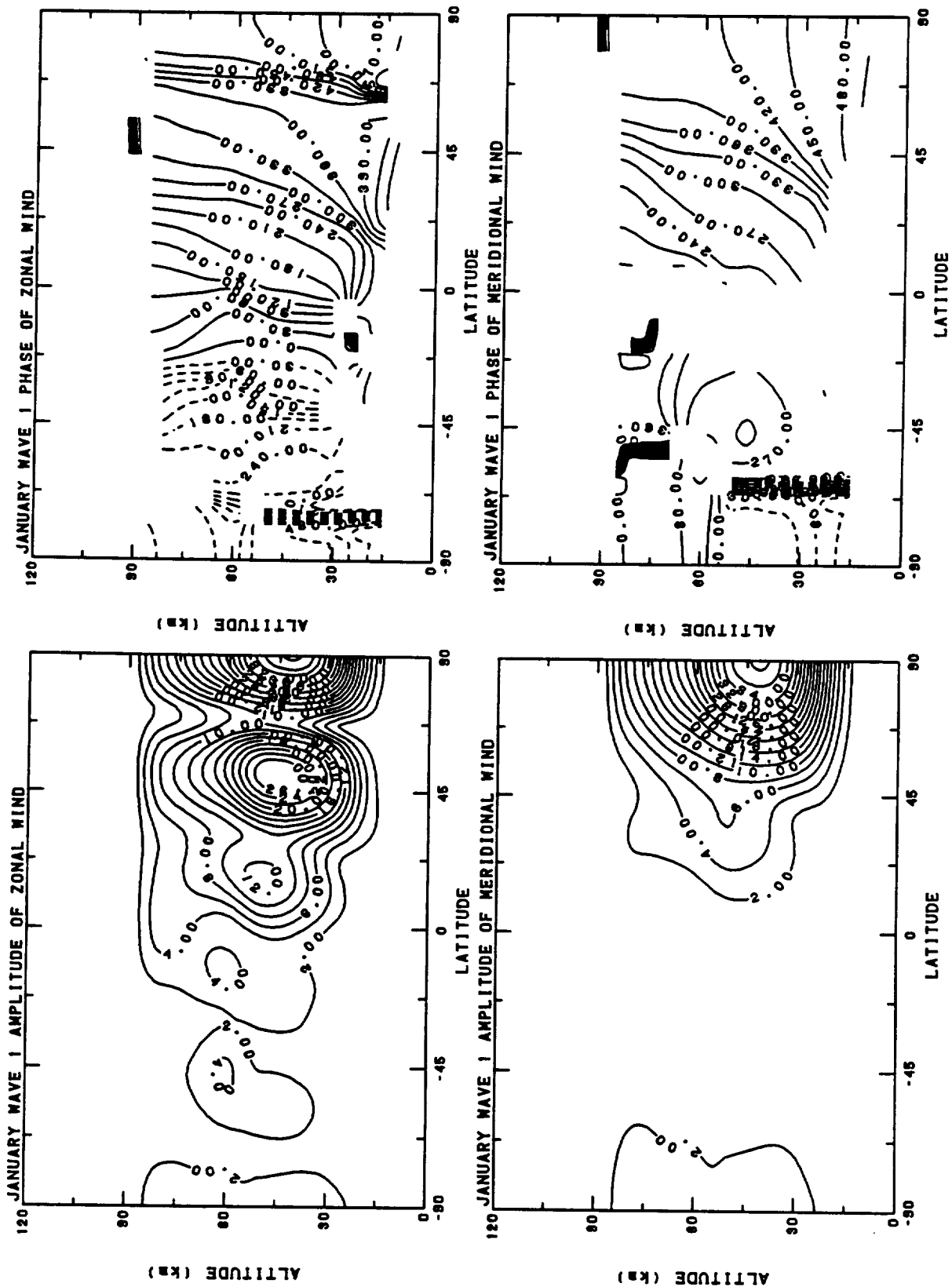
Fig. 12a. Contour plots in altitude versus latitude of the wave 1 amplitude and phase for the zonal and meridional wind for January (midmonth).

67
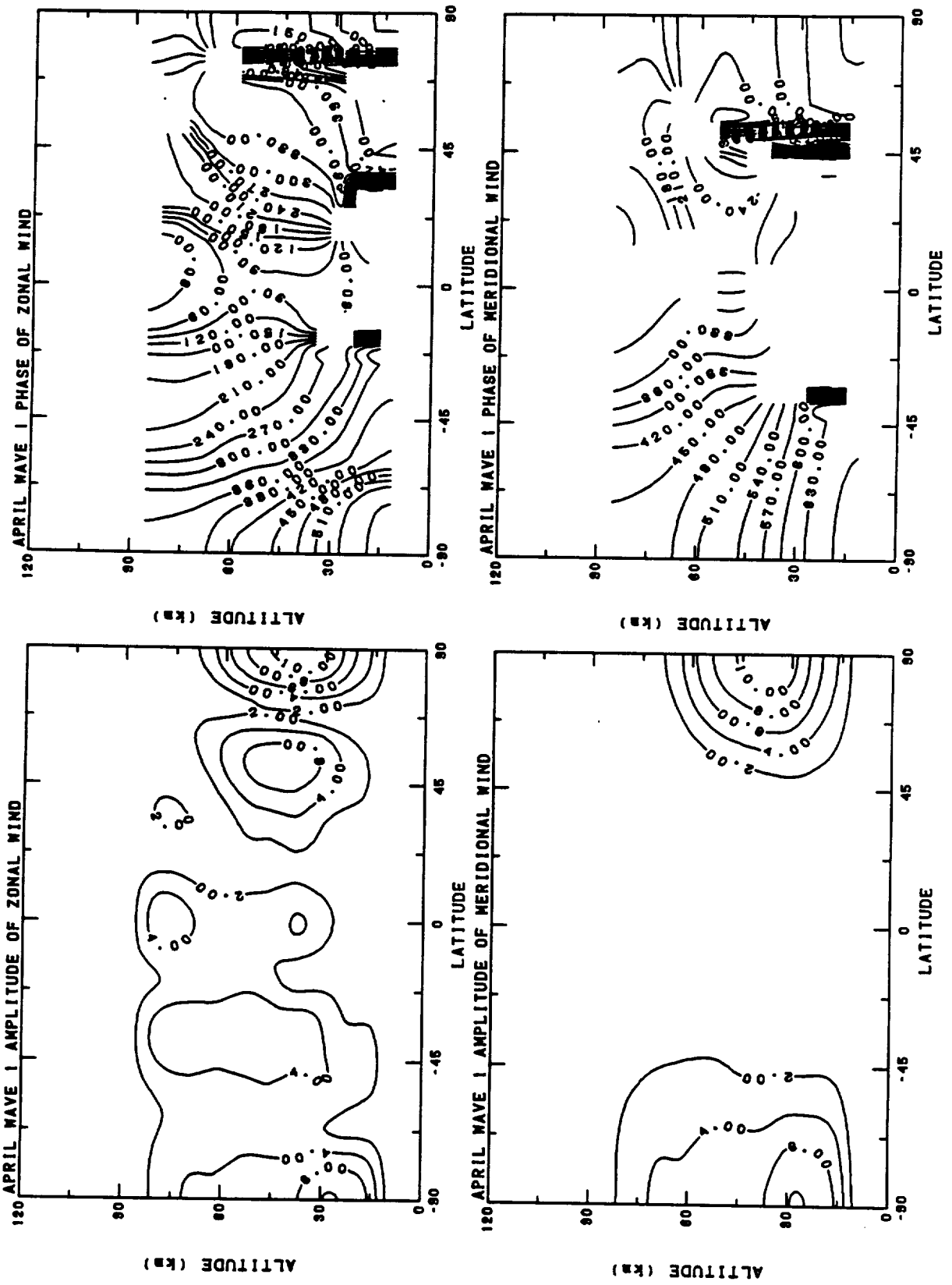
Fig. 12b. Contour plots in altitude versus latitude of the wave 1 amplitude and phase for the zonal and meridional wind for April (midmonth).
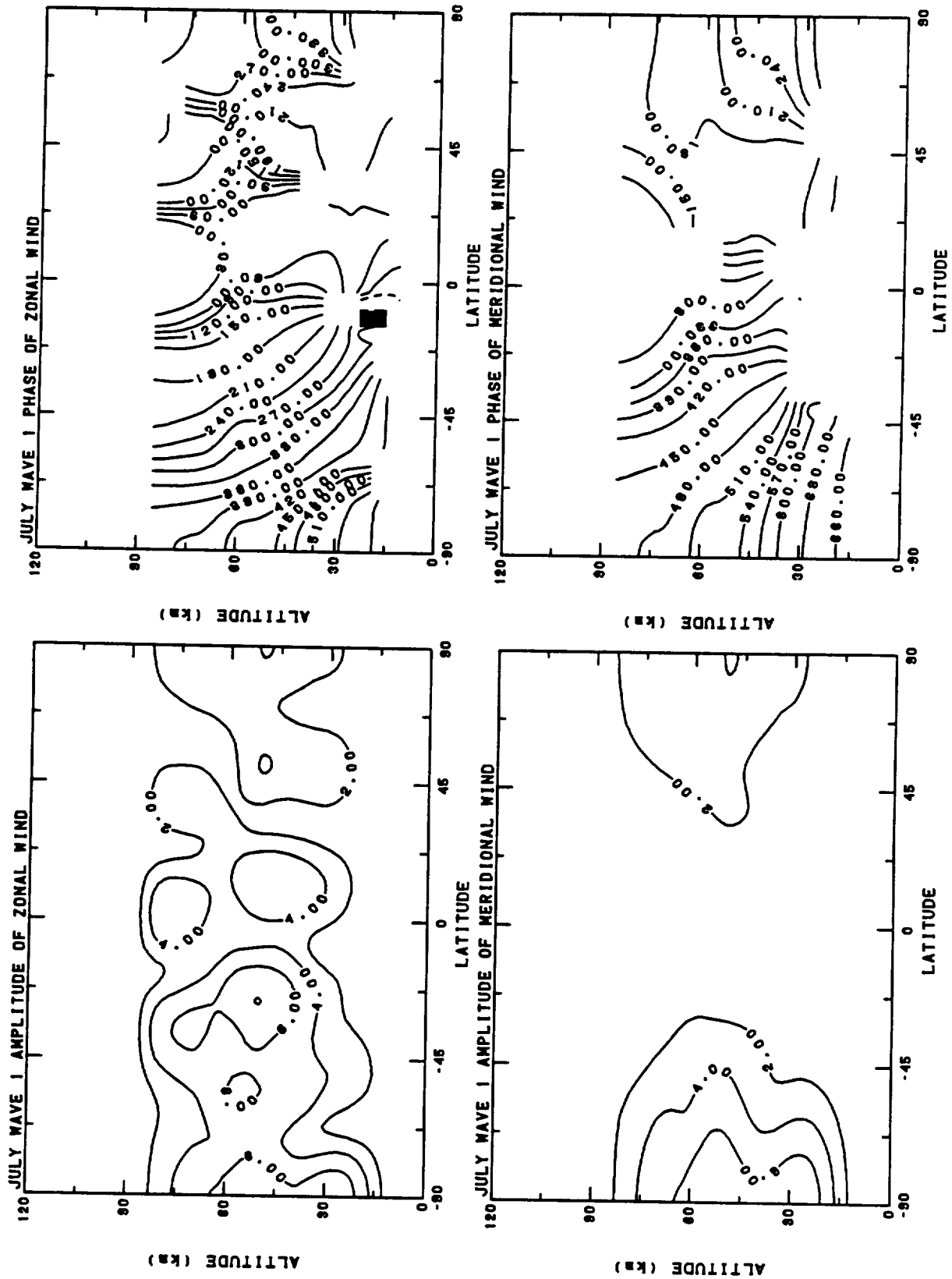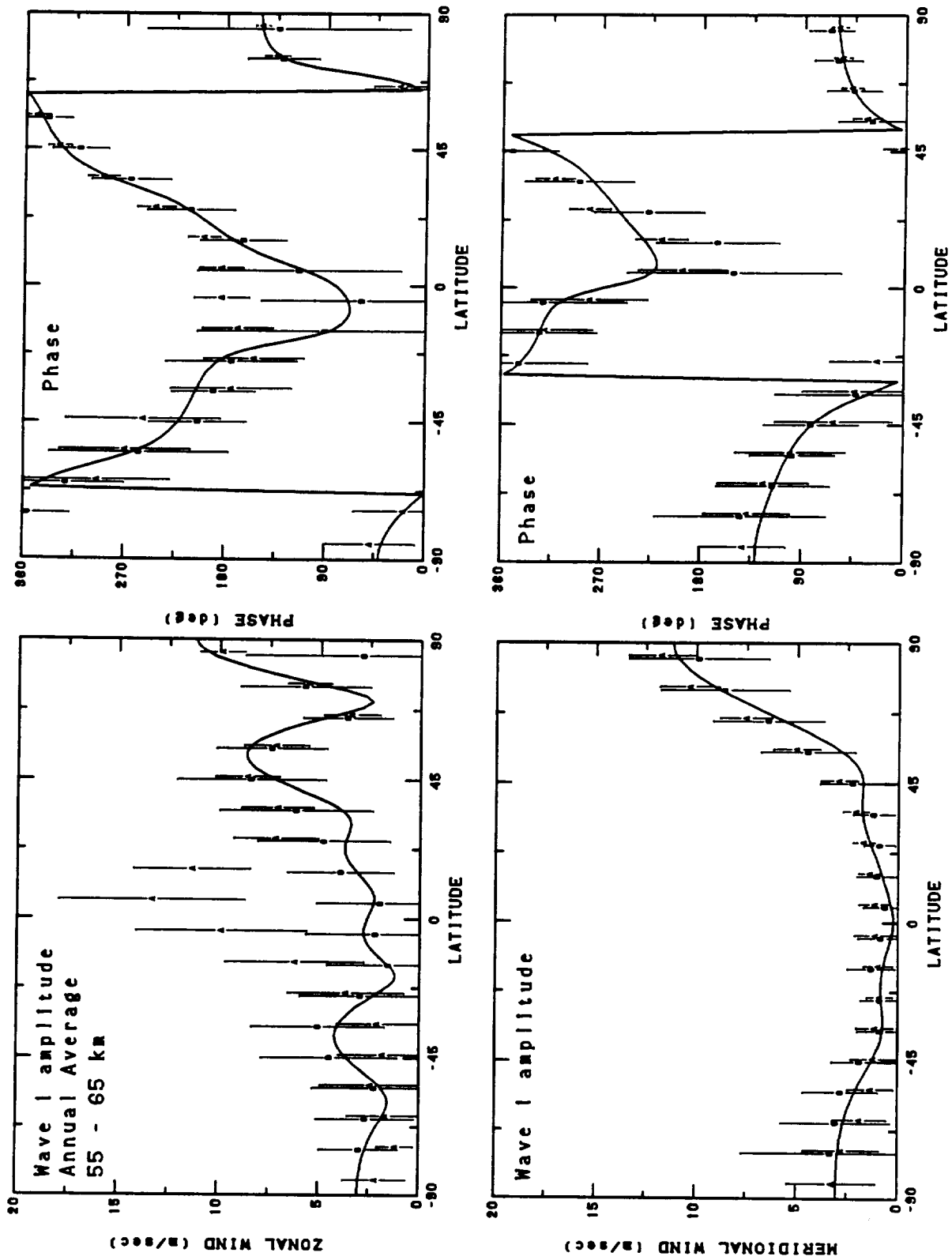
68

Fig. 12c. Contour plots in altitude versus latitude of the wave 1 amplitude and phase for the zonal and meridional wind for July (midmonth).

69
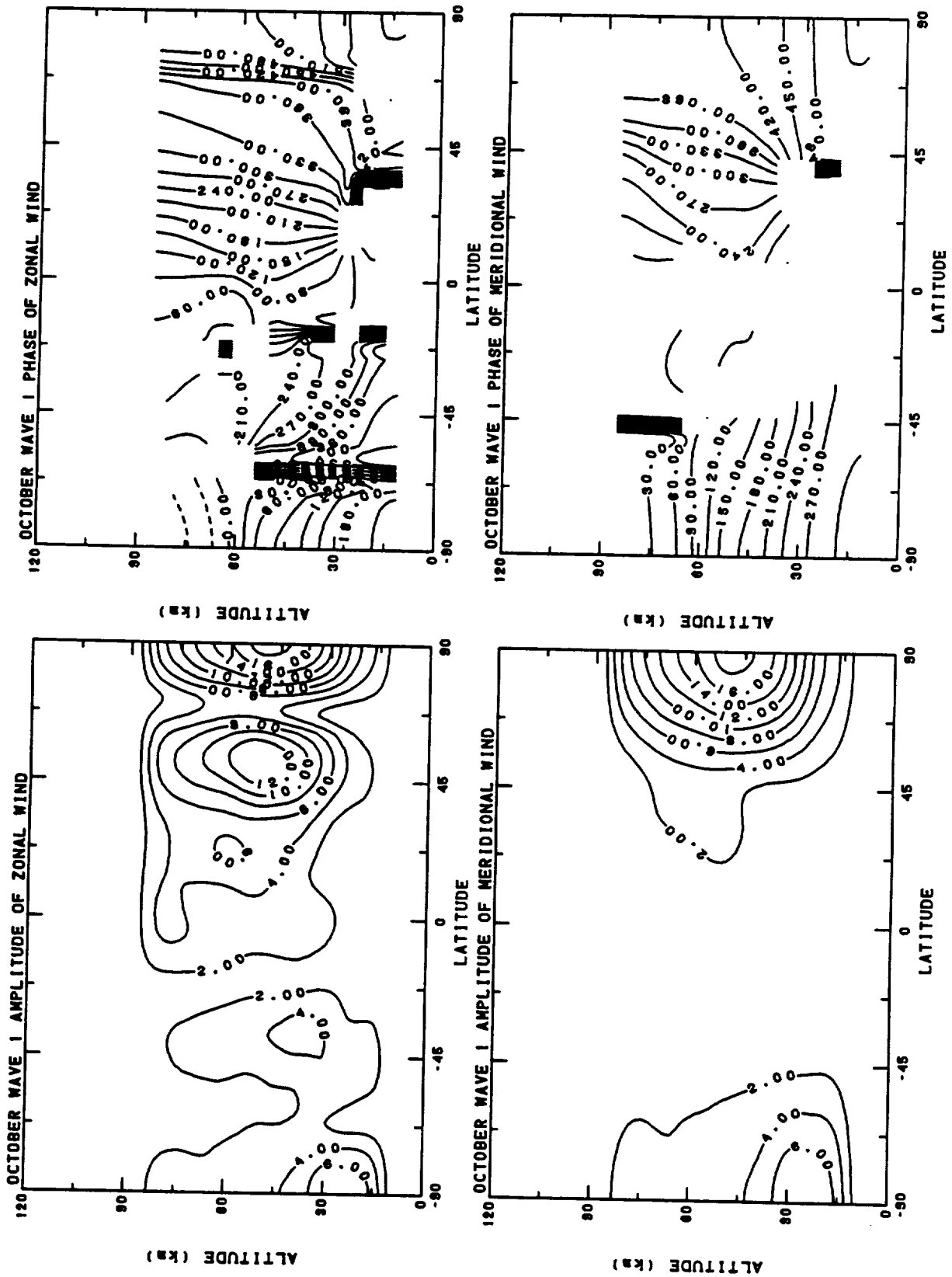
Fig. 12d. Contour plots in altitude versus latitude of the wave 1 amplitude and phase for the zonal and meridional wind for October (midmonth).

70

Fig. 13a. Amplitude and phase of wave 1 zonal and meridional wind versus latitude for seasonal (annual) average for 55 to 65 km. The HWM93 model (solid line) is shown for mid-range conditions and compared to gradient wind calculations.
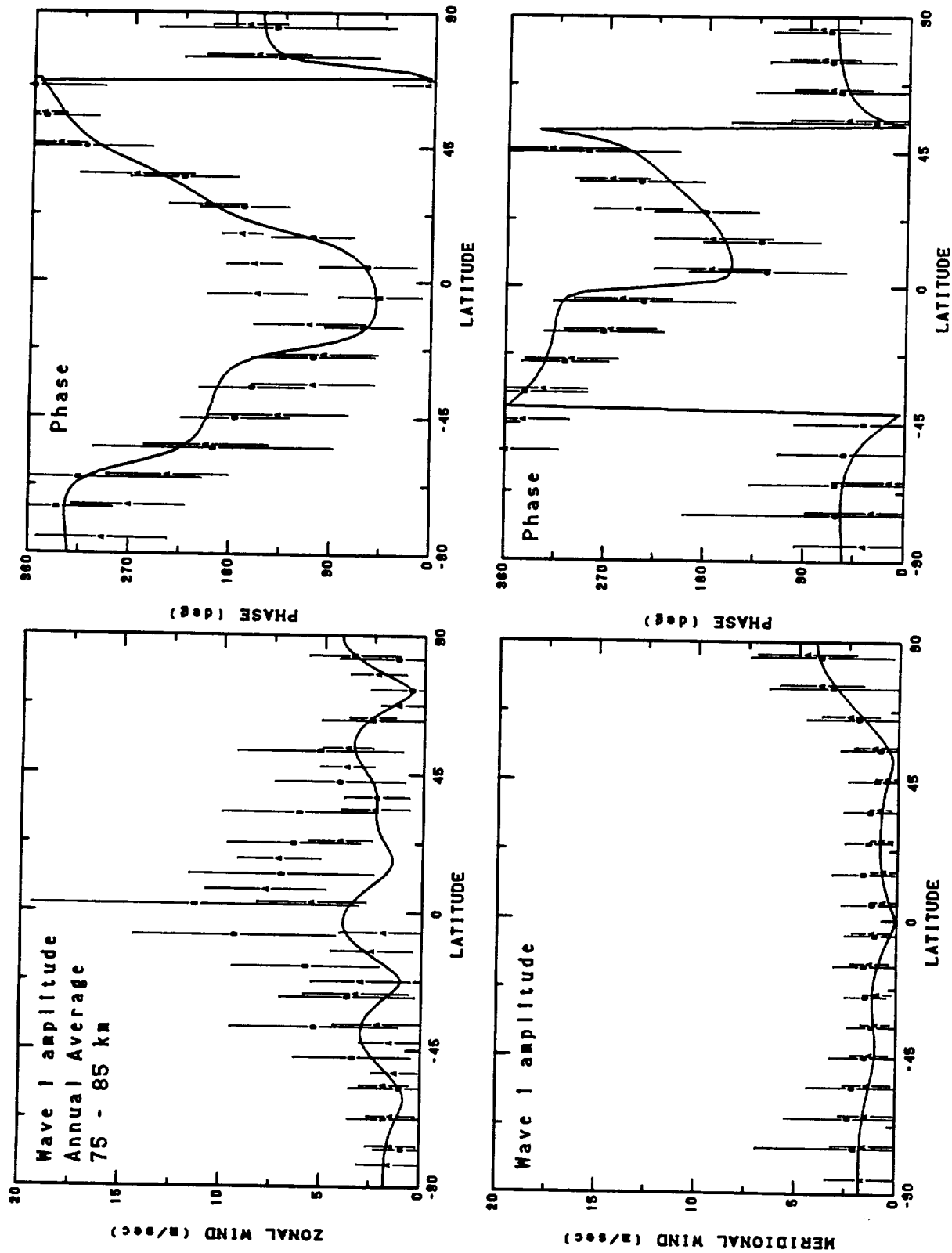
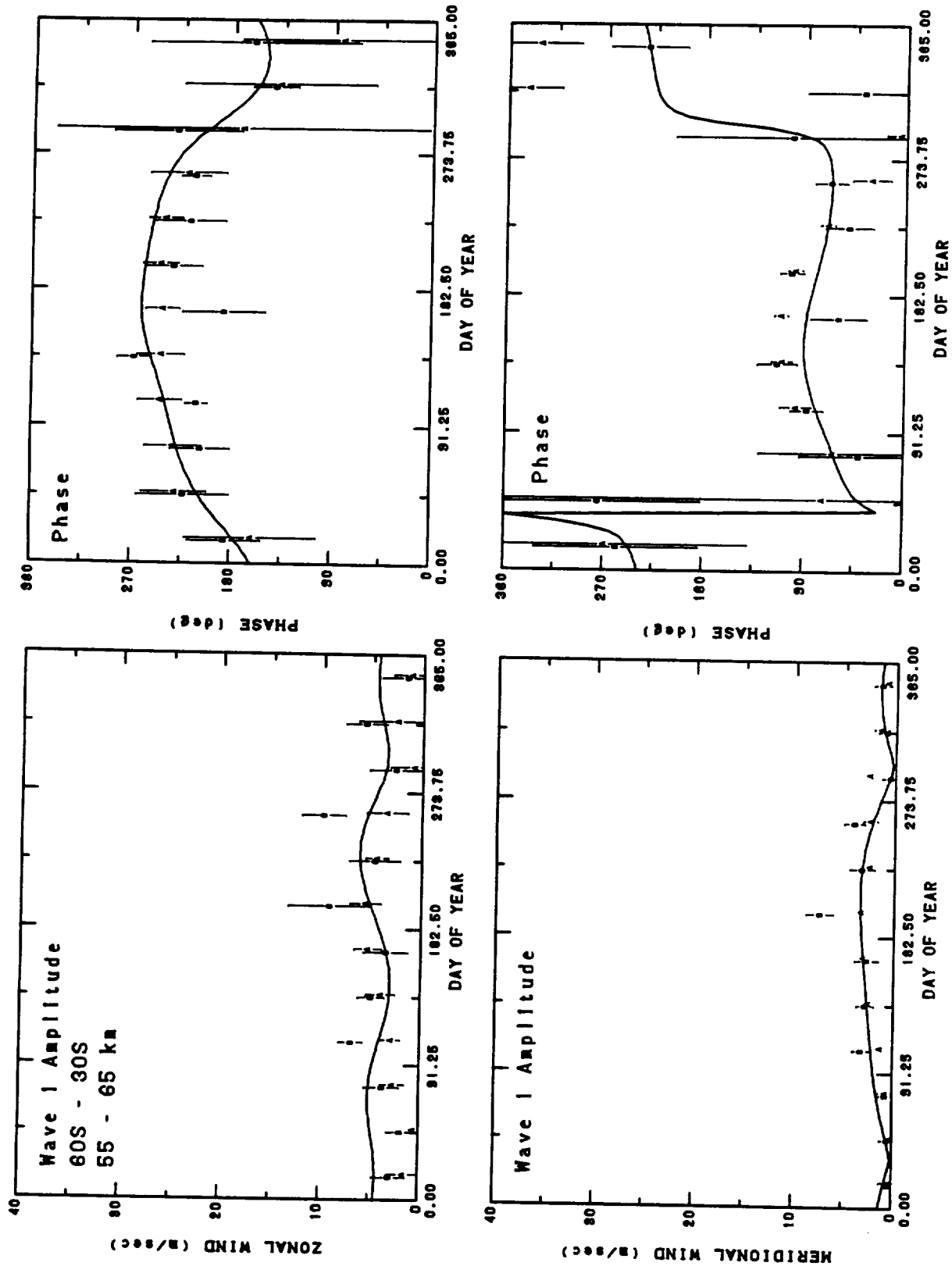Fig. 13b. Amplitude and phase of wave 1 zonal and meridional wind versus latitude for seasonal (annual) average for 75 to 85 km. The HWM93 model (solid line) is shown for mid-range conditions and compared to gradient wind calculations.
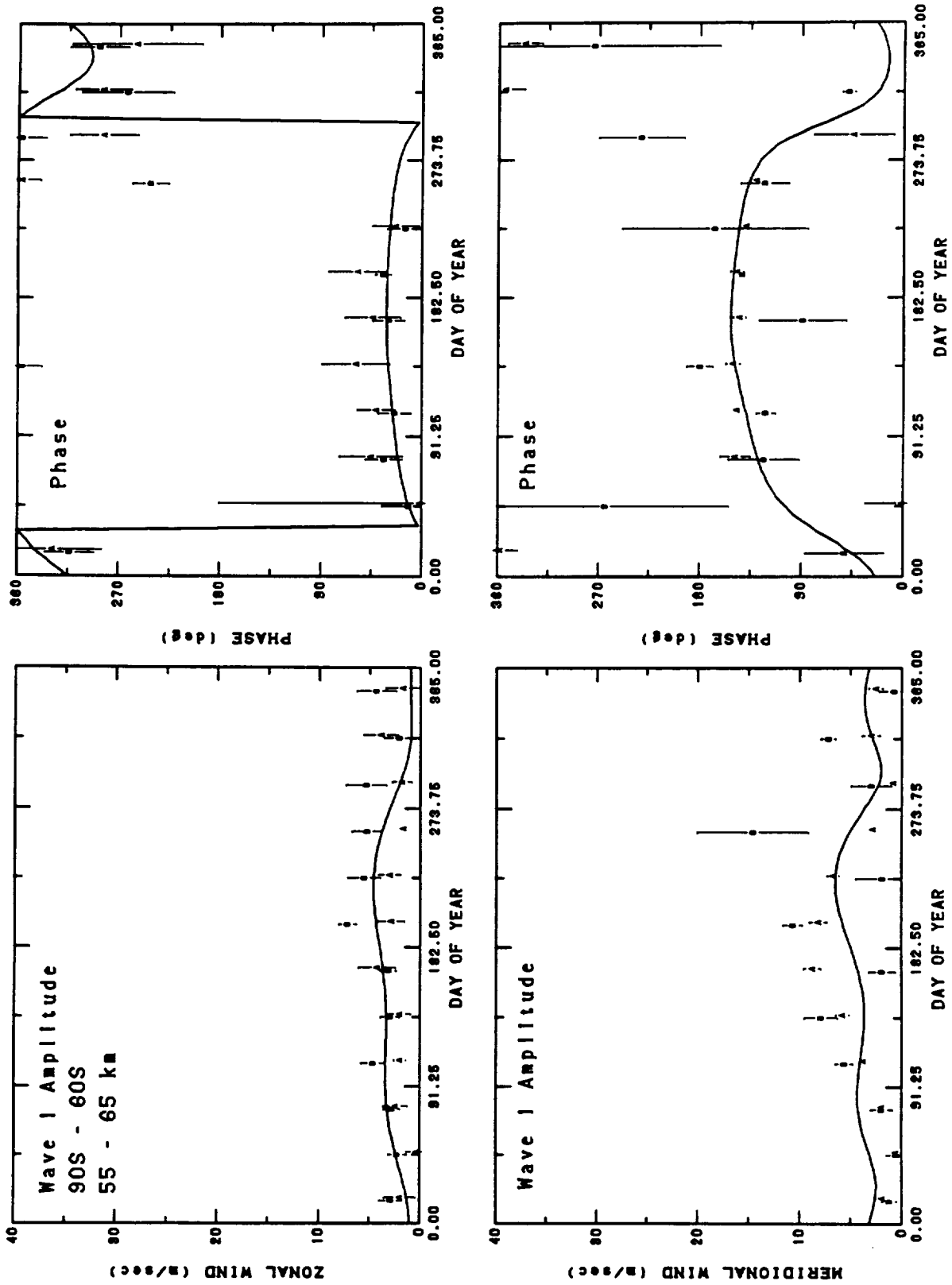
Fig. 14a. Amplitude and phase of wave 1 zonal and meridional wind versus day of year for 55 to 65 km at southern high latitudes. The HWM93 model (solid line) is shown for mid-range conditions and compared to gradient wind calculations.
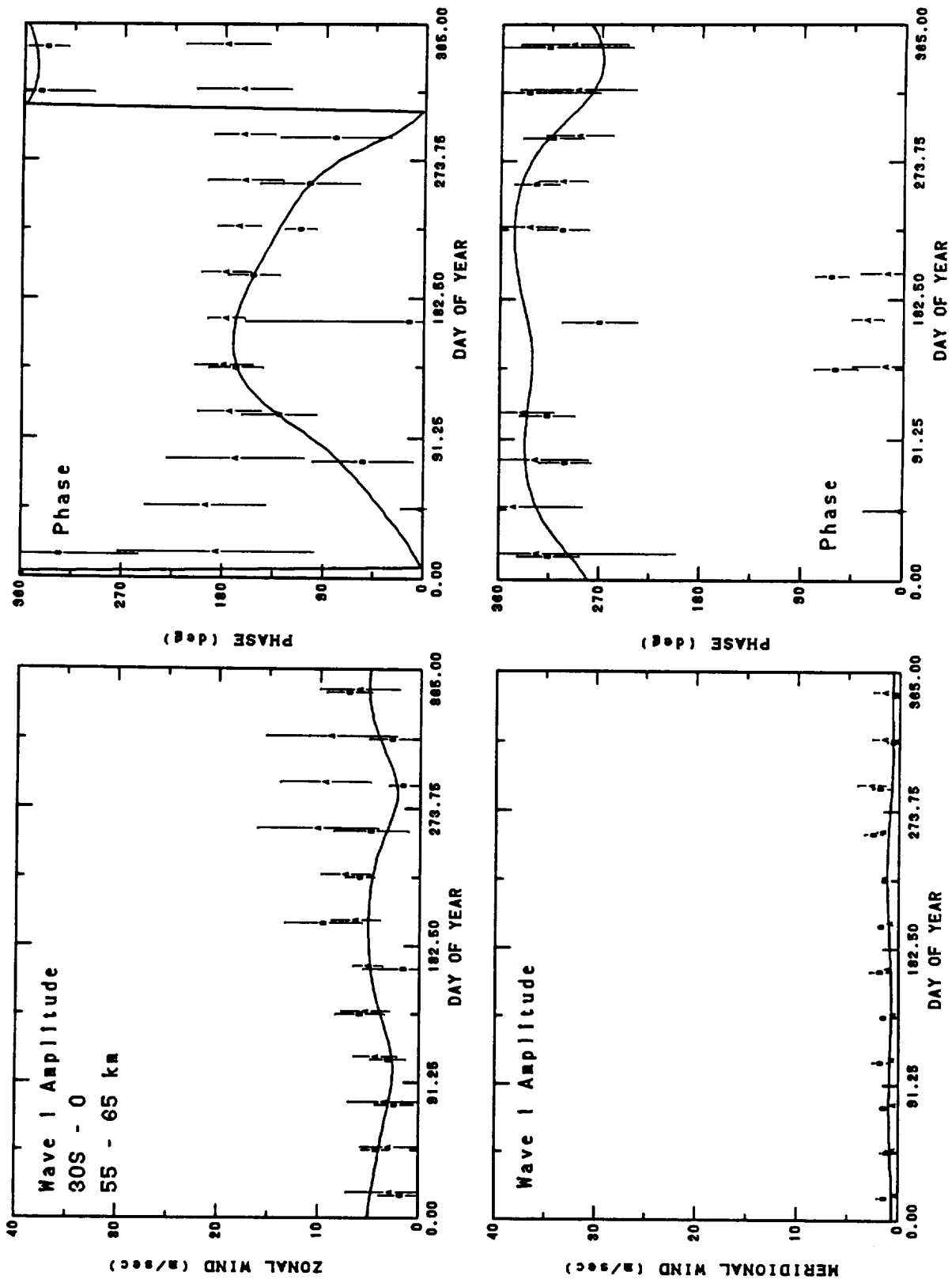
Fig. 14b. Amplitude and phase of wave 1 zonal and meridional wind versus day of year for 55 to 65 km at southern middle latitudes. The HWM93 model (solid line) is shown for mid-range conditions and compared to gradient wind calculations.
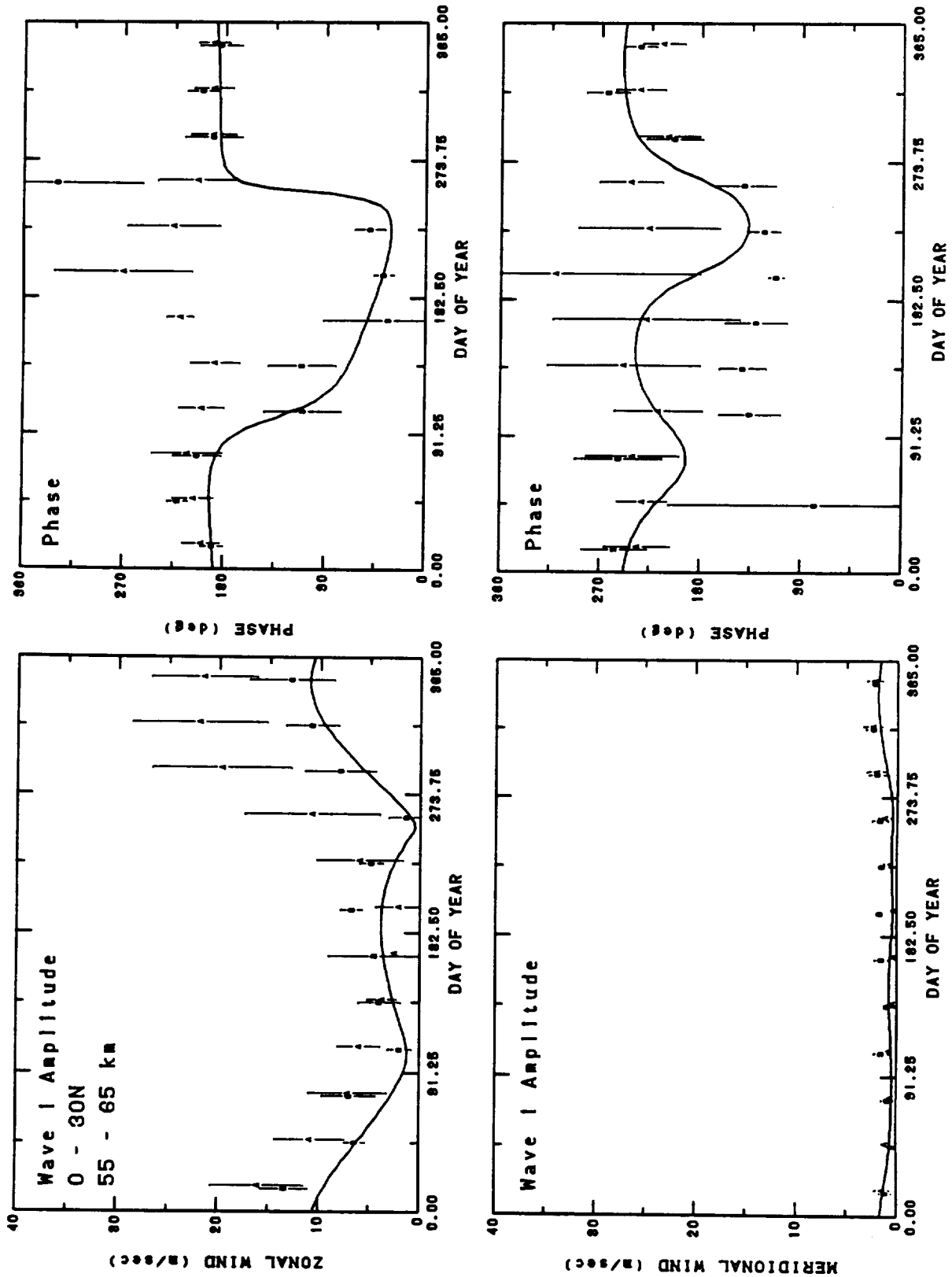
Fig. 14c. Amplitude and phase of wave 1 zonal and meridional wind versus day of year for 55 to 65 km at southern low latitudes. The HWM93 model (solid line) is shown for mid-range conditions and compared to gradient wind calculations.
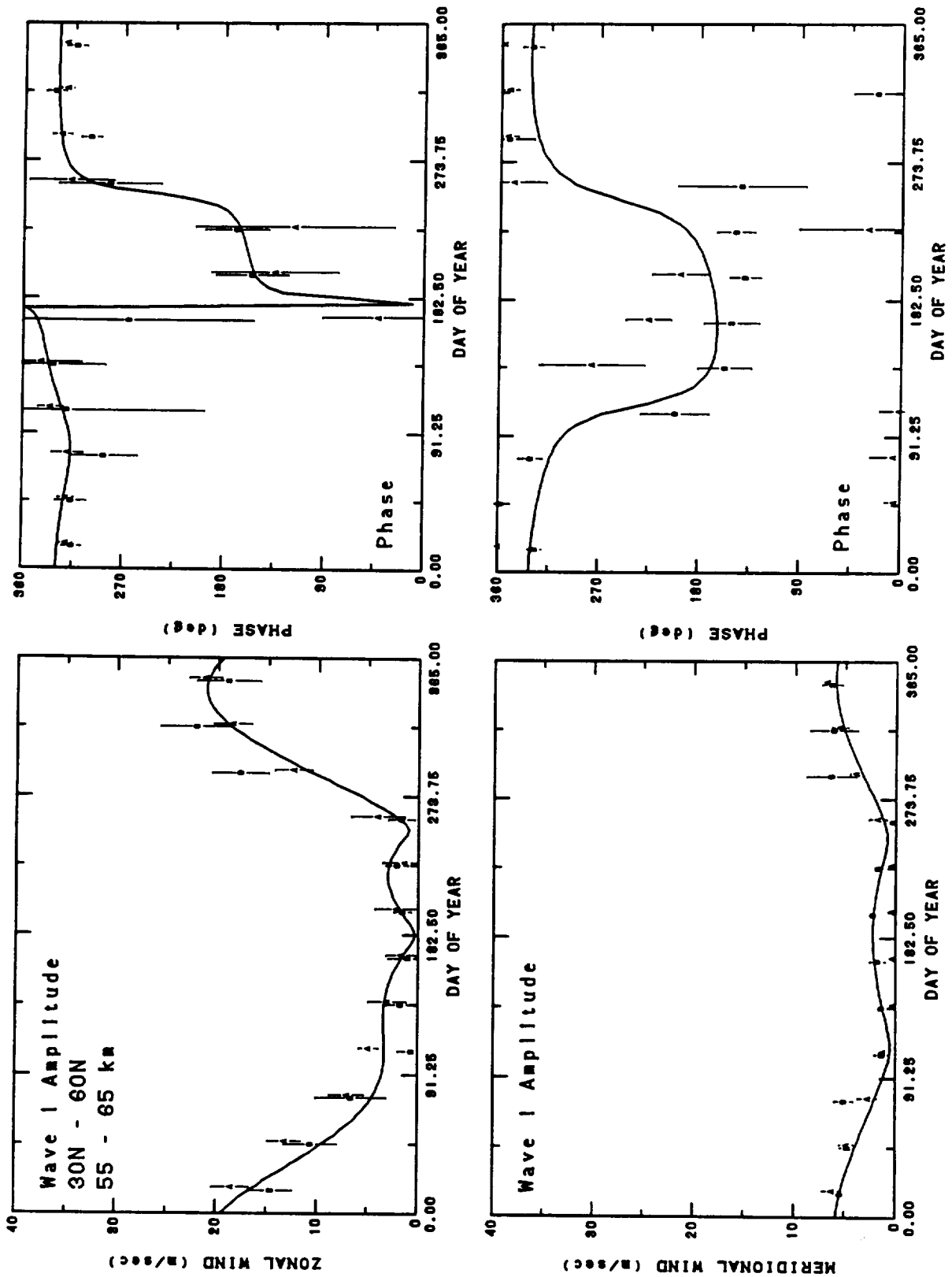
Fig. 14d. Amplitude and phase of wave 1 zonal and meridional wind versus day of year for 55 to 65 km at northern low latitudes. The HWM93 model (solid line) is shown for mid-range conditions and compared to gradient wind calculations.

76

Fig. 14e. Amplitude and phase of wave 1 zonal and meridional wind versus day of year for 55 to 65 km at northern middle latitudes. The HWM93 model (solid line) is shown for mid-range conditions and compared to gradient wind calculations.
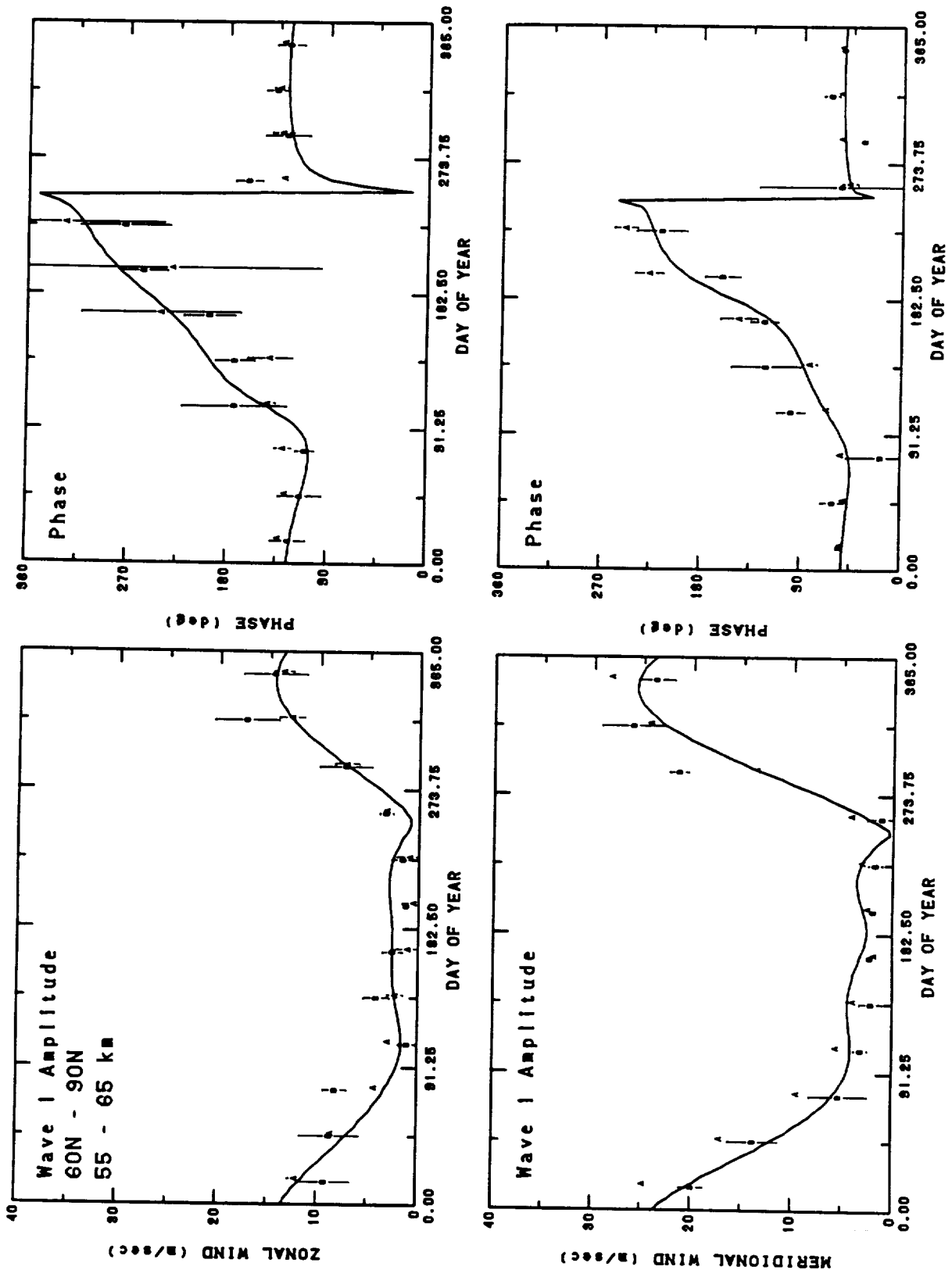
Fig. 14f. Amplitude and phase of wave 1 zonal and meridional wind versus day of year for 55 to 65 km at northern high latitudes. The HWM93 model (solid line) is shown for mid-range conditions and compared to gradient wind calculations.
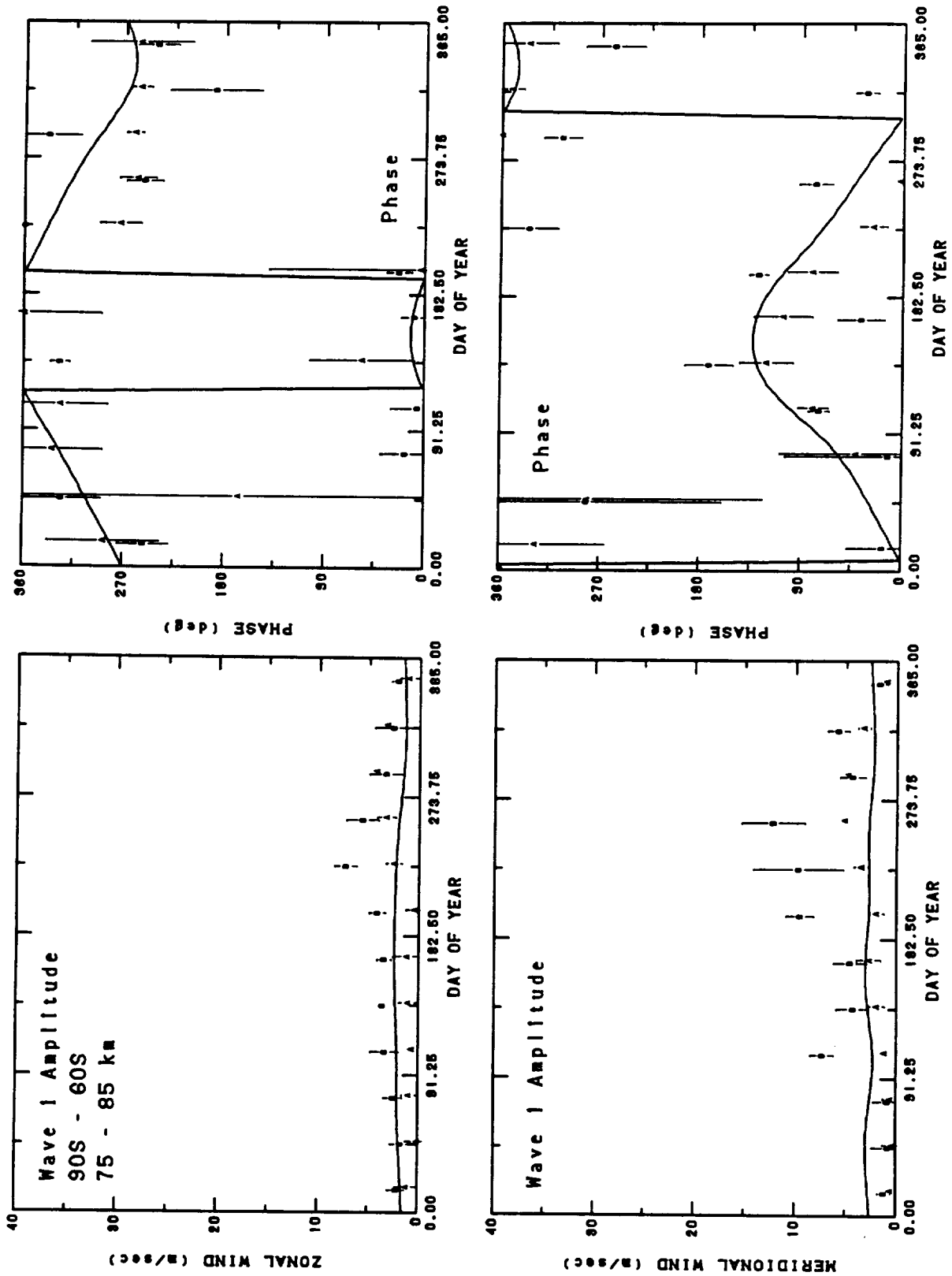
78

Fig. 14g. Amplitude and phase of wave 1 zonal and meridional wind versus day of year for 75 to 85 km at southern high latitudes. The HWM93 model (solid line) is shown for mid-range conditions and compared to gradient wind calculations.
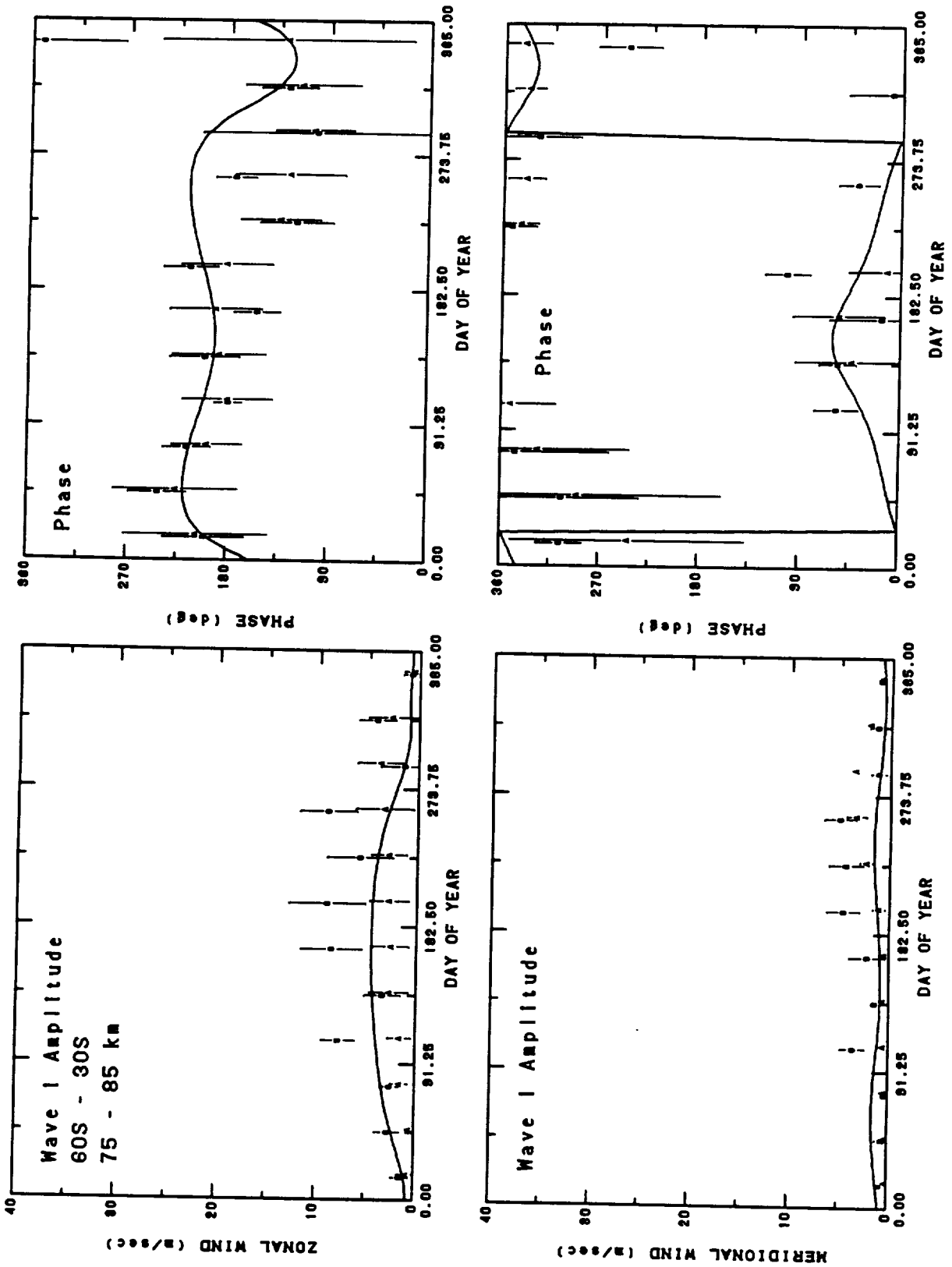
79

Fig. 14h. Amplitude and phase of wave 1 zonal and meridional wind versus day of year for 75 to 85 km at southern middle latitudes. The HWM93 model (solid line) is shown for mid-range conditions and compared to gradient wind calculations.
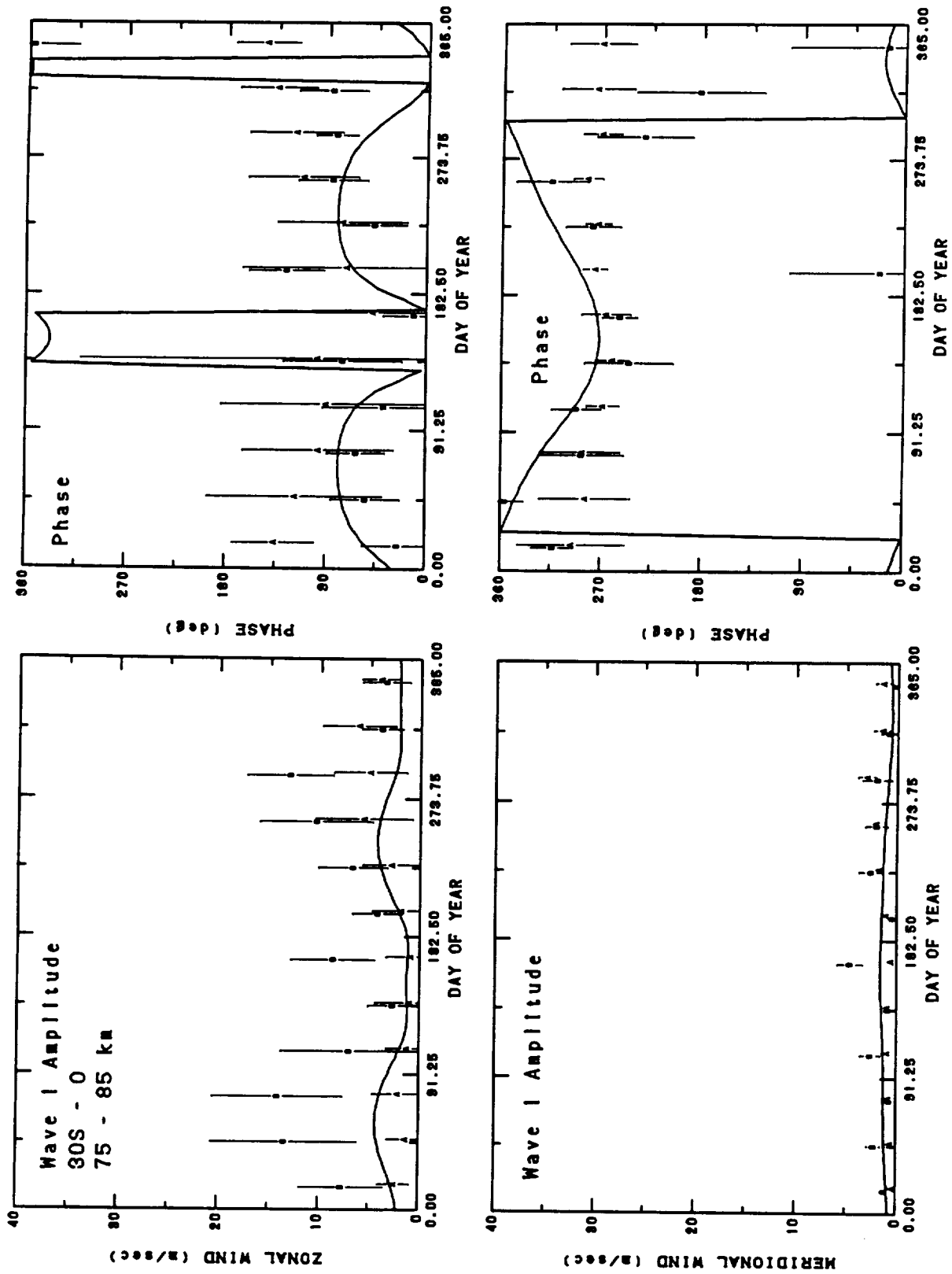
Fig. 141. Amplitude and phase of wave 1 zonal and meridional wind versus day of year for 75 to 85 km at southern low latitudes. The HWM93 model (solid line) is shown for mid-range conditions and compared to gradient wind calculations.

81

Fig. 14j. Amplitude and phase of wave 1 zonal and meridional wind versus day of year for 75 to 88 km at northern low latitudes. The HWM93 model (solid line) is shown for mid-range conditions and compared to gradient wind calculations.
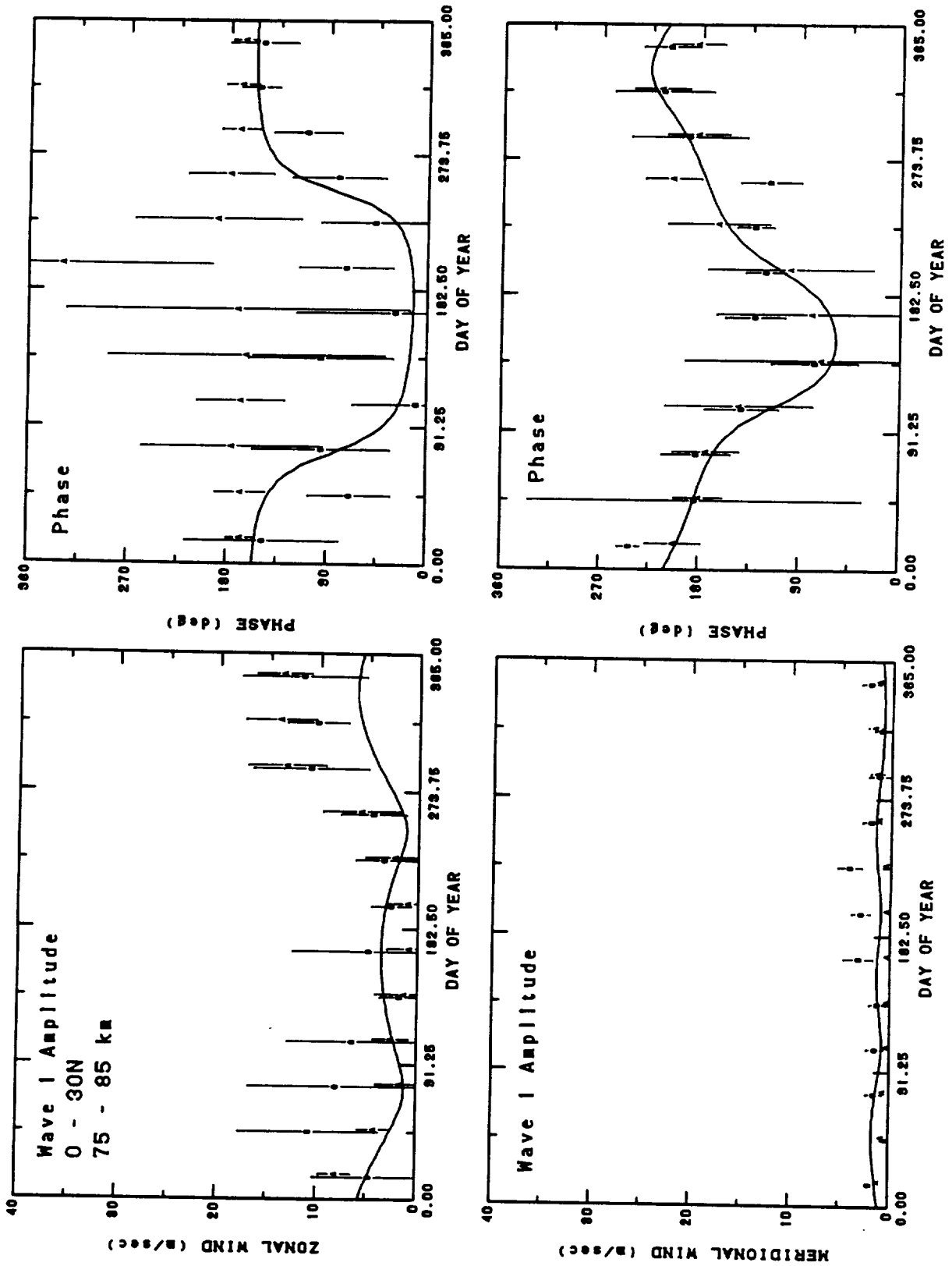
82

Fig. 14k. Amplitude and phase of wave 1 zonal and meridional wind versus day of year for 75 to 85 km at northern middle latitudes. The HWM93 model (solid line) is shown for mid-range conditions and compared to gradient wind calculations.

Fig. 141. Amplitude and phase of wave 1 zonal and meridional wind versus day of year for 75 to 85 km at northern high latitudes. The HWM93 model (solid line) is shown for mid-range conditions and compared to gradient wind calculations.
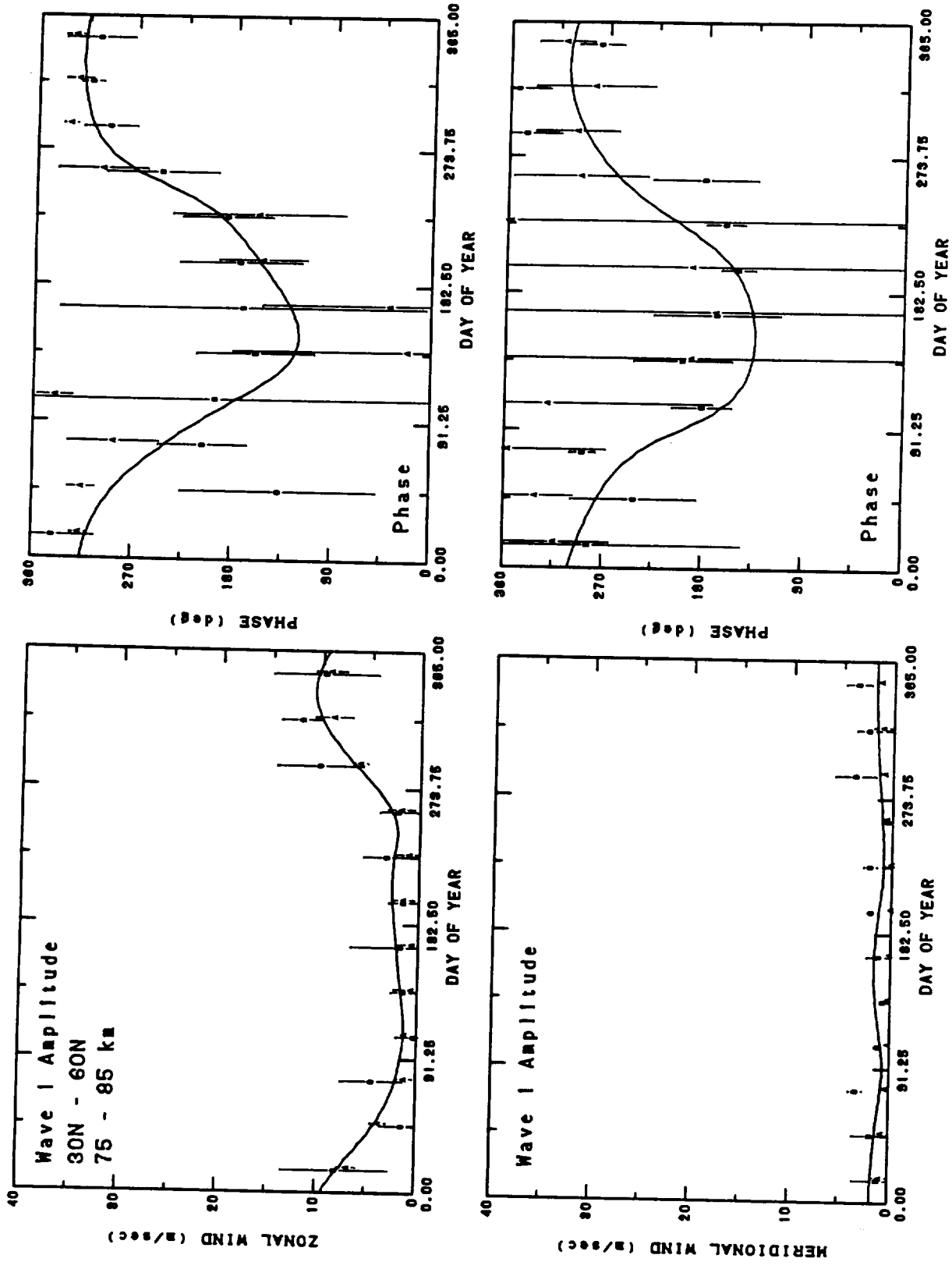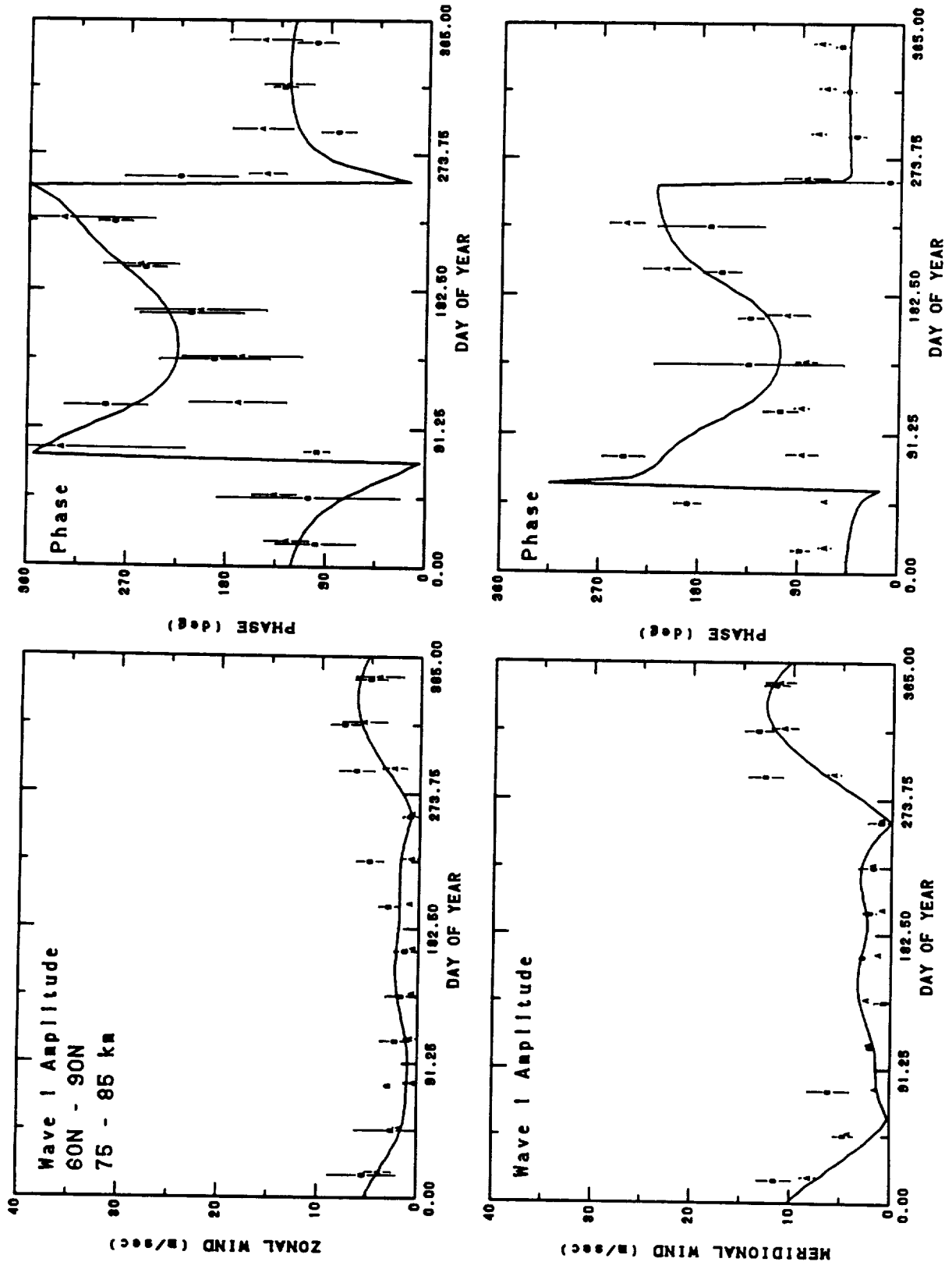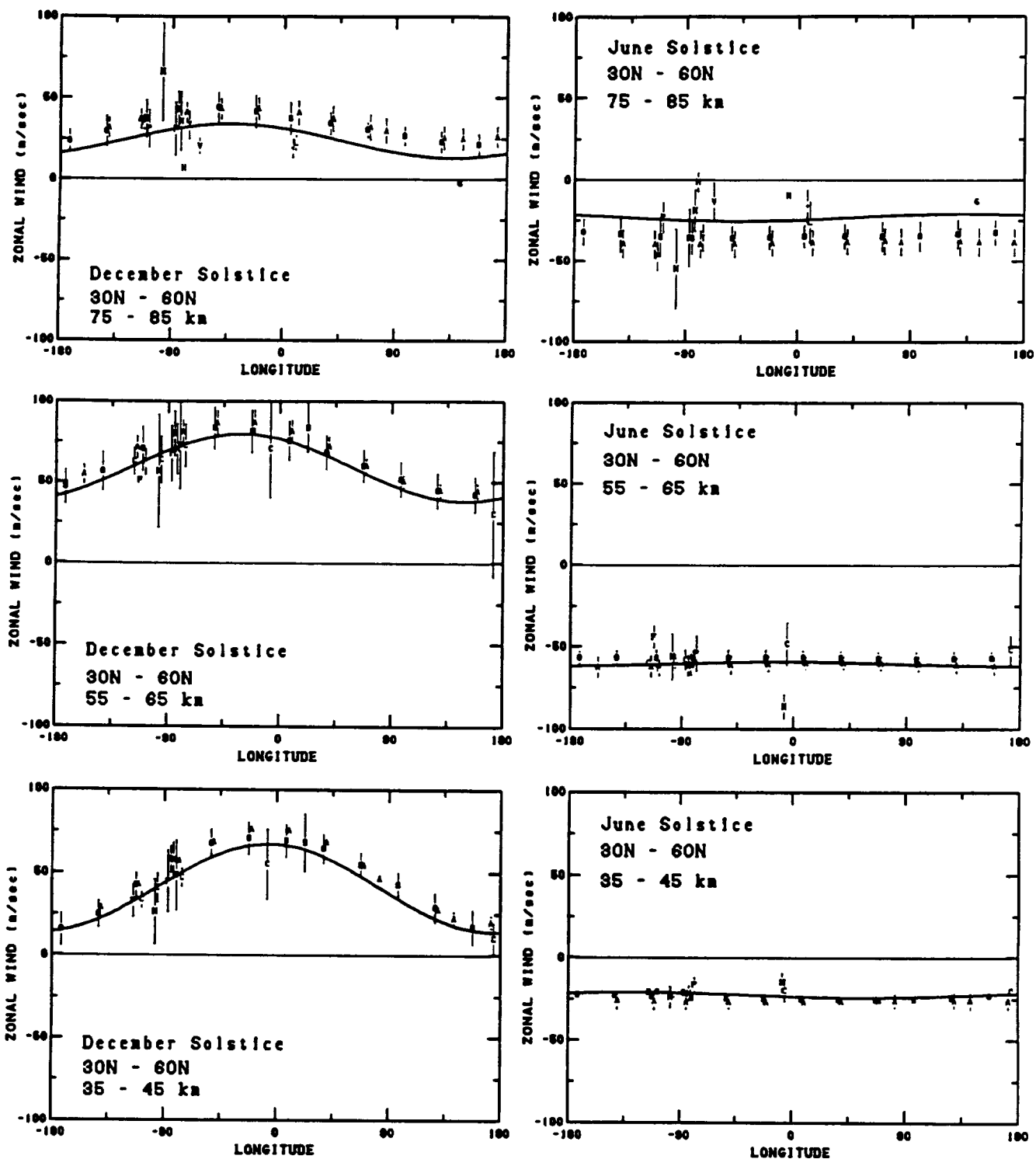
Fig. 15. Zonal wind versus longitude for model and data at northern
mid-latitudes and selected altitudes.

REPORT DOCUMENTATION PAGE

Public reporting burden for this collection of information is estimated to average 1 hour per response, including the time for reviewing instructions, searching existing data sources, gathering and maintaining the data needed, and completing and reviewing the collection of information. Send comments regarding this burden estimate or any other aspect of this collection of information, including suggestions for reducing this burden, to Washington Headquarters Services, Directorate for Information Operations and Reports, 1215 Jefferson Davis Highway, Suite 1204, Arlington, VA 22202-4302, and to the Office of Management and Budget, Paperwork Reduction Project (0704-0188), Washington, DC 20503.

1. AGENCY USE ONLY (Leave blank)	2. REPORT DATE	3. REPORT TYPE AND DATES COVERED
	April 1993	Technical Memorandum

4. TITLE AND SUBTITLE
Empirical Wind Model for the Middle and Lower Atmosphere—
Part 1: Local Time Average

5. FUNDING NUMBERS

910

6. AUTHOR(S)
A. E. Hedin, E. L. Fleming, A. H. Manson, F. J. Schmidlin,
S. K. Avery, and S. J. Franke

7. PERFORMING ORGANIZATION NAME(S) AND ADDRESS(ES)

Goddard Space Flight Center
Greenbelt, Maryland 20771

8. PERFORMING ORGANIZATION REPORT NUMBER

93B00069

9. SPONSORING/MONITORING AGENCY NAME(S) AND ADDRESS(ES)

National Aeronautics and Space Administration
Washington, D.C. 20546-0001

10. SPONSORING/MONITORING AGENCY REPORT NUMBER

TM-104581

11. SUPPLEMENTARY NOTES
Authors Hedin and Schmidlin: GSFC, Greenbelt, MD; Fleming: Applied Research Corporation, Landover, MD; Manson: University of Saskatchewan, Saskatchewan, Canada; Avery: University of Colorado, Boulder, CO; Franke: University of Illinois, Urbana, IL.

12a. DISTRIBUTION/AVAILABILITY STATEMENT
Unclassified–Unlimited
Subject Category 47
Report is available from the National Technical Information Service, U.S. Dept. of Commerce, 5285 Port Royal Road, Springfield, VA 22151; (703) 557–4650.

12b. DISTRIBUTION CODE

13. ABSTRACT (Maximum 200 words)

The HWM90 thermospheric wind model has been revised in the lower thermosphere and extended into the mesosphere and lower atmosphere to provide a single analytic model for calculating zonal and meridional wind profiles representative of the climatological average for various geophysical conditions. Gradient winds from CIRA–86 plus rocket soundings, incoherent scatter radar, MF radar and meteor radar provide the data base and are supplemented by previous data-driven model summaries. Low–order spherical harmonics and Fourier series are used to describe the major variations throughout the atmosphere including latitude, annual, semiannual, and longitude (stationary wave 1). The model represents a smoothed compromise between the data sources. Although agreement between various data sources is generally good, some systematic differences are noted, particularly near the mesopause. Root mean square differences between data and model are on the order of 15 m/s in the mesosphere and 10 m/s in the stratosphere for zonal wind, and 10 m/s and 4 m/s, respectively, for meridional wind.

14. SUBJECT TERMS

Wind; Circulation; Dynamics, Lower Thermosphere, Mesosphere; Stratosphere

15. NUMBER OF PAGES
86

16. PRICE CODE

17. SECURITY CLASSIFICATION OF REPORT	18. SECURITY CLASSIFICATION OF THIS PAGE	19. SECURITY CLASSIFICATION OF ABSTRACT	20. LIMITATION OF ABSTRACT
Unclassified	Unclassified	Unclassified	Unlimited

NSN 7540-01-280-5500